1998

Modeling and Optimal Design of Spiral-Wound Membrane Systems for Gas Separations.

Runhong Qi
Louisiana State University and Agricultural & Mechanical College

INFORMATION TO USERS

This manuscript has been reproduced from the microfilm master. UMI films the text directly from the original or copy submitted. Thus, some thesis and dissertation copies are in typewriter face, while others may be from any type of computer printer.

The quality of this reproduction is dependent upon the quality of the copy submitted. Broken or indistinct print, colored or poor quality illustrations and photographs, print bleedthrough, substandard margins, and improper alignment can adversely affect reproduction.

In the unlikely event that the author did not send UMI a complete manuscript and there are missing pages, these will be noted. Also, if unauthorized copyright material had to be removed, a note will indicate the deletion.

Oversize materials (e.g., maps, drawings, charts) are reproduced by sectioning the original, beginning at the upper left-hand corner and continuing from left to right in equal sections with small overlaps. Each original is also photographed in one exposure and is included in reduced form at the back of the book.

Photographs included in the original manuscript have been reproduced xerographically in this copy. Higher quality 6" x 9" black and white photographic prints are available for any photographs or illustrations appearing in this copy for an additional charge. Contact UMI directly to order.

UMI

A Bell & Howell Information Company
300 North Zeeb Road, Ann Arbor MI 48106-1346 USA
313/761-4700 800/521-0600

MODELING AND OPTIMAL DESIGN OF SPIRAL-WOUND MEMBRANE SYSTEMS FOR GAS SEPARATIONS

A Dissertation

Submitted to the Graduate Faculty of the
Louisiana State University and
Agricultural and Mechanical College
in partial fulfillment of the
requirements for the degree of
Doctor of Philosophy

in

The Department of Chemical Engineering

by
Runhong Qi
B.Engr. Tianjin University, China, 1984
M.Engr. Tianjin University, China, 1987
December 1998

To my wife, daughter, parents, and family.

Acknowledgments

I would like to thank my advisor, Dr. Michael A. Henson, for introducing me to the research area of modeling and design of membrane separation systems. His leadership and intensity have motivated me to do the best I can, and to become the best researcher and engineer possible. He allows me to pursue my research interests independently and always encourages higher criteria. His advice and support are truly meaningful to my professional development. Thanks also are given to the LSU Office of Research and Development and Praxair for their financial support of my research.

I need to thank many former fellow students and friends. Dr. Mike Kurtz and Dr. Rich McLain have always been ready to help me since I joined the research group. Their kind assistance in various aspects has made my transition of working environments with totally different languages and cultures much less difficult. I would also like to thank Dr. Xueyu Chen for her valuable advice and discussion of optimization problems, and Dr. Jeff Smith for his willingness to help. Thanks also to those in the office, Guang-Yan Zhu and Yongchun Zhang, for their advice, assistance and free conversations.

Thanks must also be given to my parents, parents-in-law and their families who have always supported my efforts to reach my goals. They helped take care of my daughter for more than three years during my preparation for and early attendance

at graduate school. Without their continuous support, I could not have overcome the burden and toughness of finishing my degree.

Finally and most importantly, I am truly grateful to my wife, Dawen, and daughter, Meng, for their love, support and patience which inspire me forever.

Table of Contents

List of Tables

List of Figures

Abstract

Membrane system economics can be significantly affected by process modeling and design. Available spiral-wound permeator models are difficult to use for process design because of their mathematical complexity and high computational demands. Existing sequential design methods yield suboptimal flowsheets when multiple permeation stages are required. In this dissertation, more effective modeling and design techniques for spiral-wound systems separating binary and multicomponent gas mixtures are developed.

An approximate modeling approach based on the assumption that the residue flow rate is constant in the direction of bulk permeate flow is proposed. This assumption allows a significant simplification of basic transport models which are derived from material balances and permeation relations. The approach reduces the solution of mixed-boundary nonlinear differential equations to a more computationally tractable problem involving a small number of nonlinear algebraic equations. Approximate models for both binary and multicomponent mixtures are developed. Case studies for separating CO_2 from natural gas mixtures show that the approximate models yield accurate predictions over a wide range of operating conditions with considerably less computing time than the basic transport models. An estimation technique for determining uncertain/unknown model parameters from experimental data also is proposed.

A nonlinear programming (NLP) design technique is proposed for optimizing operating conditions and analyzing parameter sensitivities for prespecified permeator configurations. The NLP method is extended to develop a mixed-integer nonlinear programming (MINLP) strategy which utilizes a permeator system superstructure to simultaneously optimize the permeator configuration and operating conditions which minimize the total process cost. Case studies for CO_2/CH_4 separations in natural gas treatment and enhanced oil recovery demonstrate that the design methodologies are sufficiently robust to handle gas separations with very demanding requirements. Optimal designs are derived for different number of separation stages for both continuous and discrete membrane areas. The proposed approach provides an efficient tool for preliminary design of multi-stage membrane systems for binary and multicomponent gas separations.

Chapter 1

Introduction

1.1 Overview

In recent years, gas separation membranes have emerged as viable alternatives to more mature technologies such as absorption and cryogenic distillation. The emergence of gas separation membranes is primarily due to three critical developments: (*i*) synthesis of high performance polymer membrane materials [47]; (*ii*) large scale production techniques for high flux asymmetric membranes [79]; and (*iii*) fabrication techniques for high surface area membrane permeators [46]. One of the most important applications of membrane technology is the use of spiral-wound permeators to upgrade natural gas mixtures encountered in natural gas treatment and enhanced oil recovery. In these applications, the success of membrane technology stems from its inherent advantages of low capital cost, operational simplicity, space and weight efficiency, easy scalability, and (in some cases) low power consumption. As noted by Spillman [71], the economic viability of membrane separation processes depends critically on *process design.*

Improved operation of spiral-wound membrane systems requires the derivation of efficient permeator models which can be used to investigate separation performance and develop systematic design methodologies. However, available models for

spiral-wound permeators are based on basic transport equations which are derived directly from material balances and permeation relations assuming cross-flow patterns for bulk flow and local permeation [57]. Basic transport models, which consist of a set of nonlinear algebraic-differential-integral equations with mixed boundary conditions, are difficult to use for process design purposes because of their mathematical complexity and high computational demands. The lack of appropriate permeator models is a major obstruction to effective simulation and design of membrane processes. An alternative approach is to develop approximation techniques to simplify the basic transport models. Such approximate models, consisting of a set of nonlinear algebraic equations, can be solved much more efficiently and effectively used for process design.

Membrane economics can be significantly affected by the design of the processes. Single-stage systems have low capital costs, but they are appropriate only for moderate product purity and recovery requirements. Multiple separation stages and recycle are required for more demanding applications. Currently, multiple-stage membrane systems are designed via a sequential procedure in which the permeator configuration is chosen and the operating conditions are then determined [9, 10, 51, 63, 71]. Sequential design procedures are inefficient because it usually is infeasible to enumerate and evaluate all possible network configurations. As a result, existing design techniques often yield suboptimal flowsheets.

During the last decade, a wide variety of process design and synthesis problems have been solved by mathematical programming [30, 34, 35]. This approach utilizes rigorous optimization methods to systematically determine the process configuration and operating conditions. A popular approach is to postulate a superstructure which embeds many process configurations, each of which is a candidate for the optimal process flowsheet [28]. The superstructure is mathematically described by a model which contains both continuous and integer variables that represent operating conditions, as well as processing units and their interconnections. The mixed-integer nonlinear programming (MINLP) model is posed as a set of constraints in an optimization problem in which the total annual process cost usually is the objective function. MINLP techniques have been proposed for the synthesis of heat exchanger networks, distillation column sequences, reactor networks, and mass-exchange networks [28, 30, 34, 35].

The purpose of this research is to develop more effective modeling and design techniques for gas separation systems comprised of spiral-wound permeators. As a first step, approximate permeator models separating binary and multicomponent gas mixtures are derived directly from basic transport models. By using the approximate models, different permeator configurations are optimized via nonlinear programming (NLP) to get a better understanding of process performance. Finally, systematic design strategies based on MINLP are developed to allow simultaneous optimization

of the system configuration and operating conditions. The research focuses on the following tasks:

1. Derivation of approximate permeator models which can be effectively used for the design of binary and multicomponent gas systems.

2. Optimization of different permeator configurations using nonlinear programming techniques.

3. Development of permeator system superstructures which efficiently represent a large number of potential permeator configurations.

4. Development of MINLP synthesis strategies to minimize the total annual cost of the membrane system.

5. Evaluation of the modeling and design techniques via case studies of methane purification in natural gas treatment and enhanced oil recovery.

1.2 Spiral-Wound Gas Permeators

The spiral-wound permeator is a common type of membrane module used in industry. Figures 1.1 and 1.2 depict a spiral-wound membrane element and its holding vessel, respectively [19, 55]. The membrane element consists of alternate layers of a feed gas channel, membrane sheet, and permeate gas channel. Spacing material is placed between two flat membrane sheets. Three edges of the two flat membrane sheets are sealed together and the open edge is sealed to a perforated collection tube.

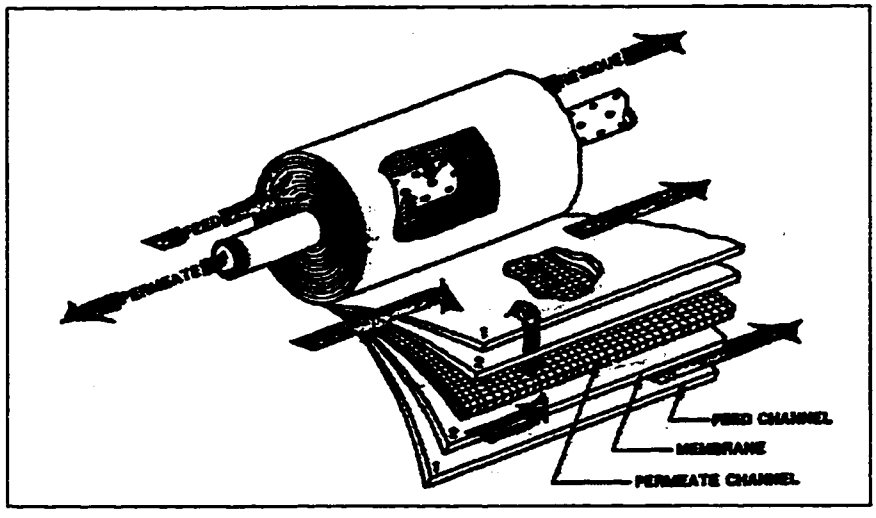

Figure 1.1: Spiral-wound membrane element [19]

A separator grid is placed on the top of the the resulting membrane leaf. Finally, the assembly is rolled around the collection tube and placed inside the cylindrical steel vessel, resulting in a very large separation area per unit volume ($\sim$3000 m^2/m^3) as compared to a simple plate-and-frame configuration ($\sim$300 m^2/m^3). As a means of incorporating more area without requiring an excessively long permeate flow path, multi-leaf assemblies can be used [46]. A pressurized feed stream is introduced on the outer surface of the membrane leaf. The more permeable components preferentially diffuse across the membrane and flow inside the permeate channel toward the collection tube as the low pressure permeate stream. The residue gas, which is enriched in the less permeable components, continues to flow within the feed channel along the outer surface of the leaf and exits at a high pressure.

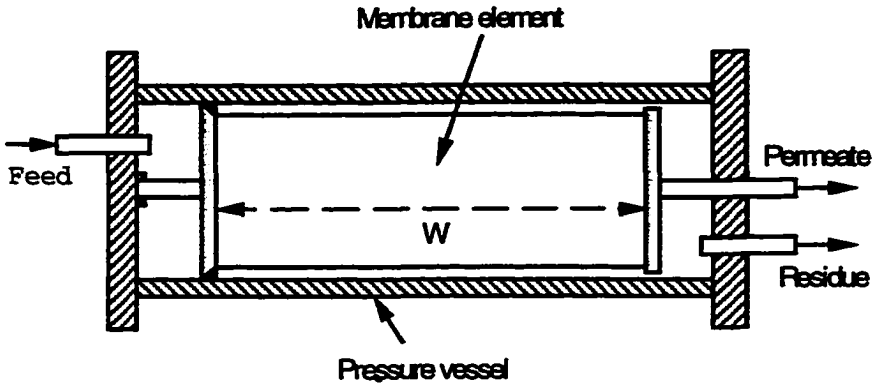

Figure 1.2: Spiral-wound membrane permeator

1.3 Carbon Dioxide/Methane Separations

Membrane processes are widely used in gas separations such as hydrogen recovery, air separation, and natural gas processing [45, 71, 79]. Spiral-wound permeators have been successfully used to separate carbon dioxide/methane mixtures encountered in natural gas treatment [19, 67, 68], and enhanced oil recovery [13, 21, 55].

In natural gas treatment, the feed gas is usually obtained directly from gas wells. The crude natural gas is a mixture of several components such as carbon dioxide (CO_2), hydrogen sulfate (H_2S), nitrogen (N_2), methane (CH_4), ethane (C_2H_6), and heavier hydrocarbons (C_2^+H). The major components are CO_2 and CH_4, while concentrations of the other components are normally small. For production of fuel-grade natural gas, acid gases (CO_2 and H_2S) need to be removed since they are corrosive and/or incombustible. A typical CH_4-enriched pipeline fuel contains less than 2% CO_2. Because the feed gas may be obtained from different gas wells, a wide range of pressures (2–7 MPa) and compositions (5–50% CO_2) can be observed. The most

common process for removing CO_2 and other acid impurities is amine absorption [44]. However, this process is very large and complex, necessitates a central processing plant for many small gas wells, and requires continuous supervision and maintenance. Membrane processes eliminate these problems, and offer lower capital investment in many situations. The CH_4-enriched residue stream is produced with essentially no pressure loss, while the CO_2-enriched permeate is produced at low pressure (0.1–0.5 MPa) with appreciable amounts of CH_4. The permeate stream has low value and can be used as a low BTU fuel or simply burned.

Enhanced oil recovery is similar to natural gas treatment in that crude gas mixtures are processed. The major difference is that in enhanced oil recovery both the permeate and residue streams have considerable value. The residue stream is used as a fuel, while the permeate stream ($\geq$ 95% CO_2) is compressed and reinjected into the gas well. As a result, the separations are more demanding than those encountered in natural gas treatment. Membrane systems are successful in this application because of their effectiveness at high CO_2 compositions and convenience in field use. To satisfy the requirements for both residue and permeate streams, multi-stage membrane processes usually are necessary.

Spiral-wound permeators for CO_2/CH_4 separations are marketed by several manufacturers, including Air Products, Dow, Hoechst-Celanese, Praxair, and Grace Membrane Systems [45, 71, 79]. It is important to note that established gas separation techniques are still used widely in these applications. As a result, spiral-wound

membrane systems must compete with more mature technologies on the basis of *overall process economics* [71, 79].

1.4 Spiral-Wound Permeator Modeling

A wide variety of permeator models have been proposed for both binary and multicomponent gas separations [49]. For the most part, available models differ with respect to assumptions concerning the flow pattern and the permeate-side pressure drop. Models based on the assumption of complete mixing on both sides of the membrane consist of simple nonlinear algebraic equations [76]. However, such models are not sufficiently accurate for process design since complete mixing is rarely achieved in practice. Models based on plug-flow and cross-flow patterns are comprised of nonlinear ordinary differential equations that typically yield mixed boundary value problems [18, 58]. While such models offer improved accuracy as compared to complete mixing models, they are likely to result in prohibitive computational requirements when utilized for process design. For asymmetric membranes, Pan [57] proposes that permeation occurs via a cross-flow pattern regardless of the flow direction of the bulk permeate stream. By using the local permeate composition rather than the bulk composition to characterize permeation, binary transport models for hollow-fiber and spiral-wound permeators accounting for permeate-side pressure drop are derived [57]. Pan [58] also formulates a multicomponent hollow-fiber model that includes pressure drop inside the fiber. A multicomponent spiral-wound model without permeate-side pressure drop is proposed by Pan and Habgood [59].

Surprisingly we have not found multicomponent transport models of spiral-wound gas permeators which include permeate-side pressure variations.

Basic transport models with permeate-side pressure drop consist of nonlinear ordinary differential equations with mixed boundary conditions. These models can be solved with a trial-and-error shooting method that requires an initial guess of the permeate-side pressure distribution [57, 58]. The differential equations are solved to generate the outlet permeate concentration, as well as a new pressure distribution. The procedure is continued until the permeate concentration converges to the desired accuracy. This solution technique usually yields accurate results, but it is computationally expensive. As a result, this solution procedure is difficult to use for process design.

An alternative approach is to develop approximate permeator models that offer a more reasonable compromise between prediction accuracy and computational efficiency. A commonly used method for hollow-fiber membrane is to approximate the variable driving force with its arithmetic average [17], logarithmic average [62] or a quadratic function of membrane area [50]. These approximations yield nonlinear algebraic equation models that can be solved very efficiently. However, they are valid only when variations in the feed-side and permeate-side concentrations are small. Moreover, it is difficult to use this method for the cross-flow pattern in spiral-wound permeators. Another method assumes a linear relationship between the permeate-side and feed-side compositions along the hollow-fiber [50] or in small

segments of the fiber [48]. This method suffers from the same limitation concerning small variations in the feed-side and permeate-side concentrations. As these variations increase, the inherently nonlinear relation between the permeate-side and feed-side compositions necessitates the use of a large number of segments (*e.g.* 40), which significantly reduces the efficiency of the method. Recently, orthogonal collocation [39] and finite element [74] methodologies have been proposed for solving hollow-fiber permeator module. Nevertheless, an effective approximation technique for spiral-wound permeators is needed.

1.5 Membrane System Design

The economic viability of membrane systems can be significantly affected by process design. The design of a membrane separation process involves the determination of: (*i*) the configuration of the permeator network; and (*ii*) the operating conditions of the individual permeators. As shown in Figure 1.3, a wide variety of permeator configurations have been proposed for CO_2/CH_4 separations. Single-stage systems (Figure 1.3a–b) are appropriate for applications in which product purity and recovery requirements are modest [21, 32, 68]. On the other hand, multiple stages with/without recycle (Figure 1.3c–g) typically are required for more demanding separations [19, 55, 65, 71]. It is important to note that an individual separation stage may actually consist of several permeators arranged in parallel since commercial permeators are designed for a specific range of flow rates.

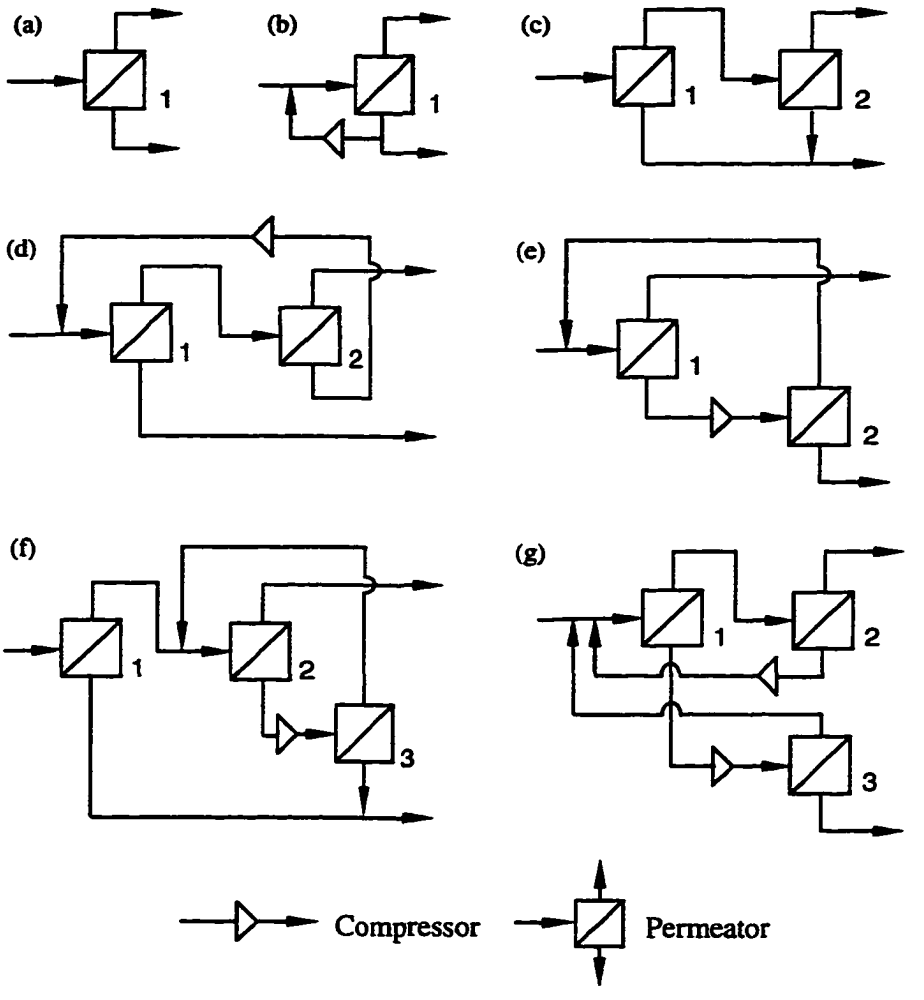

Figure 1.3: Some proposed permeator configurations for CO_2/CH_4 separations. (a) single stage; (b) single stage with recycle; (c) two stage; (d) two stage with permeate recycle; (e) two stage with residue recycle; (f) three stage with residue recycle; (g) three stage with permeate and residue recycle.

Membrane systems currently are designed via a sequential procedure in which the permeator configuration is chosen by process heuristics and the operating conditions are determined using some type of optimization procedure. Many investigators have used this method to design multi-stage gas permeation systems [2, 3, 4, 5, 7, 8, 9, 10, 18, 32, 63, 71, 72, 77]. Spillman *et al.* [72] design membrane systems to

separate CO_2/CH_4 mixtures encountered in natural gas treatment and enhanced oil recovery. Several permeator configurations are optimized for a particular feed composition. Babcock *et al.* [5] evaluate the economics of single-stage and three-stage membrane systems for natural gas treatment by providing comparisons with amine treatment processes. Bhide and Stern present detailed case studies of membrane separation systems for natural gas treatment [9, 10] and oxygen enrichment of air [7, 8]. A grid search method is used to optimize operating conditions for several different configurations. Agrawal and Xu [2, 3, 4, 77] develop a stepwise procedure for synthesis of membrane cascades using a limited number of recycle compressors. This approach is based on a master cascade which contains a large number of possible permeation stages and a specified number of recycle compressors. Substructure cascades are generated by eliminating unwanted recycle compressors and membrane stages using heuristic process analysis. A systematic method for optimizing the membrane cascades and their operating conditions is not presented.

Existing design techniques have several shortcomings including:

1. The determination of the permeator configuration and operating conditions are considered separately [71].

2. The selection of the permeator configuration is based on process heuristics rather than systematic procedures [45].

3. Design procedures are inefficient because it usually is infeasible to enumerate and evaluate all possible network configurations [46, 71].

4. Design programs which optimize operating conditions usually are proprietary and not available to the general engineering community [45, 72].

As a result, current design techniques are likely to yield suboptimal flowsheets for membrane processes which require multiple separation stages.

1.6 Process Synthesis and Optimization

Over the last three decades, process synthesis has been one of the most important research areas in chemical process design [28, 30, 35, 37]. The primary objective of process synthesis is to systematically develop process flowsheets that transform the available raw materials into desired products and which meet the specified performance criteria of: (*i*) maximum profit or minimum cost; (*ii*) energy efficiency; and (*iii*) good operability with respect to flexibility, controllability, reliability, safety, and environmental restrictions. Recently there has been a pronounced increase in the application of mixed-integer programming to process synthesis problems. Reliable and efficient optimization tools are now available, which make it possible to solve large and complex mixed-integer nonlinear programming (MINLP) problems.

These optimization-based designs involve both continuous and binary variables. The continuous variables represent flow rates, temperatures, pressures, and unit sizes, while the binary variables represent the configuration of process units. The models describing the process units are usually nonlinear. As a result, the process

synthesis problem can be classified as a MINLP problem. The MINLP optimization approach to process synthesis consists of three main steps [28]:

1. **Representation of alternatives in a superstructure**

   A superstructure is postulated in which all process alternative structures of interest are embedded and hence are candidates for the optimal process flowsheet. The superstructure features a number of different units and their interconnections.

2. **Mathematical modeling of superstructure**

   The superstructure is modeled as the following general formulation:

$$\begin{aligned} \min: \quad & f(X,Z) \\ \text{s.t.}: \quad & h(X,Z) = 0 \\ & g(X,Z) \leq 0 \\ & X \in R^n \\ & Z \in \{0,1\}^l \end{aligned} \tag{1.1}$$

   where: X is a vector of n continuous variables that represent flow rates, temperatures, pressures, compositions of the process streams, and the sizes of the process units; Z is a vector of l binary variables that denote the potential existence (*i.e.* $Z_i = 1$) or not (*i.e.* $Z_i = 0$) of different process units in the optimal process flowsheet; $f(X,Z)$ is an objective function which represents the performance criterion; $h(X,Z)$ are m equality constraints that denote total

mass and component balances, energy balances, equilibrium relations which constitute the process constraints; $g(X, Z)$ are p inequality constraints which correspond to design specifications, restrictions, feasibility constraints, and logical constraints. In many cases, the binary variables appear linearly, so the nonlinearity occurs only with respect to the continuous variables.

3. **Algorithmic development**

The MINLP optimization model is solved using various algorithms including generalized benders decomposition [33, 60], branch and bound [6, 14], outer approximation and its variants [24, 27, 42, 75], feasibility approach [54], and generalized cross decomposition [38]. Significant progress in the development of MINLP algorithms, as well as extensive computer implementations, have been made during the last decade. As a result, there now exist automated implementations of MINLP algorithms such as DICOPT++ (DIscrete and Continuous OPTimization) developed by Viswanathan and Grossmann [75] and APROS (Automatic PROcess Synthesizer) developed by Paules and Floudas [60]. These codes make use of the General Algebraic Modeling Systems (GAMS) as a modeling tool. GAMS allows problems to be specified in algebraic form and solved with various linear, nonlinear and mixed-integer solvers. While the solvers have provisions to handle nonconvexities, they do not guarantee converging the global optimum. This is a possible limitation as separation systems typically yield nonconvex MINLP problems due to the

presence of splitters and mixers [29]. In the past decade, a number of optimization techniques which ensure global solution of certain classes of nonconvex MINLP problems also have been proposed [1, 30]. These global solution techniques are not investigated in this thesis.

Chapter 2

Spiral-Wound Permeator Modeling for Binary Gas Separations

2.1 Introduction

In this chapter, we propose an approximate modeling technique for spiral-wound permeators separating binary gas mixtures. The model is based on the assumption that the residue flow rate does not vary in the direction of permeate flow. By applying this assumption to a standard fundamental model [57], the original boundary value problem is reduced to a much simpler set of nonlinear algebraic equations. Because the resulting model may contain several unknown parameters, a simple and efficient strategy for estimating model parameters from experimental data is developed. The accuracy of the approximate model is evaluated by comparing the predictions with those obtained from the fundamental model for a wide range of CO_2/CH_4 separations.

2.2 Fundamental Model

First we present the fundamental model of a spiral-wound gas permeator proposed by Pan [57]. The model development is based on Figure 2.1, which depicts permeation through an extended membrane leaf of a spiral-wound permeator. The notation is defined in Appendix A.2. The leaf is comprised of two asymmetric membranes

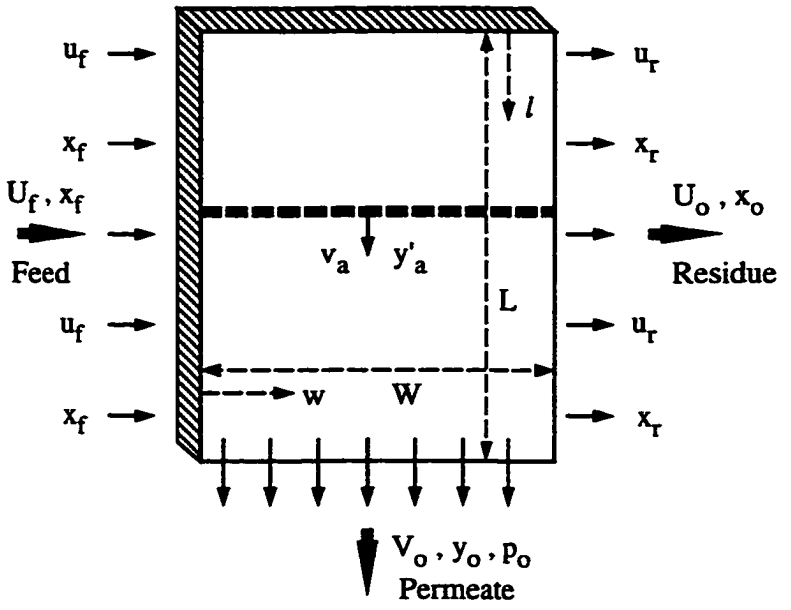

Figure 2.1: Binary gas permeation through a spiral-wound membrane.

separated by a spacing material. Three edges of the leaf are sealed and the open edge is attached to a perforated tube. The feed stream is introduced on the outside of the leaf, and gas permeates through both of the membranes into the spacing material. The permeate stream flows toward the open edge at a 90 degree angle to the feed stream. The feed gas that does not permeate is collected as the residue stream. A large surface area per volume is obtained by placing a feed spacer on top of the leaf and rolling the membrane "sandwich" around the collection tube.

The fundamental model is based on the following assumptions [57]:

1. The feed stream contains a binary gas mixture.

2. Bulk flow and local permeation are described by a cross-flow pattern.

3. There is no pressure drop on the feed side.

4. The pressure drop on the permeate side is described by Darcy's law [12].

5. Membrane permeabilities are independent of pressure and concentration.

6. The porous supporting layer offers negligible resistance to gas flow.

7. There is no mixing in the porous support.

8. The permeate pressure varies only in the direction of permeate flow.

Several of these assumption can be relaxed if necessary [18, 49, 56, 69].

The fundamental model is comprised of three ordinary differential equations, two nonlinear algebraic equations, and one nonlinear integral equation. The differential equations describe the dependence of the dimensionless permeate pressure $\gamma(h)$, dimensionless permeate flow $\theta(h)$, and bulk permeate concentration $y(h)$ on the dimensionless leaf length variable h,

$$\frac{d\gamma^2}{dh} = -C\theta \tag{2.1}$$

$$\frac{d\theta}{dh} = 1 - \phi_r \tag{2.2}$$

$$\frac{d(\theta y)}{dh} = x_f - x_r\phi_r \tag{2.3}$$

where $\phi_r(h)$ is the dimensionless residue flow rate which is defined as $\phi_r(h) = u_r(h)/u_f$; x_f and $x_r(h)$ are the feed and local residue concentrations, respectively; and:

$$C = \frac{2R_gT\mu LU_f}{Wd_mBP^2} \tag{2.4}$$

The differential equations are subject to mixed boundary conditions,

$$\theta(0) = \theta(0)y(0) = 0 \tag{2.5}$$

$$\gamma(1) = \gamma_0 \tag{2.6}$$

where γ_0 is the ratio of the permeate and feed pressures at the permeate outlet.

The first nonlinear algebraic equation describes the relation between the local feed-side concentration $x(h,s)$ and the local permeate concentration on the membrane surface $y'(h,s)$,

$$\frac{y'}{1-y'} = \frac{\alpha(x-\gamma y')}{1-x-\gamma(1-y')} \tag{2.7}$$

where α is the membrane selectivity and s is the dimensionless leaf width variable. The second algebraic equation describes the effect of the local permeate concentration on the dimensionless feed-side flow rate $\phi(h,s)$,

$$\phi = \left(\frac{y'}{y'_f}\right)^a \left(\frac{1-y'}{1-y'_f}\right)^b \left(\frac{\alpha-(\alpha-1)y'}{\alpha-(\alpha-1)y'_f}\right) \tag{2.8}$$

where $y'_f(h)$ is the local permeate concentration on the membrane surface at the feed inlet and:

$$\begin{aligned} a &= \frac{\gamma(\alpha-1)+1}{(\alpha-1)(1-\gamma)} \\ b &= \frac{\gamma(\alpha-1)-\alpha}{(\alpha-1)(1-\gamma)} \end{aligned} \tag{2.9}$$

The nonlinear integral equation describes the relation between the dimensionless permeation factor,

$$R = \frac{2WLQ_2P}{dU_f} \tag{2.10}$$

and the local permeate concentration:

$$R = \frac{1}{\alpha(1-\gamma)}\left\{\alpha - (\alpha-1)y'_f - [\alpha-(\alpha-1)y'_r]\phi_r - (\alpha-1)\int_{y'_f}^{y'_r}\phi_\gamma(y')dy'\right\} \tag{2.11}$$

Note that the integration is performed at constant pressure.

For fixed operating pressures, the model can be solved if two flow rates and/or concentrations are specified. The standard case involves the calculation of the permeate flow rate and concentration for given feed conditions. The bulk residue flow rate and concentration then can be determined by material balances around the permeator. The fundamental model is difficult to solve as a result of the nonlinear differential-algebraic-integral equations and mixed boundary conditions. For the standard calculation problem, Pan [57] proposes an iterative solution technique based on the shooting method. However, this method is computationally expensive and therefore is not well suited for process design applications.

2.3 Approximate Model

We propose an approximate modeling technique for spiral-wound gas permeators based on the fundamental model of Pan [57]. The key assumption is that the residue flow rate is constant in the direction of permeate flow, which implies that

the permeate flow rate varies linearly along the direction of permeate flow. We show that this condition is satisfied approximately by the fundamental model under most operating conditions. The assumption is used to reduce the original boundary value problem to a small number of nonlinear algebraic equations that can be solved much more efficiently. In Appendix A.1, the approximate modeling technique is compared to the one-point collocation method. Finally, a nonlinear programming method for estimating unknown parameters of the approximate model from experimental data is presented.

2.3.1 Model Development

Figure 2.2 shows predictions from the fundamental model for several feed concentrations and permeation factors. For each case, the dimensionless permeate flow rate θ and dimensionless residue flow rate ϕ_r are plotted as a function of the dimensionless leaf length variable h. Note that ϕ_r exhibits a very weak dependence on h, while θ essentially is a linear function of h. This trend is observed for a wide range of operating conditions. Motivated by this result, we assume that the residue flow rate ϕ_r is independent of h. This assumption means that ϕ_r does not vary along the direction of permeate flow, but it does not preclude ϕ variations in the direction of feed flow (see Figure 2.1). Under this condition, the differential equation (2.2) with boundary condition (2.5) is easily integrated:

$$\theta = (1 - \phi_r)\, h \tag{2.12}$$

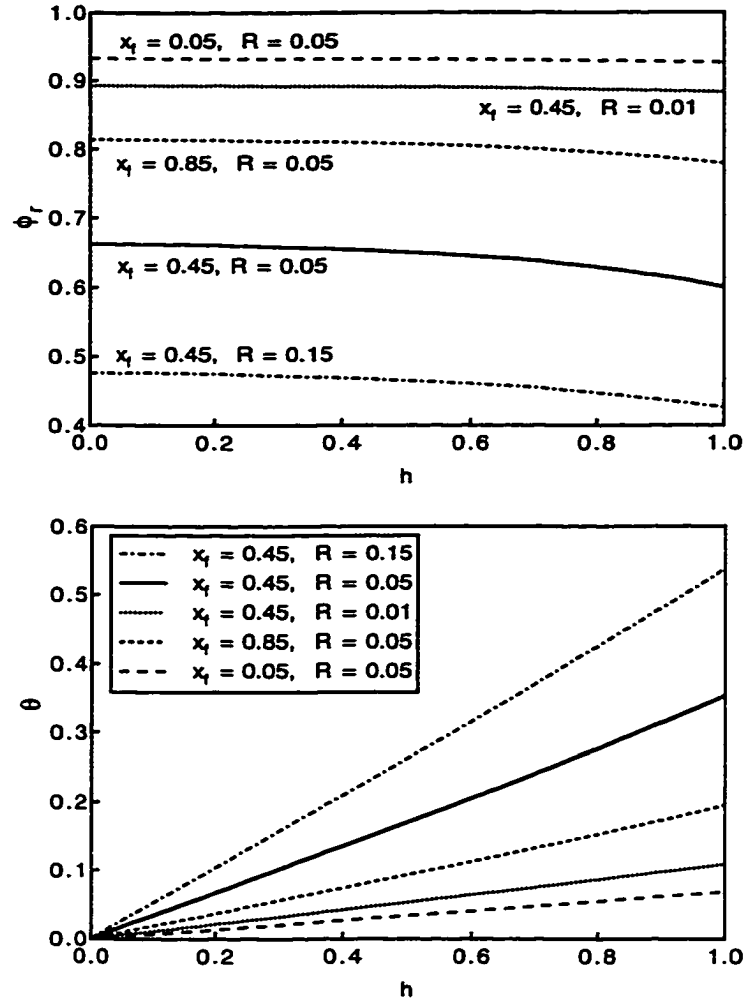

Figure 2.2: Variations of the residue and permeate flow rates along the membrane length for the fundamental model.

Note that θ is a linear function of h, as expected. Substitution of (2.12) into (2.1) and integration with the boundary condition (2.6) yields:

$$\gamma^2 = \gamma_0^2 + \frac{1}{2}C\,(1-\phi_r)\,(1-h^2) \tag{2.13}$$

Note that we allow ϕ_r to vary with h in the subsequent development. Thus, the assumption is invoked primarily to derive the approximate pressure distribution function (2.13).

The integral in (2.11) is evaluated as follows. We define the function in (2.8) as:

$$\phi(\gamma, y') \equiv \left(\frac{y'}{y'_f}\right)^a \left(\frac{1-y'}{1-y'_f}\right)^b \left(\frac{\alpha-(\alpha-1)y'}{\alpha-(\alpha-1)y'_f}\right) \tag{2.14}$$

It follows that:

$$\phi_r = \phi(\gamma, y'_r) \tag{2.15}$$

The integral is represented as,

$$I(\gamma, y'_r) = \int_{y'_f}^{y'_r} \phi_\gamma(y')dy' \tag{2.16}$$

where $\phi_\gamma(y')$ denotes that the integration is performed at constant pressure, and $\phi_\gamma(y'_f) = 1$. The integral is approximated using Gaussian quadrature [66]. The change of variable,

$$\xi \equiv \frac{y'-y'_f}{y'_r-y'_f} \tag{2.17}$$

yields the expression,

$$I(\gamma, y'_r) = (y'_r - y'_f)\int_0^1 \phi_\gamma(\xi)d\xi \cong (y'_r - y'_f)\sum_{j=1}^{N} \phi_\gamma(y'_j)w_j \tag{2.18}$$

where N is the number of quadrature points, ξ_j and w_j are the quadrature points and weights, respectively, and $y'_j = y'_f + \xi_j(y'_r - y'_f)$. Thus, the integral equation (2.11) can be represented as:

$$R = \frac{1}{\alpha(1-\gamma)}\left\{\alpha - (\alpha-1)y'_f - [\alpha - (\alpha-1)y'_r]\phi(\gamma, y'_r) - (\alpha-1)I(\gamma, y'_r)\right\} \quad (2.19)$$

Simultaneous solution of (2.13), (2.15), (2.19), and (2.7) solved for y' with $x = x_f$ [57] at each quadrature point yields $\gamma(h_i)$, $\phi_r(h_i)$, $y'_r(h_i)$, and $y'_f(h_i)$. Here h_i represents the value of h at the i-th quadrature point.

The nonlinear algebraic equation (2.7) can be rearranged as:

$$x_r = \frac{1+\gamma(\alpha-1)(1-y'_r)}{y'_r + \alpha(1-y'_r)}y'_r \quad (2.20)$$

This allows the value of the residue concentration $x_r(h_i)$ at each quadrature point to be computed from $\gamma(h_i)$ and $y'_r(h_i)$. Material balances on a differential length of membrane yield,

$$u_f = u_r + v_a \quad (2.21)$$

$$u_f x_f = u_r x_r + v_a y'_a \quad (2.22)$$

where u_f and $u_r(h)$ are the feed and residue flow rates per unit length, respectively, and $v_a(h)$ and $y'_a(h)$ are the permeate flow rate per unit length and local permeate concentration, respectively, averaged over the entire width of the membrane.

Therefore:

$$y'_a = \frac{x_f - x_r \frac{u_r}{u_f}}{1 - \frac{u_r}{u_f}} = \frac{x_f - x_r \phi_r}{1 - \phi_r} \tag{2.23}$$

The flow rate and concentration of the effluent permeate stream are calculated as follows. The flow rate is obtained from (2.2) using Gaussian quadrature,

$$\theta_0 = 1 - \int_0^1 \phi_r dh \cong 1 - \sum_{i=1}^{M} \phi_r(h_i) w_i \tag{2.24}$$

where M is the number of quadrature points. By invoking the assumption that ϕ_r is a "weak" function of h, it is easy to show that the permeate composition can be computed as:

$$y_0 = \int_0^1 y'_a dh \cong \sum_{i=1}^{M} y'_a(h_i) w_i \tag{2.25}$$

The flow rate η_0 and concentration x_0 of the effluent residue stream are determined from an overall material balance about the permeator:

$$\eta_0 = 1 - \theta_0 \tag{2.26}$$

$$x_0 = \frac{x_f - \theta_0 y_0}{1 - \theta_0} \tag{2.27}$$

The flow rates and concentrations of the effluent streams are easily calculated given the values $\gamma(h_i)$, $\phi_r(h_i)$, and $y'_r(h_i)$. Therefore, the original boundary value problem effectively is reduced to solution of the four nonlinear algebraic equations (2.7), (2.13), (2.15), and (2.19) at the quadrature points h_i. Solution complexity is

not strongly affected by the number of quadrature points N used to approximate the integral in (2.18). By contrast, the four nonlinear algebraic equations must be solved simultaneously for each quadrature point used in the computation of the permeate flow rate and concentration. Our experience indicates that one quadrature point ($M = 1$) generally provides a satisfactory solution. In this case $h_1 = 0.5$ and $w_1 = 1$, and the quadrature formulas reduce to,

$$\theta_0 = 1 - \phi_r(h_1) \tag{2.28}$$

$$y_0 = y_a'(h_1) = \frac{x_f - x_r(h_1)\phi_r(h_1)}{1 - \phi_r(h_1)} \tag{2.29}$$

where $\phi_r(h_1)$ and $x_r(h_1)$ are obtained by solving the four nonlinear algebraic equations at h_1.

It is interesting to note that the pressure distribution (2.13) has the following form in this case:

$$\gamma^2(h_1) = \gamma_0^2 + \frac{3}{8}C\left[1 - \phi_r(h_1)\right] \tag{2.30}$$

In Appendix A.1, we show that the approximate model with $M = 1$ is closely related to the model obtained when one-point collocation [66] is applied to the fundamental model. The only difference is that the collocation method yields the following pressure distribution,

$$\gamma^2(h_1) = \gamma_0^2 + \frac{1}{4}C\left[1 - \phi_r(h_1)\right] \tag{2.31}$$

where h_1 now is interpreted as the interior collocation point. The two relations are identical with the exception of the constant coefficient. While this appears to be a minor difference, the subsequent simulation results show that the proposed modeling technique can yield significant improvements in prediction accuracy.

2.3.2 Parameter Estimation

A potential disadvantage of the proposed technique is that the approximate model contains all the parameters in the original fundamental model. In most applications, detailed characteristics of the permeator are not known at the preliminary design stage. Consequently, the approximate model may contain uncertain and/or unknown parameters. We present a nonlinear programming strategy [15, 23, 40] that provides a simple and efficient means of estimating unknown/uncertain model parameters from experimental data. The primary advantage of the proposed method is that nonlinear implicit equations can be handled. Although the estimation technique is presented for one-point quadrature, it is readily extended to the more general case.

The objective is to estimate model parameters associated with the internal characteristics of the permeator. We assume that the membrane selectivity α is known. Unknown parameters may include the membrane leaf length L, the leaf width W, the leaf thickness d_m, and the asymmetric membrane thickness d. Note that these four parameters appear in the approximate model only via the terms C (2.4) and R (2.10). However, these terms are not easily estimated since they also depend on

the feed flow rate U_f and feed pressure P. This problem is handled by defining parameters that do not depend on the feed conditions:

$$C' = \frac{2R_gT\mu L}{Wd_mB} \tag{2.32}$$

$$R' = \frac{2WLQ_2}{d} \tag{2.33}$$

Then (2.4) and (2.10) can be written as:

$$C = C'\frac{U_f}{P^2} \tag{2.34}$$

$$R = R'\frac{P}{U_f} \tag{2.35}$$

Therefore, the problem is reduced to estimating the parameters C' and R'.

To facilitate parameter estimation, the model equations are formulated as follows. Equation (2.28) is rearranged as:

$$\phi_r(h_1) = 1 - \theta_0 \equiv f_1(\theta_0) \tag{2.36}$$

Combining this result with (2.29), the residue concentration is expressed as:

$$x_r(h_1) = \frac{x_f - \theta_0 y_0}{1 - \theta_0} \equiv f_2(x_f, \theta_0, y_0) \tag{2.37}$$

The following relations are obtained from (2.7),

$$y_r'(h_1) = f_3[\gamma(h_1), x_r(h_1)] \tag{2.38}$$

$$y'_f(h_1) = f_3[\gamma(h_1), x_f] \tag{2.39}$$

where f_3 represents the function obtained when (2.7) is solved for y' [57]. The following result is obtained by combining (2.30) and (2.36):

$$\gamma^2(h_1) = \gamma_0^2 + \frac{3}{8}C\theta_0 \equiv f_4(\gamma_0, \theta_0, C') \tag{2.40}$$

Equation (2.19) is represented as:

$$f_5[\gamma(h_1), y'_f(h_1), y'_r(h_1), R'] = 0 \tag{2.41}$$

The parameters C' and R' are estimated using a nonlinear programming approach. The measurement vector z and parameter vector ν are defined as:

$$z \equiv \begin{bmatrix} x_f & \gamma_0 & \theta_0 & y_0 & U_f & P \end{bmatrix}^T \tag{2.42}$$

$$\nu \equiv \begin{bmatrix} C' & R' \end{bmatrix}^T \tag{2.43}$$

Assume that N independent experiments are performed to generate the data set $\{z_1, z_2, \ldots, z_N\}$. Let $\hat{z}_i$ represent an estimate of the outcome of the i-th experiment. The parameters are determined by solving the following minimization problem,

$$\min\ \Psi(\hat{z}_1, \cdots, \hat{z}_N, \nu) = \sum_{i=1}^{N} (\hat{z}_i - z_i)^T V_i^{-1} (\hat{z}_i - z_i) \tag{2.44}$$

subject to the constraints,

$$F(\hat{z}_i, \nu) = 0, \quad i = 1, 2, \cdots, N \tag{2.45}$$

where V_i are covariance matrices, and F represents the vector function comprised of the scalar functions (2.36)–(2.41). In practice, the V_i are taken to be a constant, diagonal matrix with elements that reflect the relative accuracy of the measurements. It is important to note that reliable algorithms are available to solve the nonlinear optimization problem (2.44)–(2.45) [16, 28]. A simpler estimation problem is obtained if the feed flow rate and pressure are held constant during the experiments. In this case, the parameters C and R can be estimated directly and the dimensionality of the problem is reduced:

$$z \equiv \begin{bmatrix} x_f & \gamma_0 & \theta_0 & y_0 \end{bmatrix}^T \tag{2.46}$$

$$\nu \equiv \begin{bmatrix} C & R \end{bmatrix}^T \tag{2.47}$$

2.4 Results and Discussion

We evaluate the approximate modeling technique via a case study of CO_2/CH_4 separations. The nominal model parameters and operating conditions for the spiral-wound permeator are shown in Table 2.1. These values do not correspond to any particular application, but the range of parameters considered cover a wide variety of CO_2/CH_4 separations. Note that a nominal value is not given for the feed pressure

Table 2.1: Nominal model parameters for case study.

Parameter	Value	Variable	Value
x_f	0.45	θ_0	0.472
γ_0	0.05	y_0	0.844
α	30	η_0	0.528
C	0.1	x_0	0.099
R	0.1		

P because we work exclusively with the dimensionless model. The approximate modeling technique utilizes three quadrature points in the integral evaluation ($N = 3$) and one quadrature point in the computation of the effluent stream properties ($M = 1$). The resulting model is compared to the fundamental model and the model obtained using one-point collocation (see Appendix A.1). The effectiveness of the parameter estimation strategy also is investigated.

2.4.1 Comparison to the Fundamental Model

The fundamental and approximate models are compared in Figures 2.3–2.7. In each figure, parameters values that are not stated explicitly are given in Table 2.1. Figure 2.3 shows the predicted permeate pressure γ, permeate flow rate θ, and residue concentration x_r as a function of the membrane length h for three value of the permeation factor R. The approximate model produces very accurate predictions of the spatial variations for each value of R. The effluent permeate flow rate θ_0 and effluent residue concentration x_0 for various combinations of R and the feed concentration x_f are shown in Figure 2.4. The variable x_0 is shown rather that the

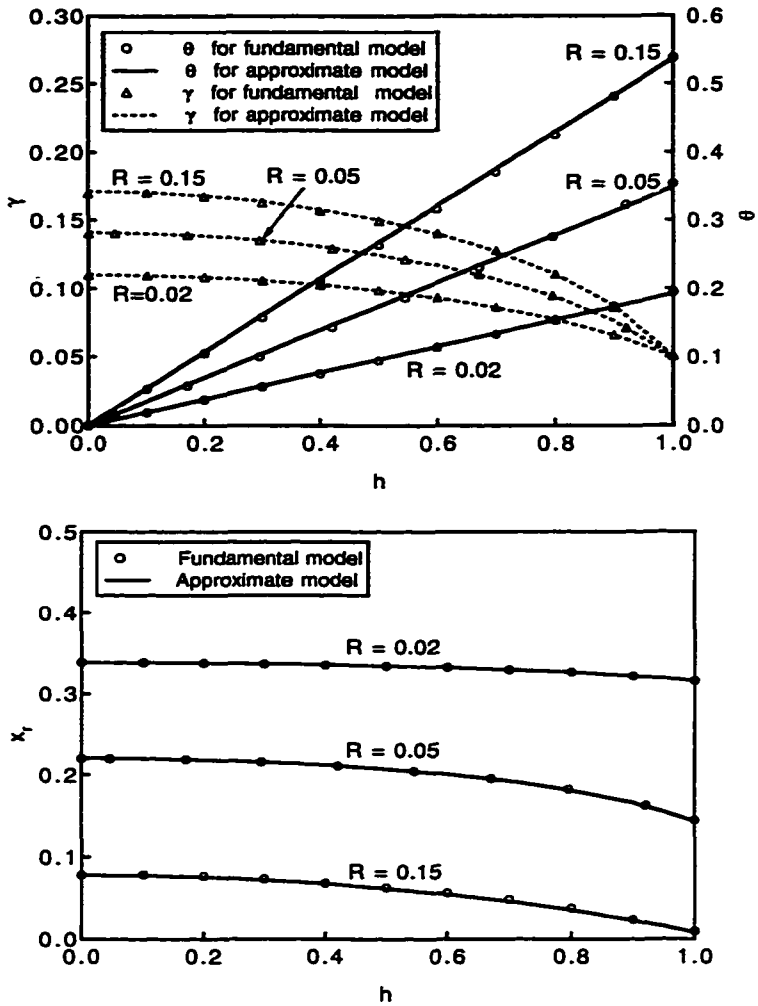

Figure 2.3: Variations of the permeate pressure, permeate flow rate, and residue concentration along the membrane length.

effluent permeate concentration y_0 because the residue concentration exhibits larger variations and therefore is more illustrative. The approximate model yields accurate predictions of both variables for all operating conditions considered. It is interesting to note that higher feed compositions yield lower residue concentrations for large value of R. Consequently, results are not shown when both x_f and R assume large values because x_0 is close to zero under these conditions.

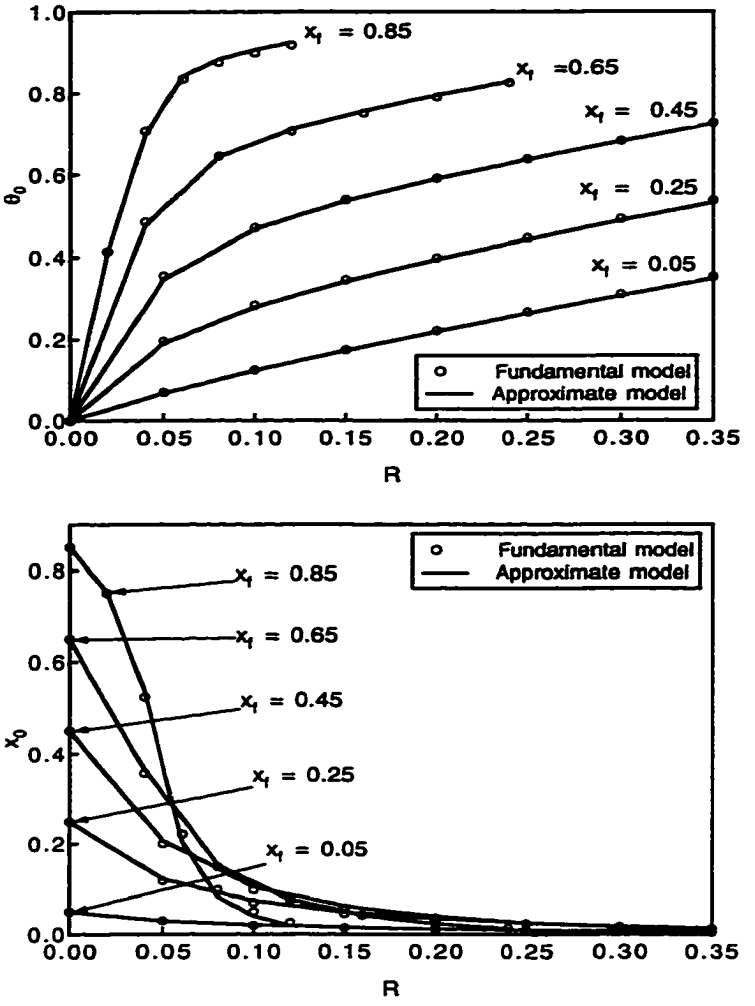

Figure 2.4: Effect of the feed composition on the permeate flow rate and residue concentration.

Figures 2.5 shows the effluent permeate flow rate and residue concentration for several combinations of R and the permeate outlet pressure γ_0. The approximate model produces very accurate predictions for each case. The effect of R and the selectivity α on the effluent stream properties is shown in Figure 2.6. The approximate model yields good predictions for all conditions considered, although small deviations between the two models are observed at intermediate values of α. Results

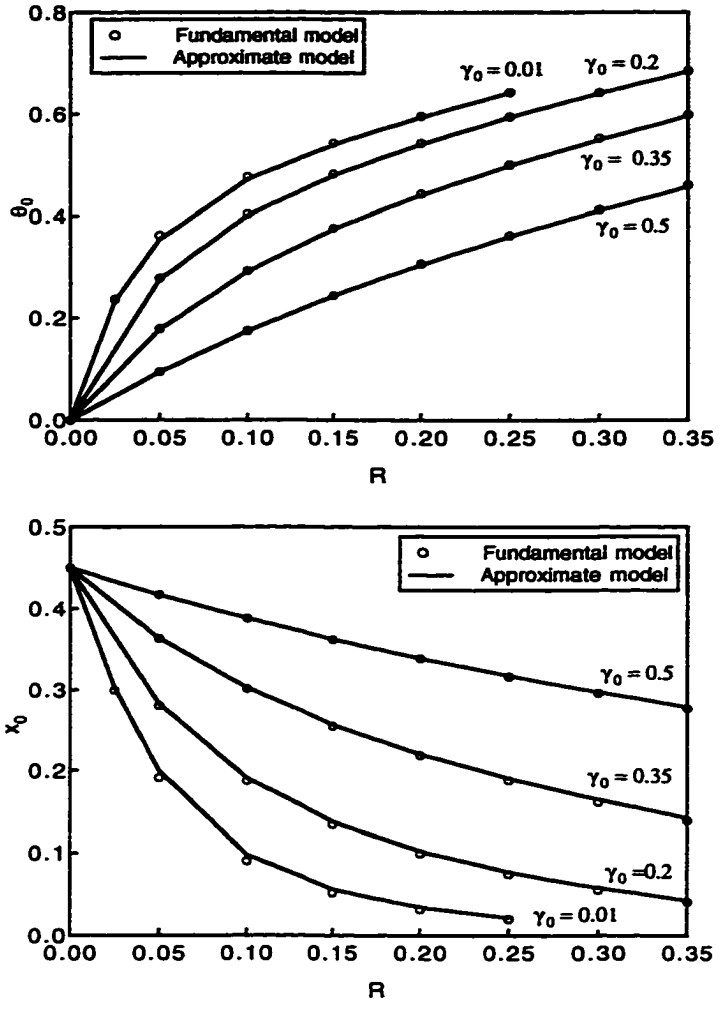

Figure 2.5: Effect of the permeate pressure on the permeate flow rate and residue concentration.

are not shown for high values of α and R since x_0 is close to zero in this case. Figure 2.7 shows the effect of the parameters R and C on the effluent permeate flow rate and residue concentration. The approximate model produces good predictions for low values of C, but becomes slightly inaccurate as C increases. The result is expected because the approximation (2.13) is less valid when C assumes large

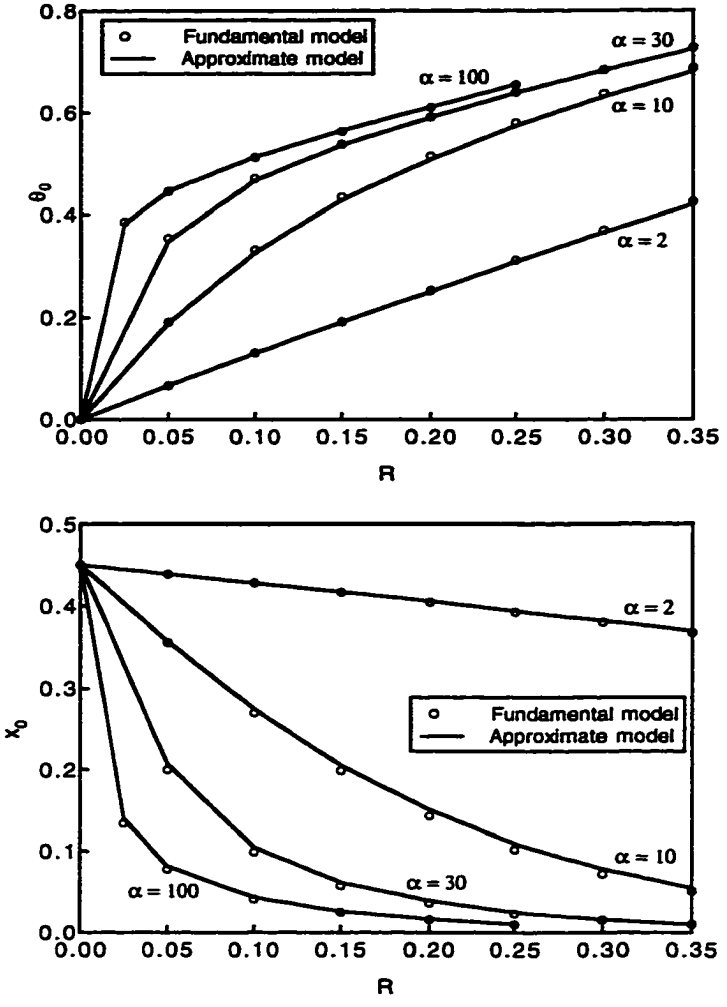

Figure 2.6: Effect of the selectivity on the permeate flow rate and residue concentration.

values. Despite this discrepancy, the approximate model yields predictions that are sufficiently accurate for process design even for large values of C.

The results in Figures 2.3–2.7 demonstrate that the approximate model provides accurate predictions over a wide range of operating conditions. The motivation for developing the approximate model is that the resulting nonlinear algebraic equations can be solved very efficiently. By contrast, the fundamental model consists of a set of

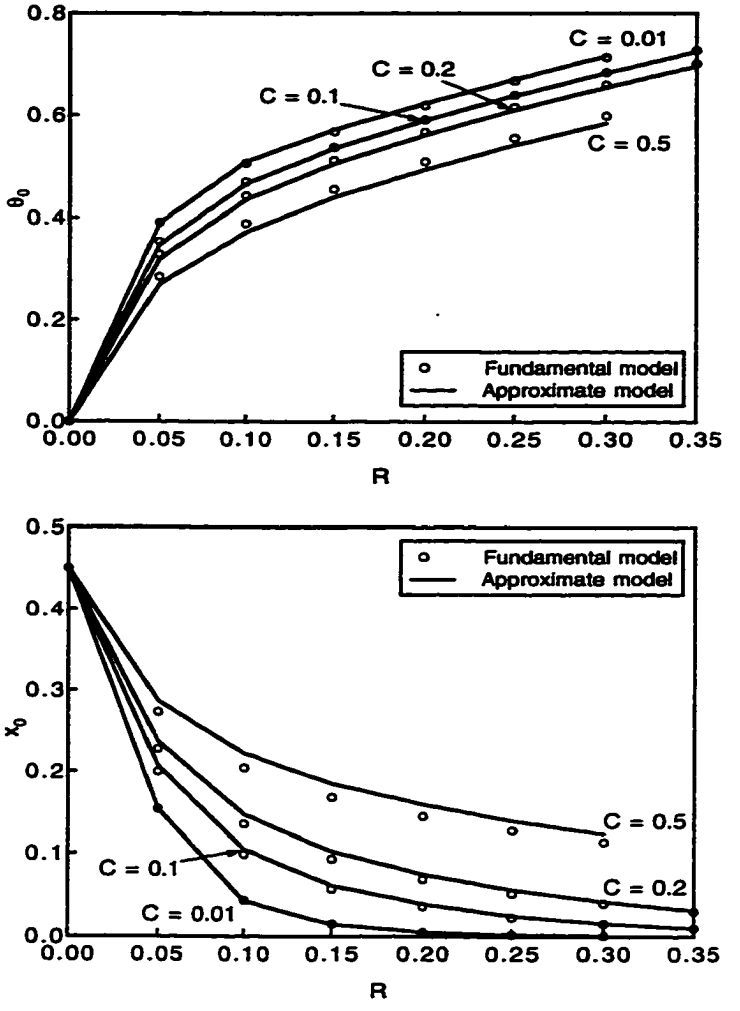

Figure 2.7: Effect of the dimensionless constant C on the permeate flow rate and residue concentration.

nonlinear differential-algebraic-integral equations with mixed boundary conditions. This model is solved using an iterative technique based on the shooting method [57]. Running MATLAB on an IBM RS-6000 workstation, we have found that the approximate model can be solved 200–400 times faster than the fundamental model. Consequently, the approximate model is well suited for process design studies.

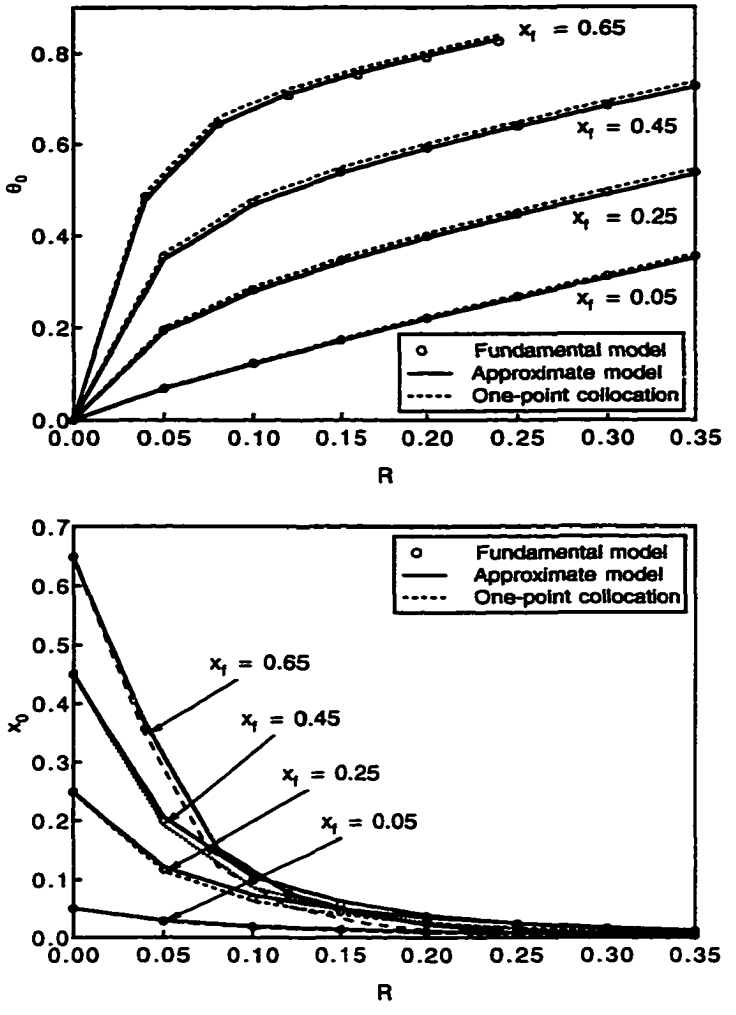

Figure 2.8: Comparison of the approximate model and one-point collocation for different feed compositions.

2.4.2 Comparison to One-Point Collocation

Next we compare the proposed model to the approximate model obtained using one-point collocation (see Appendix A.1). Results also are shown for the fundamental model to provide a basis for comparison. Figure 2.8 shows the effluent permeate flow rate and residue concentration for several combinations of the feed concentration

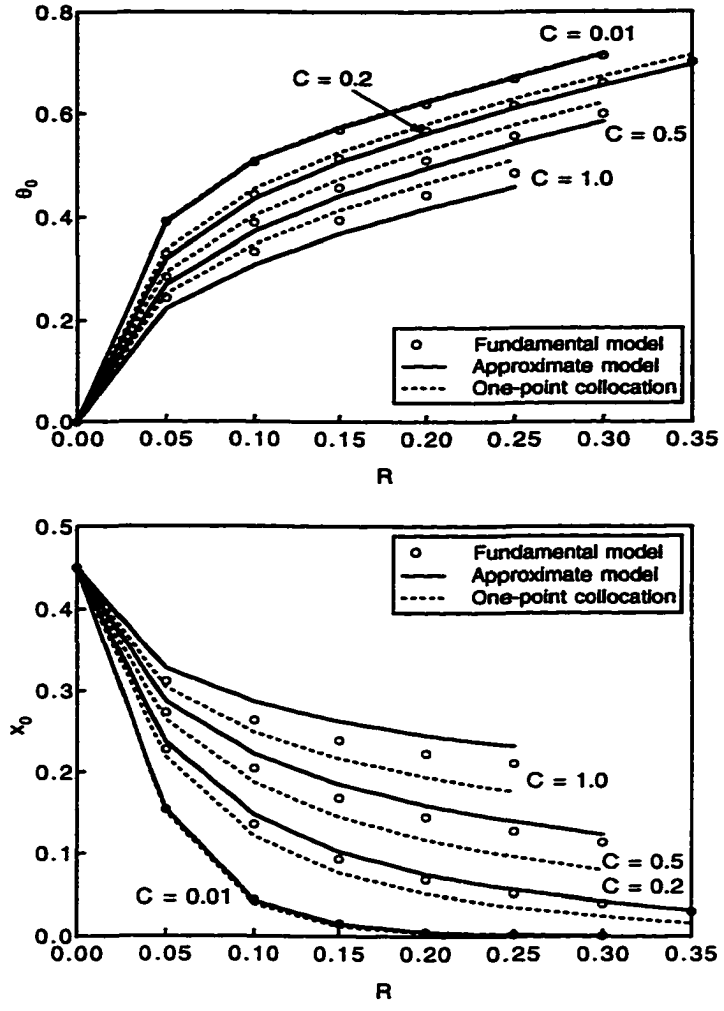

Figure 2.9: Comparison of the approximate model and one-point collocation for different values of the dimensionless constant C.

and permeation factor. Both approximate models yield good predictions, but the proposed model is slightly more accurate (maximum θ_0 error 1.5% for the proposed model and 2.2% for one-point collocation). The effect of the parameters C and R on the effluent stream properties is shown in Figure 2.9. While both models yield satisfactory results for small values of C, the proposed model is more accurate for large C values. In this case, more interior collocation points for N are required

for an accurate solution. It is important to note that the accuracy of the proposed model also can be improved by increasing the number of quadrature points M. Consequently, the proposed method is preferred since both models require the same computing effort.

2.4.3 Parameter Estimation

Finally, the effectiveness of the proposed parameter estimation strategy is investigated. As discussed previously, we assume that the membrane selectivity α is known. Two data sets are collected by utilizing the fundamental model as the actual permeator. The feed concentration x_f and effluent permeate pressure γ_0 are varied systematically, while the feed flow rate U_f and feed pressure P are held constant. This allows the unknown model parameters ($C = 0.1$, $R = 0.1$) to be estimated directly. In the second data set, we add a randomly distributed signal with standard deviation $\sigma = 0.01$ to the measurements to simulate the effects of noise.

Table 2.2 shows the result of parameter estimation for nine independent sets of data without noise. The left-hand side of the table contains the measurements, while the right-hand side shows the estimated permeate stream properties obtained with the estimated parameters listed at the bottom of the table. The parameter R is identified almost perfectly, while $\hat{C}$ has an error of 10%. However, this discrepancy has very little effect on prediction accuracy. Parameter estimation for nine sets of data with noise is shown in Table 2.3, where the true values of the measured

Table 2.2: Parameter estimation using 9 data sets without noise.

No.	Measurements				Estimates	
	x_f	γ_0	θ_0	y_0	θ_0	y_0
1	0.2000	0.0500	0.2403	0.6470	0.2391	0.6457
2	0.2000	0.1000	0.2230	0.6313	0.2225	0.6305
3	0.2000	0.2000	0.1771	0.5755	0.1771	0.5751
4	0.4000	0.0500	0.4223	0.8201	0.4218	0.8191
5	0.4000	0.1000	0.4059	0.8182	0.4057	0.8174
6	0.4000	0.2000	0.3526	0.8076	0.3525	0.8073
7	0.6000	0.0500	0.6270	0.8939	0.6311	0.8909
8	0.6000	0.1000	0.6151	0.8952	0.6190	0.8926
9	0.6000	0.2000	0.5722	0.8974	0.5745	0.8962
$\hat{C} = 0.0897, \hat{R} = 0.1001$						

Table 2.3: Parameter estimation using 9 data sets with noise.

No.	Measurements				Estimates	
	x_f	γ_0	θ_0	y_0	θ_0	y_0
1	0.2070	0.0556	0.2467	0.6474	0.2408	0.6666
2	0.1995	0.0987	0.2317	0.6065	0.2184	0.6414
3	0.2202	0.2055	0.1947	0.5871	0.1832	0.6153
4	0.4092	0.0390	0.4191	0.8099	0.4319	0.8314
5	0.3819	0.0927	0.4045	0.8297	0.3879	0.8154
6	0.4003	0.2140	0.3587	0.7998	0.3377	0.8118
7	0.5819	0.0438	0.6368	0.9003	0.6113	0.8911
8	0.6103	0.1024	0.6040	0.9034	0.6278	0.8999
9	0.6039	0.1841	0.5667	0.8957	0.5834	0.9015
$\hat{C} = 0.0704, \hat{R} = 0.0948$						

Table 2.4: Parameter estimation using experimental data [52].

No.	Measurements						Estimates	
	U_f(m^3/s)	P(MPa)	x_f	γ_0	θ_0	y_0	θ_0	y_0
1	0.0331	3.7557	0.0523	0.0272	0.3762	0.1318	0.3780	0.1338
2	0.0318	2.3767	0.0528	0.0429	0.2887	0.1564	0.2527	0.1726
3	0.0331	3.8247	0.1161	0.0267	0.4059	0.2676	0.4420	0.2570
4	0.0466	3.2041	0.1213	0.0318	0.3310	0.3345	0.2958	0.3550
5	0.0695	4.8589	0.1234	0.0210	0.3538	0.3319	0.3098	0.3609
6	0.0692	3.9626	0.1241	0.0258	0.2796	0.3732	0.2629	0.3930
7	0.0370	3.2386	0.1272	0.0315	0.3628	0.3212	0.3619	0.3266
8	0.0774	4.8589	0.1298	0.0210	0.3051	0.3766	0.2911	0.3927
9	0.0672	3.8936	0.1339	0.0262	0.2537	0.4081	0.2728	0.4114
10	0.0367	3.8936	0.2134	0.0262	0.5000	0.4115	0.5029	0.4164
$\hat{C}' = 2.08\text{x}10^{13}$ Pa^2·s/m^3, $\hat{R}' = 3.19\text{x}10^{-9}$ m^3/Pa·s								

variables are the same as in Table 2.2. The estimates $\hat{C}$ and $\hat{R}$ have errors of approximately 30% and 5%, respectively, and therefore the model predictions are slightly less accurate than in the noise-free case.

Table 2.4 shows the results of parameter estimation using ten experimental data sets from [52]. Binary CO_2/CH_4 data are generated from the original multicomponent data by considering the additional components (N_2 and hydrocarbons) as the slower permeating component (CH_4). Because the feed flow rate U_f and feed pressure P vary, it is necessary to estimate the parameters C' and R' rather than the dimensionless parameters. Note that the predictions are much less accurate than those obtained from the simulation data. This is expected since the experimental system has complications that are not present in simulation:

1. The separation is multicomponent.

2. There are differences in operating conditions that are not completely reflected in the experimental data sets (*e.g.* temperature variations).

3. The approximate model does not account for non-ideal effects such as concentration polarization, flow channeling, CO_2 plasticization, etc.

Nevertheless, predictions suitably accurate for preliminary process design are obtained by systematic estimation of the unknown model parameters.

2.5 Summary and Conclusions

An approximate modeling technique for spiral-wound permeators separating binary gas mixtures has been proposed and evaluated. The approach is based on the assumption that the residue flow rate is constant in the direction of permeate flow. The approximate model is derived by applying this assumption to an accepted fundamental model [57]. The original boundary value problem is reduced to a more tractable problem involving a small number of nonlinear algebraic equations. Additional justification for the modeling technique is obtained via comparison to one-point collocation. Because the approximate model may contain unknown/uncertain parameters, a nonlinear programming strategy for estimating parameters from experimental data has been proposed. A case study of CO_2/CH_4 separations has shown that the proposed model yields accurate predictions with considerably less computing time than the fundamental model.

Chapter 3

Spiral-Wound Permeator Modeling for Multicomponent Gas Separations

3.1 Introduction

The development of multicomponent permeator models is of considerable significance since most industrial applications involve multicomponent separations. As mentioned in Chapter 1, it appears that multicomponent models of spiral-wound permeators with permeate-side pressure drop are not available in the open literature. Motivated by this fact, two multicomponent models for spiral-wound gas permeators are proposed in this chapter. The *basic transport model* is derived directly from material balances and permeation relations assuming cross-flow patterns for bulk flow and local permeation. Permeate-side pressure variations are described by Darcy's law. As compared to the binary case, the principal difficulty is that the multicomponent model does not yield an explicit expression for the local feed-side flow rate. We show that the local feed-side flow rate and the local feed-side compositions can be calculated for a given permeate-side pressure distribution by solving an initial value problem. The basic transport equations then are solved via an iterative shooting method. The *approximate model* is derived directly from the basic transport model by assuming that the residue flow rate is constant along the

direction of bulk permeate flow. Integral expressions are approximated via Gaussian quadrature, and the feed-side flow rate and compositions are determined by solving the associated initial value problem using a fourth-order Runge-Kutta-Gill algorithm. The basic and approximate models are compared for gas separations involving four and eight components. We show that the approximate model provides very close agreement while requiring significantly less computing effort. An estimation technique for determining uncertain/unknown model parameters from experimental data is proposed and applied to CO_2/CH_4 mixtures containing small amounts of N_2 and other hydrocarbons.

3.2 Basic Transport Model

The development of the basic transport model is based on Figure 3.1, which illustrates the feed and permeate flows in an extended membrane leaf. The variables are defined in Appendix B. The feed stream is introduced on the outside of the leaf, and gas permeates through the two membranes into the spacing material. The more permeable components preferentially diffuse through the membranes in a cross-flow pattern, and the bulk permeate stream flows at a right-angle with respect to the feed stream (*i.e.* the l-direction shown in Figure 3.1). The feed-side gas that does not permeate is collected as the residue stream.

The main assumptions are similar to those used in the binary case [57]:

1. Local permeation and bulk permeate flow are described by a cross-flow pattern.

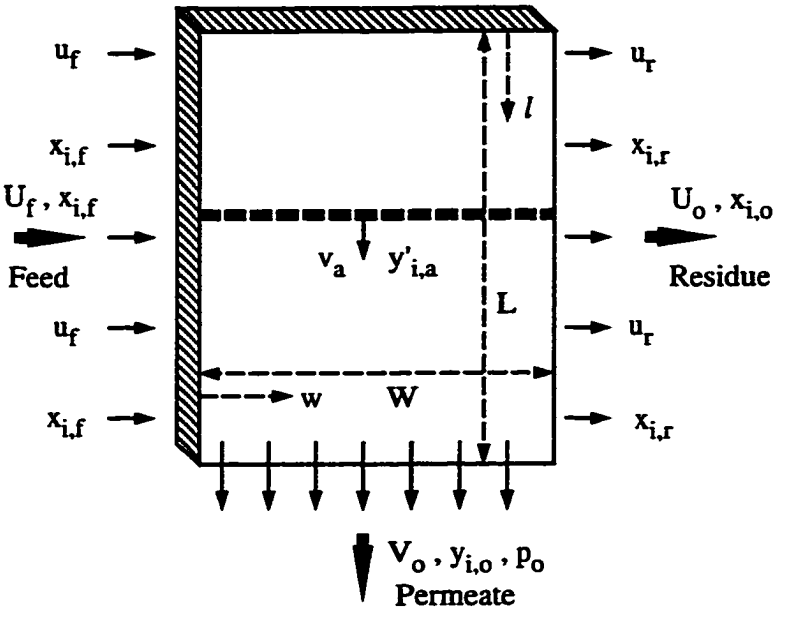

Figure 3.1: Multicomponent gas permeation through a spiral-wound membrane.

2. The feed-side pressure drop is negligible. This is a reasonable assumption for sufficiently low feed flow rates and/or short membrane leaf widths.

3. The porous supporting layer of the asymmetric membrane offers negligible resistance to gas flow.

4. There is no permeate mixing in the direction of bulk permeate flow.

5. The bulk permeate stream is accumulated by mixing the local permeate stream with the bulk permeate stream.

6. The permeate pressure varies only in the direction of permeate flow and the variations are described by Darcy's law [12].

7. The membrane selectivities are independent of pressure and concentration.

3.2.1 Model Derivation

Under the preceding assumptions, the transport equations for a multicomponent spiral-wound permeator are as follows [57, 59]:

- permeation

$$\left[\frac{\partial(ux_i)}{\partial w}\right]_l = -2\left(\frac{Q_i}{d}\right)(Px_i - py_i'), \quad i = 1, \ldots, n \tag{3.1}$$

$$\left[\frac{\partial(ux_i)}{\partial u}\right]_l = y_i', \quad i = 1, \ldots, n \tag{3.2}$$

- permeate pressure

$$\frac{dp^2}{dl} = -\frac{2R_gT\mu V}{Wd_mB} \tag{3.3}$$

- material balance

$$\frac{dV}{dl} = u_f - u_r \tag{3.4}$$

$$\frac{d(Vy_i)}{dl} = u_f x_{i,f} - u_r x_{i,r} \quad i = 2, \ldots, n \tag{3.5}$$

- composition sums

$$\sum_{i=1}^{n} x_i = 1, \quad \sum_{i=1}^{n} y_i = 1, \quad \sum_{i=1}^{n} y_i' = 1 \tag{3.6}$$

The variables are defined in Appendix B. Although only $n-1$ equations in (3.1) and (3.2) are independent, we list all the equations to facilitate the subsequent development. Equations (3.1)–(3.5) can be rewritten in the following dimensionless

form:

$$\left[\frac{\partial(\phi x_i)}{\partial r}\right]_h = -\alpha_i(x_i - \gamma y_i'), \quad i = 1, \ldots, n \tag{3.7}$$

$$\left[\frac{\partial(\phi x_i)}{\partial \phi}\right]_h = y_i', \quad i = 1, \ldots, n \tag{3.8}$$

$$\frac{d\gamma^2}{dh} = -C\theta \tag{3.9}$$

$$\frac{d\theta}{dh} = 1 - \phi_r \tag{3.10}$$

$$\frac{d(\theta y_i)}{dh} = x_{i,f} - \phi_r x_{i,r} \quad i = 2, \ldots, n \tag{3.11}$$

where:

$$r = \left(\frac{2Q_b P}{d \cdot u_f}\right) w \tag{3.12}$$

$$C = \frac{2R_g T \mu L^2 u_f}{W d_m B P^2} = \frac{2R_g T \mu L U_f}{W d_m B P^2} \tag{3.13}$$

The subscript b represents the base component to which the selectivities α_i are referred (*i.e.* $\alpha_b = 1$). The base component can be any component for which $Q_b \neq 0$.

Equation (3.8) may be written as:

$$\left[\frac{\partial(\ln\phi)}{\partial x_i}\right]_h = \frac{1}{y_i' - x_i}, \quad i = 1, \ldots, n \tag{3.14}$$

Dividing (3.7) by (3.8) yields:

$$\left[\frac{\partial \phi}{\partial r}\right]_h = -\frac{x_i - \gamma y_i'}{y_i'/\alpha_i}, \quad i = 1, \ldots, n \tag{3.15}$$

Using (3.6), the right-hand side of (3.15) can be summed from $i = 1$ to n without changing the ratio value, which yields:

$$\frac{x_i - \gamma y_i'}{y_i'/\alpha_i} = \frac{1-\gamma}{\bar{y}'} \tag{3.16}$$

where:

$$\bar{y}' = \sum_{i=1}^{n} \frac{y_i'}{\alpha_i} \tag{3.17}$$

Therefore:

$$\left[\frac{\partial \phi}{\partial r}\right]_h = -\frac{1-\gamma}{\bar{y}'} \tag{3.18}$$

The following relations between the feed-side and permeate-side compositions are obtained from (3.16):

$$x_i = \gamma y_i' + \frac{(1-\gamma)y_i'}{\alpha_i \bar{y}'} \tag{3.19}$$

$$y_i' = \frac{\alpha_i x_i \bar{y}'}{1 - \gamma + \gamma \alpha_i \bar{y}'} \tag{3.20}$$

$$\sum_{i=1}^{n} \frac{\alpha_i x_i \bar{y}'}{1 - \gamma + \gamma \alpha_i \bar{y}'} = 1 \tag{3.21}$$

Note that the dimensionless permeate pressure γ only is a function of h from Assumption 6; thus (3.19)–(3.21) relate x_i, y_i', and $\bar{y}'$ at a constant value of h. Therefore substituting (3.19) into (3.14) yields the following relations at constant h (or γ):

$$d(\ln\phi) = \frac{1 + \gamma(\alpha_i \bar{y}' - 1)}{(1-\gamma)(\alpha_i \bar{y}' - 1)} \frac{dy_i'}{y_i'} - \frac{d\bar{y}'}{(\alpha_i \bar{y}' - 1)\bar{y}'}, \quad i = 1, \cdots, n \tag{3.22}$$

Equations (3.19)–(3.22) are similar to expressions derived by Pan [58] in modeling multicomponent hollow-fiber permeators. However, Pan's model contains differential equations with several independent variables. As a result, the model is difficult to solve. Below we reformulate the model equations to facilitate numerical solution by allowing $\bar{y}'$ to be the only independent variable.

Rearranging (3.22) to express dy_i' in terms of $d(\ln\phi)$ and $d\bar{y}'$, and then taking the sum from $i = 1$ to n noting that $\sum_1^n dy_i' = 0$, yields an expression for $d(\ln\phi)$ in terms of $d\bar{y}'$:

$$\frac{d(\ln\phi)}{d\bar{y}'} = -\frac{\sum_1^n A_j y_j'}{\sum_1^n B_j y_j'} \tag{3.23}$$

where:

$$A_j = \frac{1-\gamma}{(1-\gamma+\gamma\alpha_j\bar{y}')\bar{y}'} \tag{3.24}$$

$$B_j = \frac{(1-\gamma)(\alpha_j\bar{y}'-1)}{1-\gamma+\gamma\alpha_j\bar{y}'} \tag{3.25}$$

Substituting $d(\ln\phi)$ from (3.23) into (3.22) and choosing $n-1$ independent equations yields dy_i' in terms of $d\bar{y}'$:

$$\frac{dy_i'}{d\bar{y}'} = y_i'\left(A_i - \frac{B_i\sum_1^n A_j y_j'}{\sum_1^n B_j y_j'}\right) \quad i = 2, \cdots, n \tag{3.26}$$

At constant γ, solving (3.23) and (3.26) simultaneously and then using (3.6) to determine the composition of the first component yield functions $\phi(\bar{y}')$ and $y_i'(\bar{y}')$.

Integrating (3.18) at constant γ with the boundary conditions:

$$w = 0, \quad r = 0, \quad \phi = \phi_f = 1, \quad \bar{y}' = \bar{y}'_f$$

$$w = W, \quad r = R, \quad \phi = \phi_r \quad \bar{y}' = \bar{y}'_r$$

yields:

$$\begin{aligned} R &= -\frac{1}{1-\gamma}\int_1^{\phi_r} \bar{y}' d\phi \\ &= \frac{1}{1-\gamma}\left(\bar{y}'_f - \phi_r \bar{y}'_r + \int_{\bar{y}'_f}^{\bar{y}'_r} \phi d\bar{y}'\right) \end{aligned} \tag{3.27}$$

where R is the the dimensionless permeation factor:

$$R = \frac{2Q_b WP}{d \cdot u_f} = \frac{2Q_b LWP}{d \cdot U_f} \tag{3.28}$$

Equations (3.9)–(3.11), (3.19)–(3.21), (3.23), (3.26), and (3.27) represent the multicomponent transport model for the spiral-wound permeator.

3.2.2 Calculation Procedure

The multicomponent model can be solved via an iterative shooting method. As compared to the binary case discussed by Pan [57], the major difficulty in solving the multicomponent model is that an explicit expression for the dimensionless residue flow rate ϕ_r is not available. Consequently for each step in integrating the differential equations (3.10)–(3.11), the initial-value differential equations (3.23) and (3.26) and

the nonlinear algebraic equation (3.27) must be solved to obtain $\phi_r(h)$ and $x_{i,r}(h)$. As shown below, this makes the calculation procedure very complicated and time consuming.

For a spiral-wound permeator with specified separation properties (α_i, R, and C), outlet pressure ratio (γ_0), and feed composition ($x_{i,f}$), the iterative solution procedure may be outlined as follows:

1. Calculation of ϕ_r and $x_{i,r}$ for a given value of γ.

   (a) For a given $x_{i,f}$, solve (3.21) for $\bar{y}'_f$ and use (3.20) to calculate $y'_{i,f}$.

   (b) Solve (3.23), (3.26), and (3.27) simultaneously with initial conditions $\bar{y}' = \bar{y}'_f$, $y'_i = y'_{i,f}$, and $\phi = \phi_f = 1$ to obtain $\bar{y}'_r$, $y'_{i,r}$, and ϕ_r, and then calculate $x_{i,r}$ using (3.19).

2. Shooting method to solve the differential equations (3.9)–(3.11).

   (a) Initially assume that γ is equal to γ_0 for all h.

   (b) Using this γ–h relation and the calculation procedure in step 1, integrate (3.10) and (3.11) from $h = 0$ (where $\theta = \theta y_i = 0$) to $h = 1$ to obtain θ–h and y_i–h relations, and then evaluate the relations at $h = 1$ to obtain θ_0 and $y_{i,0}$.

   (c) Utilizing the θ–h relation obtained in step 2(b), integrate (3.9) from $h = 1$ (where $\gamma = \gamma_0$) to $h = 0$ to obtain a new γ–h relation.

(d) Repeat steps 2(b) and 2(c) until θ_0 converges to the desired accuracy. The outlet residue stream flow rate and concentrations are calculated by overall material balance.

3.3 Approximate Model

3.3.1 Model Development

As in the binary case shown in Chapter 2, the approximate model is developed by assuming that the residue flow rate ϕ_r is constant with respect to h in order to develop an approximate pressure distribution function $\gamma(h)$. It is important to note that ϕ_r is allowed to vary with h in the subsequent model development. Under this assumption, the differential equation (3.10) for the dimensionless permeate flow rate is easily integrated with boundary condition $\theta(0) = 0$:

$$\theta = (1 - \phi_r)\, h \tag{3.29}$$

In Section 3.4 we show this assumption is valid for a wide range of operating conditions by demonstrating that ϕ_r exhibits a very weak dependence on h, while θ effectively is a linear function of h. Substitution of (3.29) into (3.9) and integration with the boundary condition $\gamma(1) = \gamma_0$ yields the approximate pressure distribution function:

$$\gamma^2 = \gamma_0^2 + \frac{1}{2} C\,(1 - \phi_r)\,(1 - h^2) \tag{3.30}$$

The subsequent model development is based on this γ–h relation.

The integral in (3.27) is approximated using Gaussian quadrature [66]:

$$I \equiv \int_{\bar{y}'_f}^{\bar{y}'_r} \phi d\bar{y}' \cong (\bar{y}'_r - \bar{y}'_f) \sum_{j=1}^{N} \phi_j w_j \tag{3.31}$$

where:

$$\bar{y}'_j = \bar{y}'_f + \xi_j(\bar{y}'_r - \bar{y}'_f) \tag{3.32}$$

Here N is the number of quadrature points, ξ_j and w_j are the quadrature points and quadrature weights, respectively, and ϕ_j is the feed-side flow rate at the quadrature point $\bar{y}'_j$. Now the integral equation (3.27) can be represented as:

$$R = \frac{1}{1-\gamma}\left(\bar{y}'_f - \phi_r \bar{y}'_r + (\bar{y}'_r - \bar{y}'_f)\sum_{j=1}^{N} \phi_j w_j\right) \tag{3.33}$$

The flow rates ϕ_j and ϕ_r are obtained by integrating the initial-value differential equations (3.23) and (3.26). Numerical solutions are obtained by using a fourth-order Runge-Kutta-Gill approximation at each quadrature point $\bar{y}'_j$ and the outlet point $\bar{y}'_r$. The resulting expressions are [66]:

$$Y_j = Y_{j-1} + \frac{1}{6}(K_1 + K_4) + \frac{1}{3}(\lambda_2 K_2 + \lambda_4 K_3) \tag{3.34}$$

$$K_1 = \delta_j \cdot F(\bar{y}'_{j-1},\ Y_{j-1}) \tag{3.35}$$

$$K_2 = \delta_j \cdot F(\bar{y}'_{j-1} + \frac{\delta_j}{2},\ Y_{j-1} + \frac{1}{2}K_1) \tag{3.36}$$

$$K_3 = \delta_j \cdot F(\bar{y}'_{j-1} + \frac{\delta_j}{2},\ Y_{j-1} + \lambda_1 K_1 + \lambda_2 K_2) \tag{3.37}$$

$$K_4 = \delta_j \cdot F(\bar{y}'_{j-1} + \delta_j,\ Y_{j-1} + \lambda_3 K_2 + \lambda_4 K_3) \tag{3.38}$$

where:

$$Y_j = \left[\ln\phi_j,\ y'_{2,j},\ \cdots,\ y'_{n,j}\right]^T \tag{3.39}$$

$$F = [f_\phi,\ f_2,\ \cdots,\ f_n]^T \tag{3.40}$$

$$\delta_j = \bar{y}'_j - \bar{y}'_{j-1} \tag{3.41}$$

$$\lambda_1 = \frac{\sqrt{2}-1}{2}, \quad \lambda_2 = \frac{2-\sqrt{2}}{2}, \quad \lambda_3 = -\frac{\sqrt{2}}{2}, \quad \lambda_4 = \frac{2+\sqrt{2}}{2} \tag{3.42}$$

The functions $f_\phi,\ f_2,\ \cdots,\ f_n$ represent the right-hand sides of (3.23) and (3.26), and $y'_{i,j}$ represents the permeate concentration of the i-th component at the quadrature point $\bar{y}'_j$. The initial conditions are:

$$Y_0 = \left[0,\ y'_{2,f},\ \cdots,\ y'_{n,f}\right]^T \tag{3.43}$$

where $y'_{i,f}$ is determined from $\bar{y}'_f$ using (3.20). Equations (3.34)–(3.38) represent n nonlinear algebraic equations that must be solved simultaneously at each quadrature point and the outlet point to yield ϕ_j, $y'_{i,j}$, ϕ_r, and $y'_{i,r}$ for $i = 2, \cdots, n$. Note that (3.34)–(3.38) are solved for a given value of γ, and therefore $\bar{y}'$ is the only independent variable. When γ is taken as a variable, the resulting functions for ϕ_r, $y'_{i,r}$ and ϕ_j can be expressed as:

$$\phi_r = \Phi_1(\gamma,\ \bar{y}'_f,\ \bar{y}'_r) \tag{3.44}$$

$$y'_{i,r} = \Phi_i(\gamma,\ \bar{y}'_f,\ \bar{y}'_r), \quad i = 2, \cdots, n \tag{3.45}$$

$$\phi_j = \Phi'_j(\gamma,\ \bar{y}'_f,\ \bar{y}'_r), \quad j = 1, \cdots, N \tag{3.46}$$

Substitution of ϕ_j and ϕ_r into (3.33) yields the relation:

$$R = \Psi(\gamma,\ \vec{y}'_f,\ \vec{y}'_r) \tag{3.47}$$

Simultaneous solution of the nonlinear algebraic equations (3.21), (3.30), (3.44), and (3.47) at each quadrature point yields $\vec{y}'_f(h_k)$, $\gamma(h_k)$, $\phi_r(h_k)$, and $\vec{y}'_r(h_k)$, where h_k represents the value of h at the k-th quadrature point. Substitution of these variables into (3.45) yields $y'_{i,r}(h_k)$, which then is used to calculate $x_{i,r}(h_k)$ via (3.19).

As in the binary case, Gaussian quadrature is used to determine the effluent permeate flow rate and bulk concentration. From (3.10):

$$\theta_0 = 1 - \int_0^1 \phi_r dh \cong 1 - \sum_{k=1}^{M} \phi_r(h_k) w_k \tag{3.48}$$

where M is the number of quadrature points employed, w_k are the quadrature weights, and $\phi_r(h_k)$ is the value of ϕ_r at the k-th quadrature point. By performing a material balance on a differential length of membrane and invoking the assumption that ϕ_r does not vary with h, the permeate compositions are approximated as:

$$y_{i,0} = \int_0^1 y'_{i,a} dh \cong \sum_{k=1}^{M} y'_{i,a}(h_k) w_k, \qquad i = 2, \cdots, n \tag{3.49}$$

where:

$$y'_{i,a}(h_k) = \frac{x_{i,f} - x_{i,r}(h_k)\phi_r(h_k)}{1 - \phi_r(h_k)}, \qquad i = 2, \cdots, n \tag{3.50}$$

The bulk concentration for the first component is determined via (3.6). The flow rate η_0 and bulk concentration $x_{i,0}$ of the effluent residue stream are determined from an overall material balance about the permeator:

$$\eta_0 = 1 - \theta_0 \tag{3.51}$$

$$x_0 = \frac{x_{i,f} - \theta_0 y_{i,0}}{1 - \theta_0} \tag{3.52}$$

It will be shown that a single quadrature point ($M = 1$) provides a satisfactory solution for most operating conditions. In this case $h_1 = 0.5$ and $w_1 = 1$, and the quadrature formulas reduce to:

$$\theta_0 = 1 - \phi_r(h_1) \tag{3.53}$$

$$y_{i,0} = y'_{i,a}(h_1) = \frac{x_{i,f} - x_{i,r}(h_1)\phi_r(h_1)}{1 - \phi_r(h_1)} \tag{3.54}$$

3.3.2 Parameter Estimation

A potential drawback of the proposed modeling approach is that detailed characteristics of spiral-wound permeators often are not known at the preliminary design stage. Consequently, the approximate model may contain uncertain and/or unknown parameters. One way to address this problem is to use estimation techniques to determine the model parameters from experimental data. In Chapter 2, a nonlinear programming strategy to estimate C (3.13) and R (3.28) for binary systems was developed by noting that all unknown parameters in the approximate model

appear only via these two terms. Using the least square error between the measured and estimated variables as the objective function and all binary model equations as constraints, "optimal" parameters are determined by solving a minimization problem. A similar technique also could be developed for multicomponent systems by using the multicomponent model equations as constraints. Potential difficulties in using the multicomponent model for parameter estimation include: (*i*) the permeate concentrations for the least permeable components normally are very small; and (*ii*) the multicomponent model is considerably more complicated than the binary model. As a result, parameter estimation could be less reliable and less efficient than in the binary case.

A simplified method of parameter estimation for multicomponent systems may be developed by using the approximate binary model. Similar to multicomponent distillation [41], we divide the different components into five groups according to their relative permeabilities. The most important two components are denoted as the light key component (LK) and heavy key component (HK). Components more permeable than the LK are called light components (L), while components less permeable than the HK are called heavy components (H). Components between the two key components are called intermediate components (I). A *sharp cut* is defined as a separation in which there are no heavy components in permeate stream and no light components in residue stream. By assuming a sharp cut, an analogous binary system may be constructed under the following conditions:

1. There are no light components or the concentrations of the light components are sufficiently small.

2. There are no intermediate components or the concentrations of the intermediate components are sufficiently small.

Under these conditions, we formulate a binary model by defining a relative flow rate, a relative pressure, and relative concentrations:

$$U_f^b = U_f(x_{f,LK} + x_{f,HK}) \tag{3.55}$$

$$P^b = P(x_{f,LK} + x_{f,HK}) \tag{3.56}$$

$$x_0^b = \frac{x_{f,LK}}{x_{f,LK} + x_{f,HK}} \tag{3.57}$$

$$\gamma_0^b = \frac{p_0}{P^b} = \frac{\gamma_0}{x_{f,LK} + x_{f,HK}} \tag{3.58}$$

$$\theta_0^b = \frac{V_0}{U_f^b} = \frac{\theta_0}{x_{f,LK} + x_{f,HK}} \tag{3.59}$$

$$y_0^b = \frac{y_{0,LK}}{y_{0,LK} + y_{0,HK}} \tag{3.60}$$

Because the parameters C and R depend on the feed flow rate (U_f) and the feed pressure (P), we define two parameters C' and R' that do not vary with the operating conditions:

$$C' = \frac{2R_g T \mu L}{W d_m B} \tag{3.61}$$

$$R' = \frac{2Q_b LW}{d} \tag{3.62}$$

From (3.13) and (3.28):

$$C = C' \frac{U_f}{P^2} \tag{3.63}$$

$$R = R' \frac{P}{U_f} \tag{3.64}$$

In this way, the multicomponent estimation problem is reduced to estimating the parameters C' and R' using the binary model and the binary variables. Detailed formulation of the estimation problem is described in Chapter 2.

3.4 Case Studies

We compare the basic transport model and the approximate model for the separation of gas mixtures containing four and eight components. The four component example involves CO_2 separation from a hydrocarbon mixture containing CH_4, C_2H_6, and C_3H_8 [58]. The eight component example does not represent any specific gas separation system, but it does demonstrate the potential for modeling mixtures with a large number of components. The proposed models are evaluated for a wide range of model parameters and operating conditions. In addition, the parameter estimation technique is applied to experimental data for the separation of CO_2/CH_4 mixtures containing small amounts of N_2 and other hydrocarbons [52].

For binary mixtures, the multicomponent models yield the same results as the binary models in Chapter 2. The models differ only because an explicit expression for the feed-side flow rate cannot be derived in the multicomponent case. In this

Table 3.1: Nominal operating conditions for four component system.

Parameter	Value	Variable	BTM Value	APM Value
$x_{i,f}$	0.30	$x_{i,0}$	0.0808	0.0862
	0.55		0.7067	0.7027
	0.10		0.1405	0.1395
	0.05		0.0720	0.0715
α_i	30	$y_{i,0}$	0.7880	0.7845
	1		0.2011	0.2038
	0.25		0.0099	0.0104
	0.05		0.0010	0.0013
γ_0	0.05	η_0	0.6900	0.6939
C	0.1	θ_0	0.3100	0.3061
R	0.1	BTM – Basic transport model		
		APM – Approximate permeator model		

sense, the multicomponent models can be regarded as generalizations of the binary models. Therefore, results for binary mixtures are not shown here.

3.4.1 Four Component System

The basic transport model and the approximate model are compared in Figures 3.2–3.9. Table 3.1 contains the parameter values not shown explicitly in each figure. The operating conditions are based on data from Pan [58] for CO_2 separation from hydrocarbon mixtures containing CH_4, C_2H_6, and C_3H_8. The values of C and R are obtained from our previous study of binary separations (see Chapter 2). The approximate model is solved using three quadrature points for the integral (3.31) and one quadrature point for integrals (3.48) and (3.49) (*i.e.* $N = 3$, $M = 1$). The second component CH_4 is chosen as the base component for calculating the

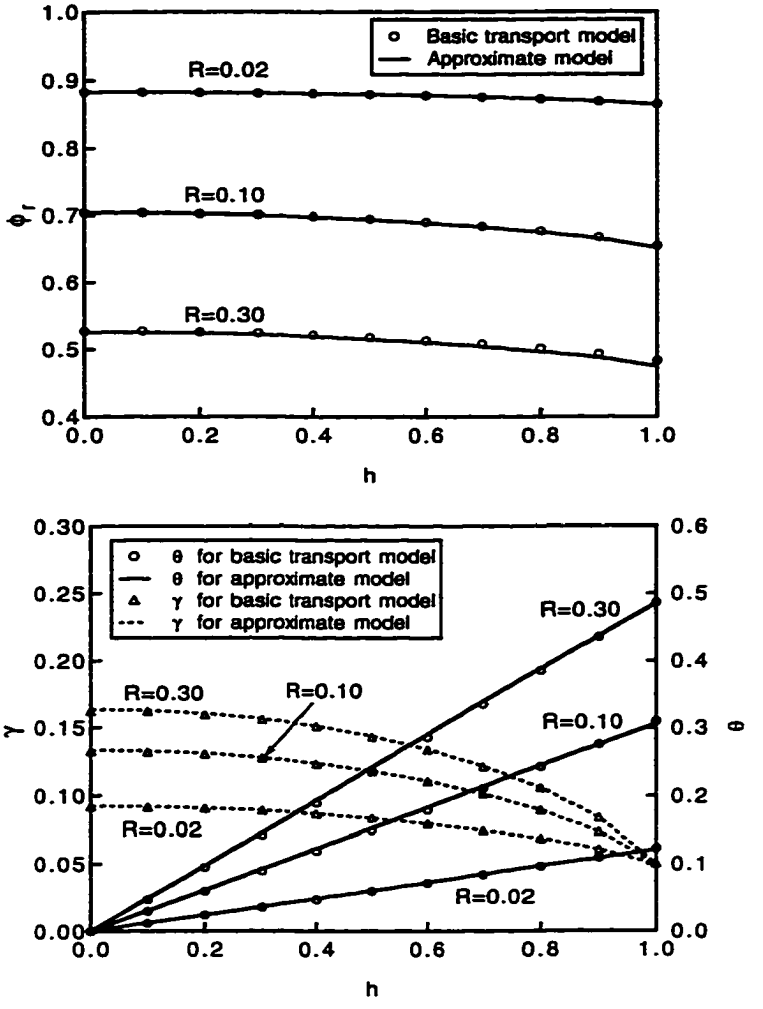

Figure 3.2: Variations of residue flow rate, permeate pressure, and permeate flow rate along the membrane length.

selectivities α_i. Note that any component can be chosen as the base component, but the value of the permeation factor R is determined by the permeability of the selected component.

Figure 3.2 shows the residue flow rate ϕ_r, permeate flow rate θ, and permeate-side pressure γ as a function of the membrane length h for three values of the permeation factor R. As assumed in the development of the approximate model, ϕ_r

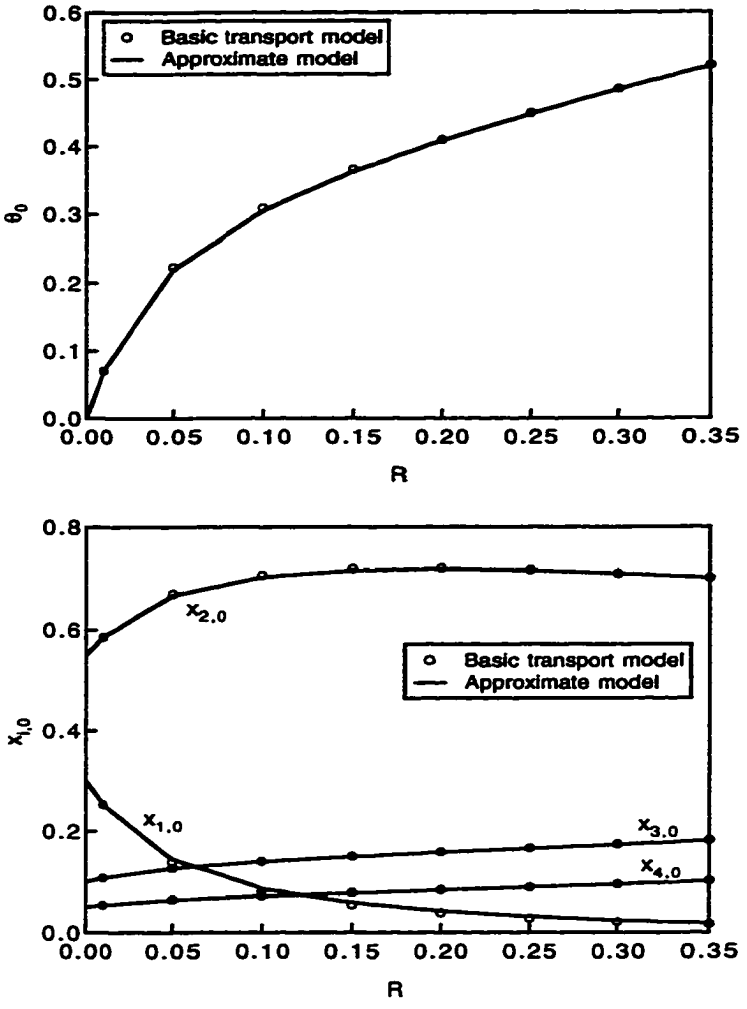

Figure 3.3: Effect of permeation factor on permeate flow rate and residue concentrations (four component system).

is a weak function of h and θ exhibits a linear dependence on h. The approximate model produces very accurate predictions of the three variables for each value of R. Figure 3.3 illustrates the effect of R on the outlet permeate flow rate θ_0 and the outlet residue concentration $x_{i,0}$ for all four components. The two models yield almost identical predictions for all values of R. Note that as R increases, the residue concentration of the most permeable component ($x_{1,0}$) decreases, the concentration

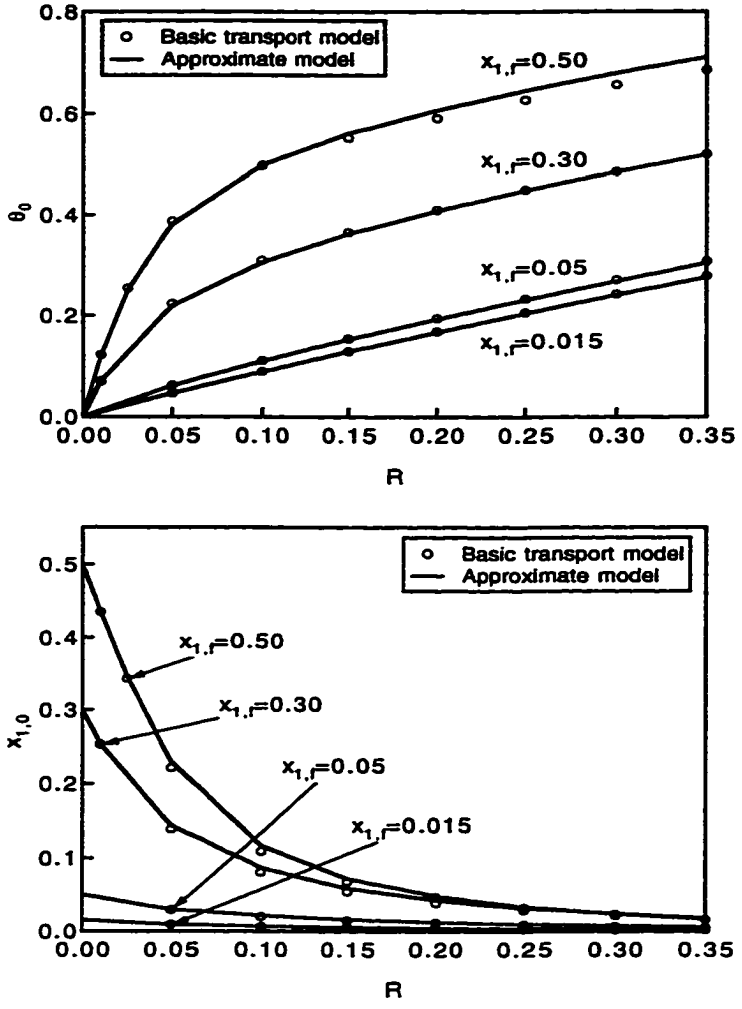

Figure 3.4: Effect of feed composition on permeate flow rate and residue concentration of the first component (four component system).

of the moderately permeable component ($x_{2,0}$) exhibits a maximum, and the concentrations of the least permeable components ($x_{3,0}$ and $x_{4,0}$) increase.

The permeate flow rate θ_0 and the residue concentration of the first component $x_{1,0}$ for various combinations of R and the feed concentrations $x_{i,f}$ are shown in Figure 3.4. The feed concentrations of components 1 and 2 are changed to keep the sum of the mole fraction unity, while the concentrations of components 3 and 4 are

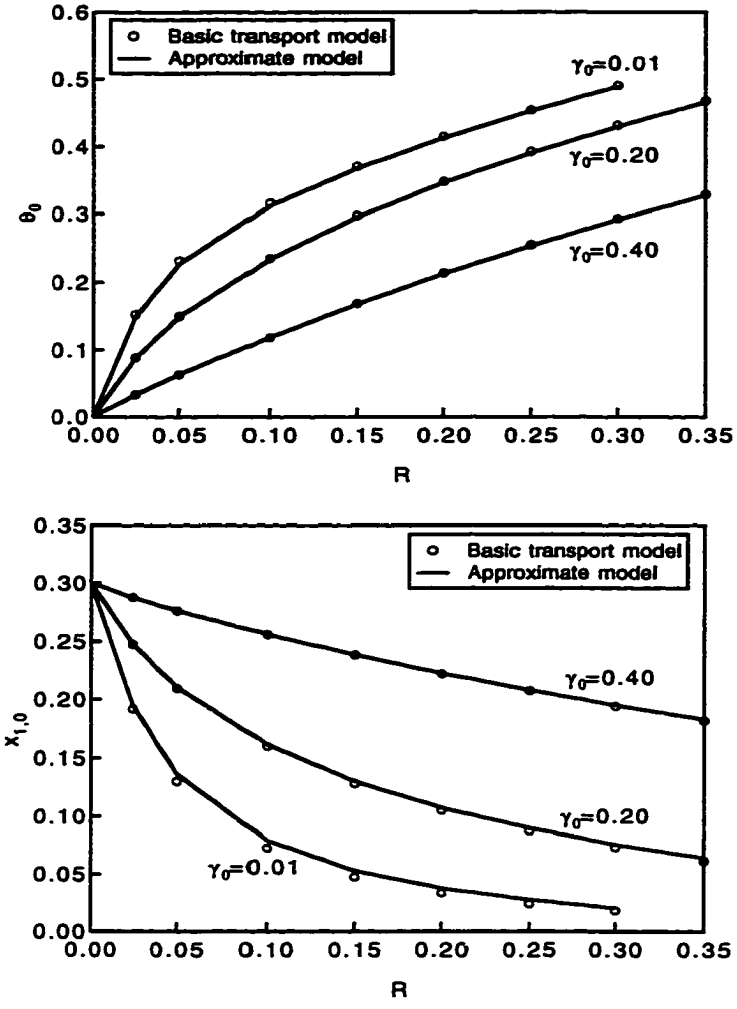

Figure 3.5: Effect of permeate pressure on permeate flow rate and residue concentration of the first component (four component system).

the same as shown in Table 3.1. The predictions of θ_0 and $x_{1,0}$ obtained from the approximate model are very accurate except for small deviations at large values of $x_{1,f}$ and R. Figure 3.5 shows the effect of R and the outlet permeate pressure γ_0 on θ_0 and $x_{1,0}$. The two models show very close agreement for all operating conditions considered. The effect of R and the selectivity on θ_0 and $x_{1,0}$ is illustrated in Figure 3.6. The selectivity of the first component α_1 is changed, while the selectivities of

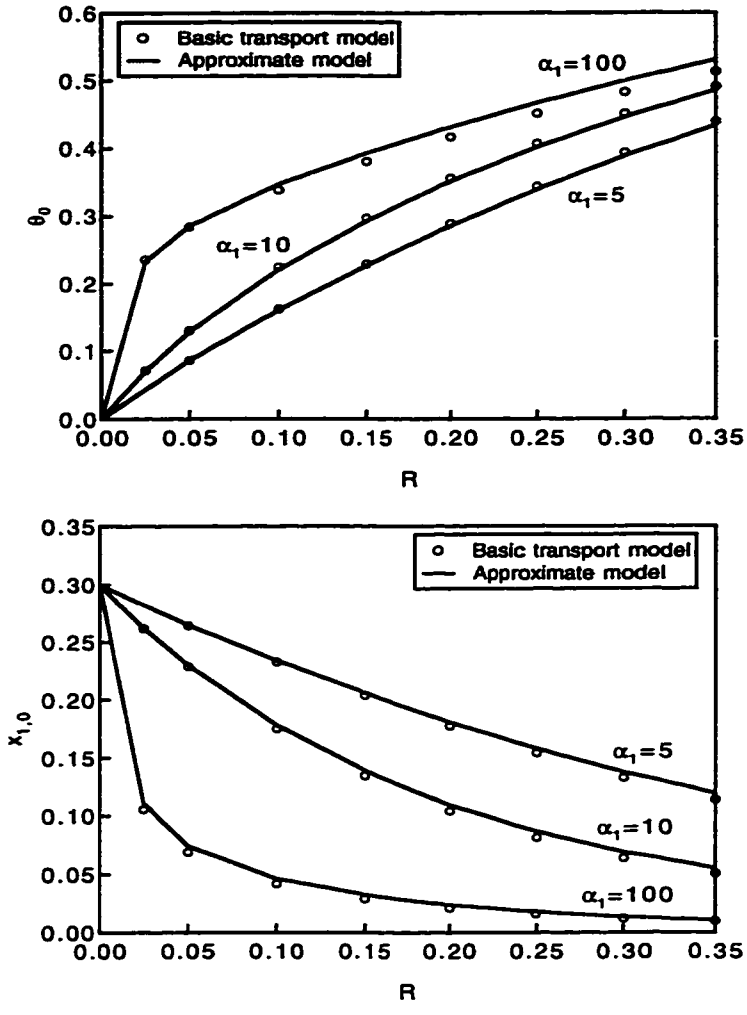

Figure 3.6: Effect of selectivity on permeate flow rate and residue concentration of the first component (four component system).

the other components remain constant. The predictions of the approximate model are very accurate for most conditions, although small deviations in θ_0 are observed for large values of R and α_1. Figure 3.7 shows the effect of R and the parameter C on θ_0 and $x_{1,0}$. The approximate model produces accurate predictions for low values of C, but deviations are observed as C is increased. This is expected as

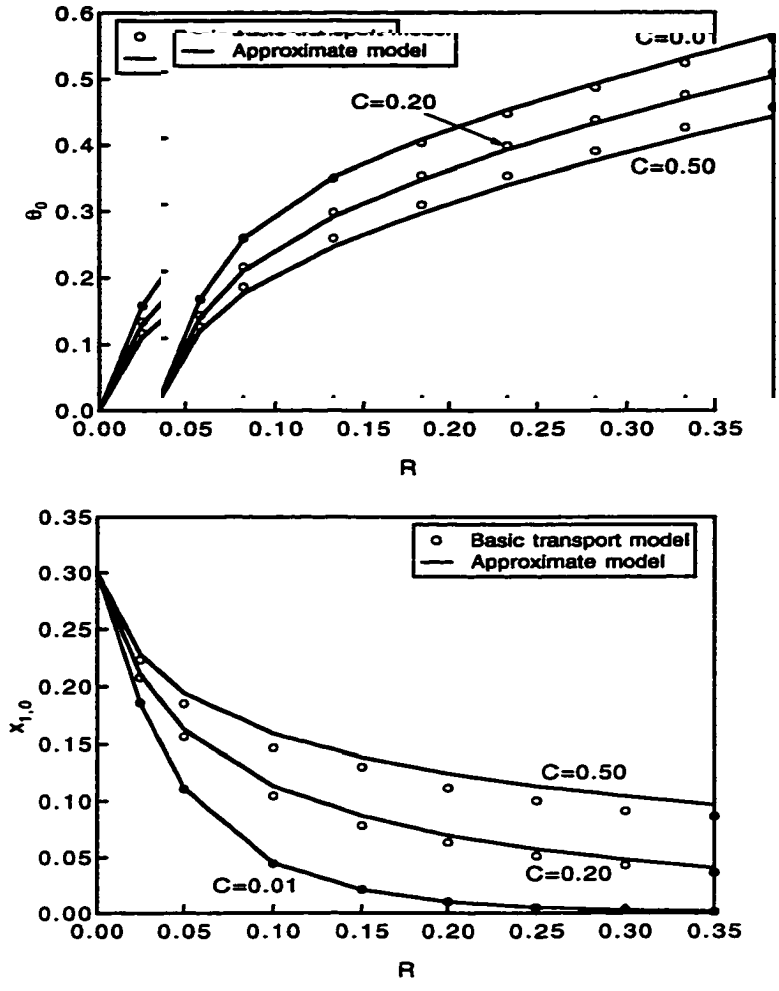

Figure 3.7: Effect of dimensionless constant C on permeate flow rate and residue concentration of the first component (four component system).

the approximate pressure distribution function (3.30) becomes less accurate as C increases.

The results in Figures 3.6 and 3.7 show that the approximate model becomes less accurate for large values of α_1 and C. The accuracy of the approximate model can be improved by increasing the numbers of quadrature points used to approximate integrals in the basic transport model. Figure 3.8 shows the improvement obtained

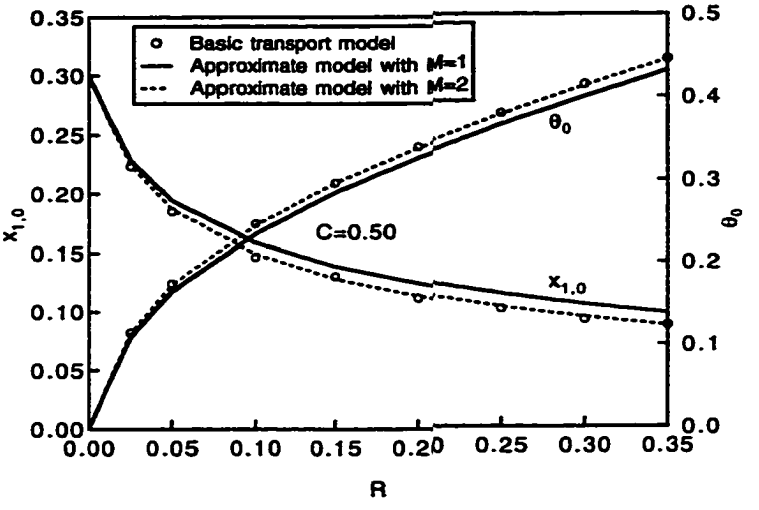

Figure 3.8: Accuracy improvement of the approximate model by increasing the number of quadrature points M.

when the number of quadrature points in (3.48) is changed from $M = 1$ to $M = 2$. The operating conditions are identical to those in Figure 3.8 for $C = 0.50$. The approximate model produces very accurate results when $M = 2$. Figure 3.9 shows the improvement obtained by increasing the number of quadrature points in (3.31) from $N = 3$ to $N = 4$. The operating conditions are the same as in Figure 3.6 for $\alpha_1 = 100$. In this case, we show predictions of the permeate concentration $y_{1,0}$ rather than $x_{1,0}$ because the differences are more pronounced. As expected, improved accuracy is obtained when $N = 4$. Accuracy of the approximate model also can be improved by adding some intermediate points between the N quadrature points when performing integration via the Runge-Kutta-Gill algorithm (3.34)–(3.38); this does not require N to be increased. Note that the computation time increases almost linearly with the increase in M, while increasing N has much less effect.

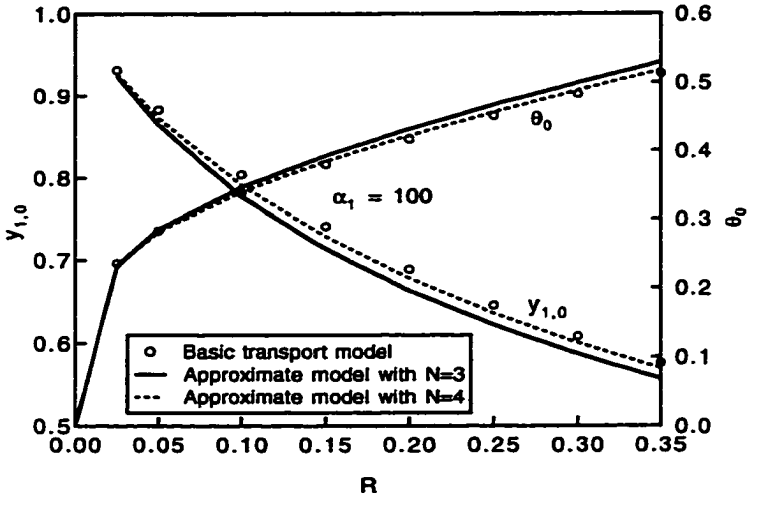

Figure 3.9: Accuracy improvement of the approximate model by increasing the number of quadrature points N.

The results in Figures 3.2–3.9 demonstrate that the approximate model provides very close agreement to the basic transport model for the four component system over a wide range of operating conditions. The major advantage of the approximate model is that the resulting nonlinear algebraic equations can be solved very efficiently with little effect on prediction accuracy. On the other hand, solution of the basic transport model is very computationally intensive as a result of the nonlinear differential-algebraic-integral equations, mixed boundary conditions, and implicit expression for the feed-side flow rate. Running MATLAB on an IBM RS-6000 workstation, the computing time for a single simulation is 1.2–3 seconds with the approximate model as compared to 6–20 minutes with the basic model. Thus, the approximate model can be solved 200–600 faster than the basic transport model for the cases in Figures 3.2–3.9. This represents a substantial reduction

Table 3.2: Nominal operating conditions for eight component system.

Parameter	Value	Variable	BTM Value	APM Value
$x_{i,f}$	0.20	$x_{i,0}$	0.0664	0.0697
	0.20		0.1259	0.1281
	0.20		0.1973	0.1974
	0.20		0.2750	0.2729
	0.05		0.0778	0.0771
	0.05		0.0830	0.0822
	0.05		0.0864	0.0855
	0.05		0.0882	0.0872
α_i	20	$y_{i,0}$	0.3724	0.3723
	10		0.2957	0.2951
	5		0.2035	0.2035
	2		0.1032	0.1036
	1		0.0141	0.0142
	0.5		0.0074	0.0074
	0.2		0.0030	0.0031
	0.05		0.0008	0.0008
γ_0	0.05	η_0	0.5634	0.5694
C	0.1	θ_0	0.4366	0.4306
R	0.1	BTM – Basic transport model		
		APM – Approximate permeator model		

in computing effort for the optimal design of complex permeator configurations, in which hundreds of model solutions may be required.

3.4.2 Eight Component System

Figures 3.10–3.12 compare the basic transport model and the approximate model for an eight component system. Operating conditions not shown explicitly in each figure are listed in Table 3.2. The fifth component is taken as the base component

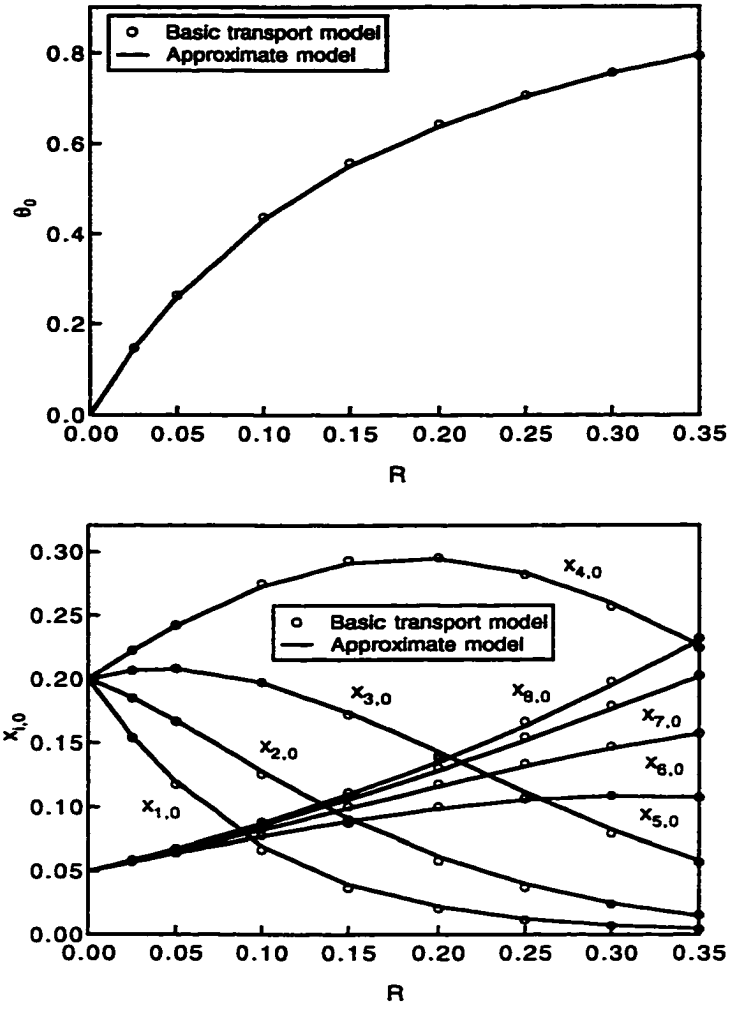

Figure 3.10: Effect of permeation factor on permeate flow rate and residue concentrations (eight component system).

for determining α_i and R. As in the four component case, Gaussian quadrature is performed with $M = 1$ and $N = 3$.

Figure 3.10 shows the outlet permeate flow rate θ_0 and the residue concentrations $x_{i,0}$ of all eight components as a function of the permeation factor R. The two models produce almost identical results for all values of R. The effect of R and γ_0 on θ_0 and $x_{1,0}$ is shown in Figure 3.11. The approximate model yields accurate predictions for

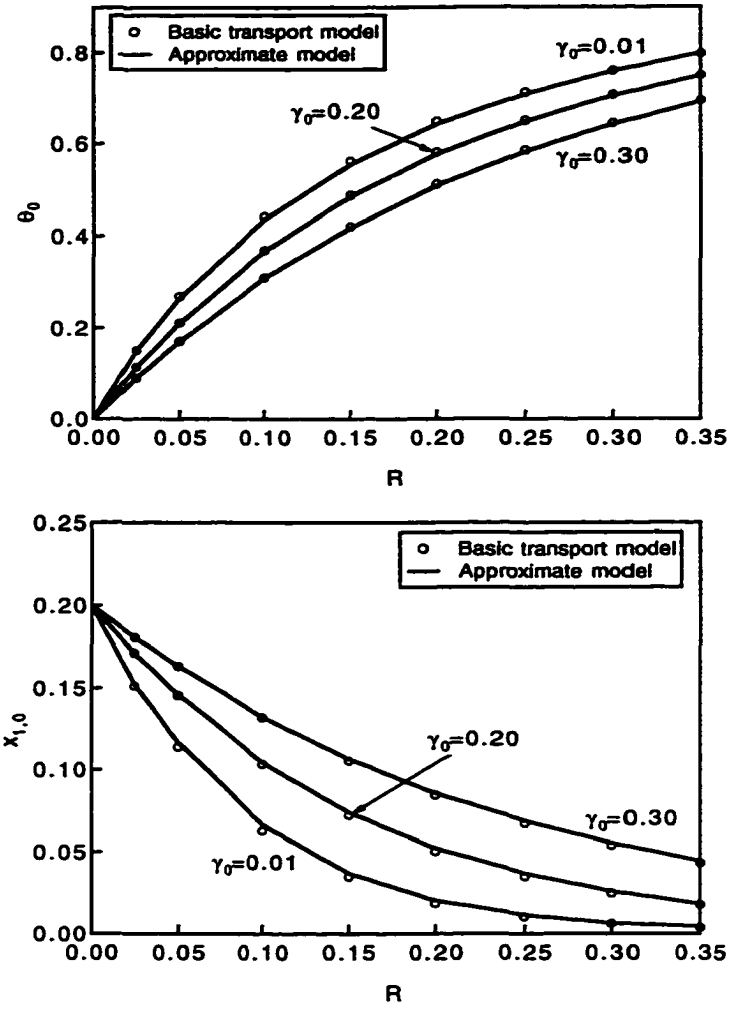

Figure 3.11: Effect of permeate pressure on permeate flow rate and residue concentration of the first component (eight component system).

all operating conditions considered. Figure 3.12 shows the effect of R and C on θ_0 and $x_{1,0}$. The approximate model yields accurate predictions under most conditions, although small deviations are observed for large values of C as expected.

These results demonstrate that the basic transport model and the approximate model can be applied to gas mixtures with a large number of components. It is important to note that the computational effort associated with solving the

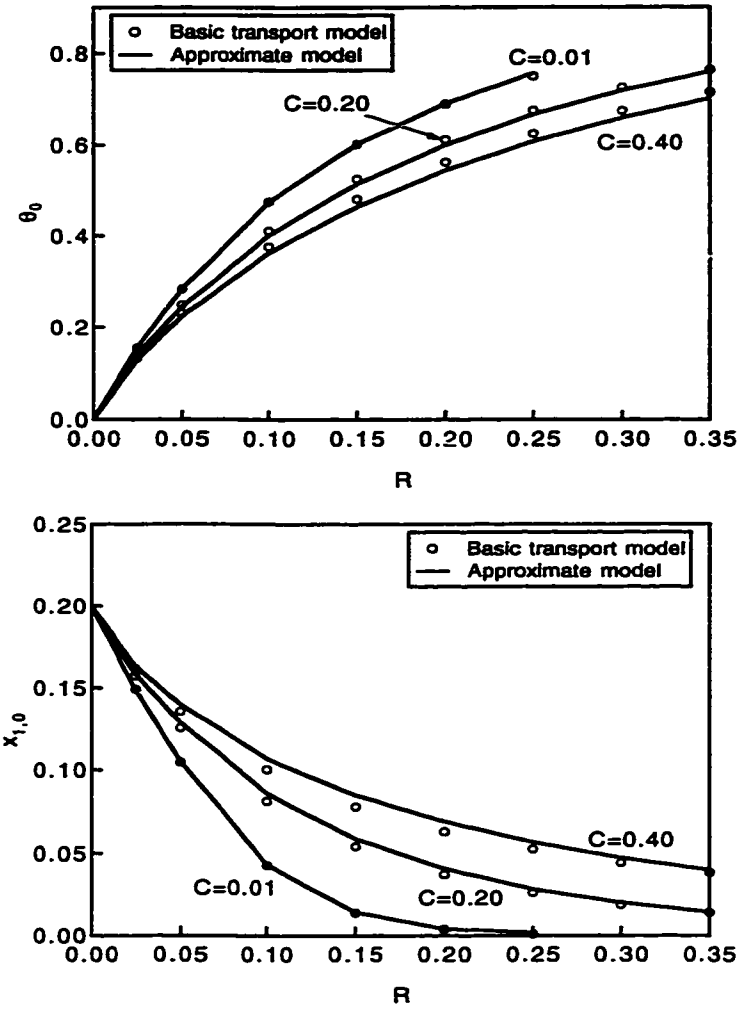

Figure 3.12: Effect of dimensionless constant C on permeate flow rate and residue concentration of the first component (eight component system).

approximate model does not increase dramatically as the number of components increases. The computing time for a single simulation in Figures 3.10–3.12 is 1.5–3.5 seconds with the approximate model and 8–25 minutes with the basic model. As in the four component case, the approximate model is 200–700 times faster than the basic transport model.

Table 3.3: Operating conditions and parameters for experimental data [52].

No.	U_f	P	γ_0	% feed composition ($x_{i,f}$)				Parameters	
	(m^3/s)	(MPa)		CO_2	CH_4	N_2	C^+H	$\hat{R}$	$\hat{C}$
1	0.0331	3.756	0.0272	5.23	86.67	1.22	6.88	0.4058	0.0442
2	0.0318	2.377	0.0429	5.28	86.86	1.35	6.51	0.2674	0.1061
3	0.0331	3.825	0.0267	11.61	80.72	1.14	6.53	0.4133	0.0426
4	0.0466	3.204	0.0318	12.13	79.69	1.07	7.11	0.2462	0.0854
5	0.0695	4.859	0.0210	12.34	80.16	1.05	6.45	0.2501	0.0555
6	0.0692	3.963	0.0258	12.41	79.59	1.05	6.95	0.2049	0.0830
7	0.0370	3.239	0.0315	12.72	78.79	1.05	7.44	0.3128	0.0665
8	0.0774	4.859	0.0210	12.98	79.05	1.05	6.92	0.2247	0.0617
9	0.0672	3.894	0.0262	13.39	79.19	1.05	6.37	0.2073	0.0835

3.4.3 Parameter Estimation

The effectiveness of the proposed parameter estimation strategy is investigated using experimental data for separation of CO_2/CH_4 mixtures containing small amounts of N_2 and other hydrocarbons [52]. Nine sets of experimental data are selected for a permeator after checking the consistency of the operating temperature and the closure of material balances. The selectivities are chosen as in Lee *et al.* [53]: CO_2/CH_4 selectivity=20; N_2/CH_4 selectivity=1.0; and C^+H/CH_4 selectivity=0.4. The C^+H represents all the hydrocarbons higher than CH_4, but it consists mostly of C_2H_6. Parameter estimation is achieved by transforming the experimental measurements into relative values according to (3.55)–(3.60), and then using the binary model to estimate the parameters C' and R'. The estimation results are: $C' = 1.884 \times 10^{13}$ m^3/Pa, and $R' = 3.578 \times 10^{-9}$ $Pa^2\ s/m^3$.

Table 3.4: Comparison of experimental data and simulation results.

No.	Cut ratio		% outlet permeate composition ($y_{i,0}$)							
			CO_2		CH_4		N_2		C^+H	
	θ_0	$\hat{\theta}_0$	$y_{1,0}$	$\hat{y}_{1,0}$	$y_{2,0}$	$\hat{y}_{2,0}$	$y_{3,0}$	$\hat{y}_{3,0}$	$y_{4,0}$	$\hat{y}_{4,0}$
1	0.3762	0.4005	13.18	12.75	82.14	82.92	0.95	1.17	3.73	3.16
2	0.2887	0.2693	15.64	16.77	79.11	79.26	0.89	1.23	4.36	2.74
3	0.4059	0.4651	26.76	24.60	69.08	71.58	0.77	1.01	3.39	2.81
4	0.3310	0.3114	33.45	34.70	62.75	61.95	0.64	0.83	3.16	2.51
5	0.3538	0.3266	33.19	35.04	63.08	61.90	0.62	0.81	3.11	2.25
6	0.2796	0.2773	37.32	38.54	59.56	58.42	0.59	0.77	2.53	2.27
7	0.3628	0.3790	32.12	31.75	63.98	64.55	0.69	0.86	3.21	2.85
8	0.3051	0.3063	37.66	38.35	59.28	58.58	0.66	0.78	2.40	2.30
9	0.2537	0.2883	40.81	40.26	55.90	56.94	0.56	0.76	2.73	2.04
e	6.74%		3.94%		1.53%		29.04%		18.73%	

These parameters are used to simulate the multicomponent separation. Table 3.3 shows the operating conditions and calculated C and R derived from the estimated C' and R'. Table 3.4 compares the experimental data and the predicted values, as well as their average relative errors. The θ_i and $y_{i,0}$ represent experimental measurements, and the $\hat{\theta}_i$ and $\hat{y}_{i,0}$ represent values predicted by the approximate multicomponent model using the estimated parameters. The errors are calculated as follows:

$$e_{\theta_0} = \frac{1}{N}\sum_{j=1}^{N}\left|\frac{\hat{\theta}_{0,j}-\theta_{0,j}}{\theta_{0,j}}\right| \times 100\% \tag{3.65}$$

$$e_{y_{i0}} = \frac{1}{N}\sum_{j=1}^{N}\left|\frac{\hat{y}_{i0,j}-y_{i0,j}}{y_{i0,j}}\right| \times 100\% \tag{3.66}$$

where N represents the number of experiments. The predictions are sufficiently accurate for preliminary process design. The large relative errors associated with the N_2 and C^+H components are attributable to their low concentrations in the permeate stream.

3.5 Summary and Conclusions

Two multicomponent models for spiral-wound gas permeators which account for permeate-side pressure variations have been proposed. The basic transport model is derived from fundamental material balances and permeation relations, while the approximate model is derived directly from the basic model by assuming the residue flow rate is constant along the direction of permeate flow. The approximate model is developed by using Gaussian quadrature to approximate integral expressions and the fourth-order Runge-Kutta-Gill algorithm to solve the initial value problem for the feed-side flow rate and compositions. The two models compare favorably for gas mixtures containing four and eight components. The major shortcoming of the basic transport model is the computational effort required to generate a solution. On the other hand, the approximate model provides very accurate predictions with less than 1% of the computation time required for the basic model. In addition, a simple method for estimating uncertain/unknown model parameters from experimental data has been proposed and successfully applied to a CO_2/CH_4 separation system. As result of its accuracy and efficiency, the approximate model is well suited for simulation and design of complex membrane separation systems.

Chapter 4

Membrane System Design via Nonlinear Programming

4.1 Introduction

As discussed in Chapter 1, the conventional design approach for multi-stage membrane systems is to select a small number of system configurations and then optimize the operating conditions of each network. The final design is chosen to be the system which yields the most favorable economics. This procedure is useful for the design of simple membrane processes, comparison of different configurations, and investigation of parameter sensitivities. Several investigators have utilized this design approach for CO_2/CH_4 separations [5, 9, 10, 18, 32, 63, 71, 72]. Despite these studies, more general comparisons of CO_2/CH_4 membrane system designs and more detailed description of the associated optimization methods also are needed.

In the previous chapters, an approximate modeling technique for spiral-wound permeators separating binary and multicomponent gas mixtures is proposed. The development of the approximate models is based on simplifying basic transport models which include permeate-side pressure drop. The resulting models are well suited for process design because the nonlinear algebraic equations can be solved very efficiently and yield excellent prediction accuracy over a wide range of operating

conditions. In this chapter, the approximate binary model is utilized to develop a design strategy for spiral-wound membrane processes. Nonlinear programming (NLP) techniques are used to determine operating conditions which satisfy the separation requirements while minimizing the annual process cost. The design procedure is applied to the separation of CO_2/CH_4 mixtures in natural gas treatment and enhanced oil recovery. The performance of different permeator configurations is compared and parameter sensitivities are analyzed. The NLP design methodology provides guidance on the development of permeator superstructures and synthesis strategies that allow simultaneous optimization of the permeator configuration and operating conditions.

4.2 Nonlinear Programming Strategy

The optimal design of a gas membrane separation system involves a tradeoff between capital investment and operating expenses. Using the following nonlinear programming strategy and the approximate binary permeator model, we compare the system configurations shown in Figure 1.3 for CO_2/CH_4 separations. Both natural gas treatment and enhanced oil recovery applications are considered. The design strategy is based on the following nonlinear optimization problem:

Minimize: annual process cost

Subject to: operating requirements

material balances for each mixing/splitting point

model equations for each permeator

nonnegativity constraints

An example of the mathematical formulation for a three-stage configuration (Figure 1.3g) is shown in Appendix C.1. Other configurations in Figure 1.3 are formulated similarly. Note that in this work we assume the membrane area can be varied continuously by changing the membrane width. As a result, the pressure coefficient C in equation (2.4) can be factored into a form involving the membrane area and the feed conditions:

$$C = C'' \frac{U_f}{AP^2} \tag{4.1}$$

where C'' is a parameter that depends on the internal properties of the permeator. The nominal economic costs and operating parameters are obtained from Spillman *et al.* [72], Babcock *et al.* [5], and Lee *et al.* [52, 53].

- Operating conditions
  - natural gas processing capacity: $U_{f,0} = 10$ mol/s (19,353 m^3/day)
  - working time: $t_{wk} = 300$ days/year
  - feed pressure: $P = 3.5$ MPa
  - product permeate pressure: $p_0 = 0.105$ MPa
  - temperature: $T = 40°C$
  - feed CO_2 concentration: $x_{f,0} = 0.20$

- Operating requirements
  - outlet residue CO_2 concentration less than 2% (both applications)
  - outlet permeate CO_2 concentration greater than 95% (enhanced oil recovery only)
  - outlet permeate pressure for each stage not less than 0.105 MPa to avoid negative pressure operation
- Membrane properties
  - CH_4 permeability: $Q_2/d = 1.48 \times 10^{-3}$ mol/MPa·m^{2}s (0.0119 $m^3_{STP}/m^2h\cdot bar$)
  - CO_2/CH_4 selectivity: $\alpha = 20$
  - pressure parameter: $C'' = 9.32$ MPa^{2}m^{2}s/mol
- Capital investment
  - membrane housing: $f_{mh} = 200$ \$/m^2 membrane
  - gas-powered compressors: $f_{cp} = 1000$ \$/KW
  - compressor efficiency: $\eta_{cp} = 70\%$
  - working capital: $f_{wk} = 10\%$ of fixed capital investment
  - capital charge: $f_{cc} = 27\%$ per year
- Operating expenses

- membrane replacements: $f_{mr} = 90$ \$/m^2 membrane
- membrane lifetime: $t_m = 3$ years
- maintenance: $f_{mt} = 5\%$ of fixed capital investment
- utility and sale gas price: $f_{sg} = 35$ \$/Km^3
- sale gas gross heating value: $f_{hv} = 43$ MJ/m^3
- lost CH_4 is converted to sales gas value

The gas volumes are calculated at standard conditions (0.102 MPa, 273 K). The pressure parameter C'' is based on an estimated value derived in Chapter 2.

4.3 Natural Gas Treatment

For natural gas treatment, the residue CO_2 concentration must be less than 2%, while no constraint is placed on the permeate concentration. For the nominal operating conditions presented earlier, each configuration in Figure 1.3 is optimized to minimize the annual cost of the membrane system. The results are shown in Table 4.1. The configuration with three stages and residue recycle (f) yields the lowest cost, while the two-stage system with residue recycle (e) is most expensive.

4.3.1 Effect of Feed Conditions

Figure 4.1 shows the effect of feed composition on the process cost, total membrane area, compressor power, and CH_4 recovery for each configuration in Figure 1.3. Note that each configuration has a maximum cost with respect to the CO_2 concentration

Table 4.1: Optimal separation systems at nominal conditions for natural gas treatment.

CF[a]	F ($\frac{\$}{Km^3}$)	n	A_n (m^2)	$W_{cp,n}$ (KW)	$p_{0,n}$ (MPa)	$U_{f,n}$ ($\frac{mol}{s}$)	$x_{f,n}$	$U_{0,n}$ ($\frac{mol}{s}$)	$x_{0,n}$	$V_{0,n}$ ($\frac{mol}{s}$)	$y_{0,n}$
a,b	11.874	1	352.75	–	0.105	10.00	0.200	6.51	0.020	3.49	0.535
c	11.692	1	142.15	–	0.105	10.00	0.200	8.07	0.085	1.93	0.677
		2	205.40	–	0.105	8.07	0.085	6.53	0.020	1.53	0.362
d	11.276	1	231.54	–	0.105	11.08	0.210	8.20	0.057	2.88	0.644
		2	157.96	9.86	0.105	8.20	0.057	7.12	0.020	1.08	0.298
e	12.747	1	424.30	37.96	0.105	12.09	0.195	7.93	0.020	4.16	0.530
		2	67.81	–	0.105	4.16	0.530	2.09	0.174	2.07	0.891
f	11.204	1	180.89	–	0.105	10.00	0.200	7.71	0.066	2.29	0.651
		2	184.97	11.90	0.105	8.52	0.066	7.22	0.020	1.30	0.321
		3	29.84	–	0.105	1.30	0.321	0.82	0.068	0.49	0.744
g	12.574	1	320.16	31.98	0.105	12.10	0.196	8.59	0.037	3.51	0.586
		2	101.15	5.89	0.105	8.59	0.037	7.95	0.020	0.65	0.243
		3	64.30	–	0.105	3.51	0.586	1.45	0.147	2.05	0.897

[a]CF–configuration; F–annual process cost; n–permeator stage number; A–membrane area; W_{cp}–compressor power; p_0–outlet permeate pressure; U_f–feed flow rate; x_f–feed concentration; U_0–residue flow rate; x_0–residue concentration; V_0–permeate flow rate; y_0–permeate concentration.

of the feed gas. Single stage with recycle (configuration *b*) always yields single stage without recycle (configuration *a*), which indicates permeate recycle is not favorable for single-stage systems. As expected, systems without recycle (configurations *a* and *c*) provide low CH_4 recoveries. However, they yield moderate process costs because of small membrane areas and the lack of compressors. The two-stage system with permeate recycle (configuration *d*) and three-stage system with residue recycle (configuration *f*) have the lowest process costs, mainly because they can increase CH_4 recovery with moderate power consumption. The two-stage system with residue recycle (configuration *e*) and three-stage system with permeate and residue recycle

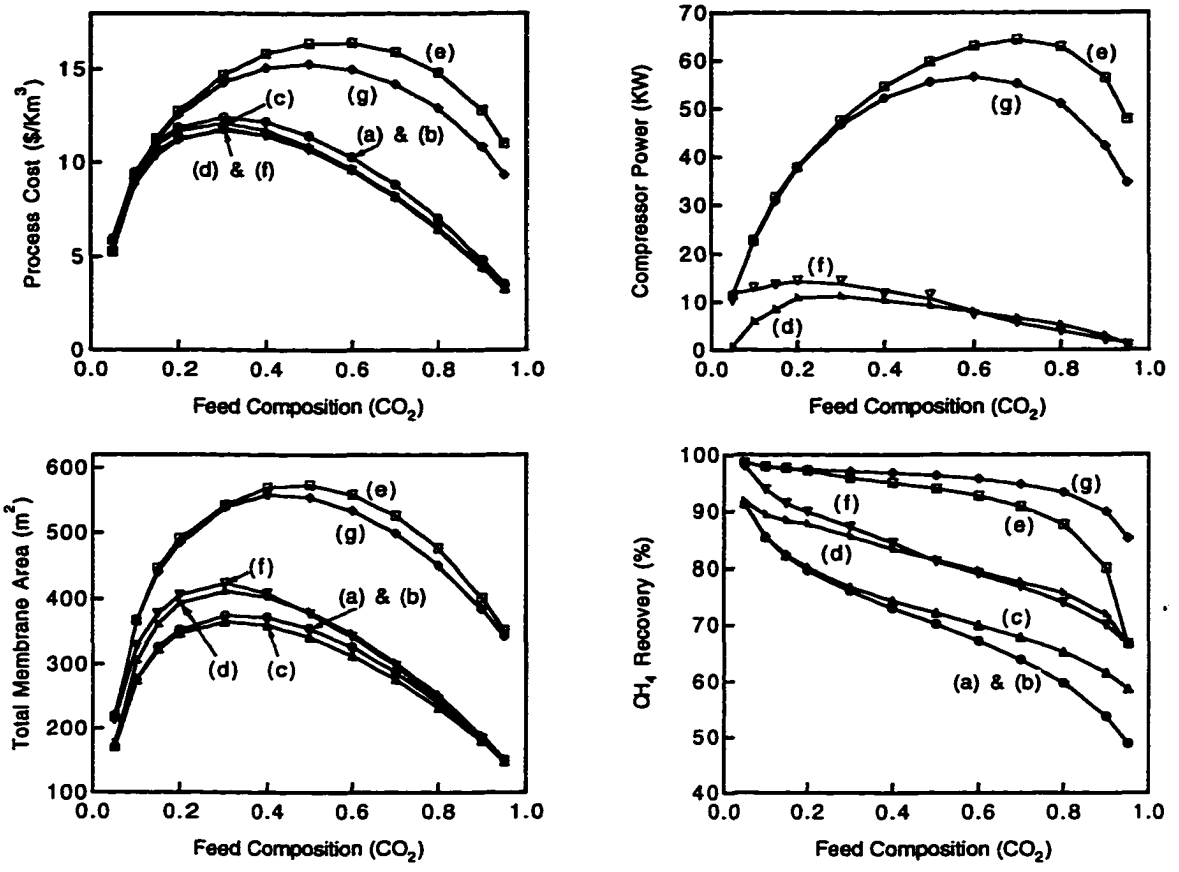

Figure 4.1: Effect of feed composition on optimal separation system for natural gas treatment: (a) single stage; (b) single stage with recycle; (c) two stage; (d) two stage with permeate recycle; (e) two stage with residue recycle; (f) three stage with residue recycle; (g) three stage with permeate and residue recycle.

(configuration *g*) provide unnecessarily high CH_4 recoveries at the expense of large membrane area and high power consumption. Therefore, the process costs for these two configurations are very high. These results are consistent with those obtained by Spillman *et al.* [72] and Babcock *et al.* [5].

The effect of feed pressure on different configurations is shown in Figure 4.2. Only three configurations (*a*, *d*, and *f*) are investigated as a result of their relatively

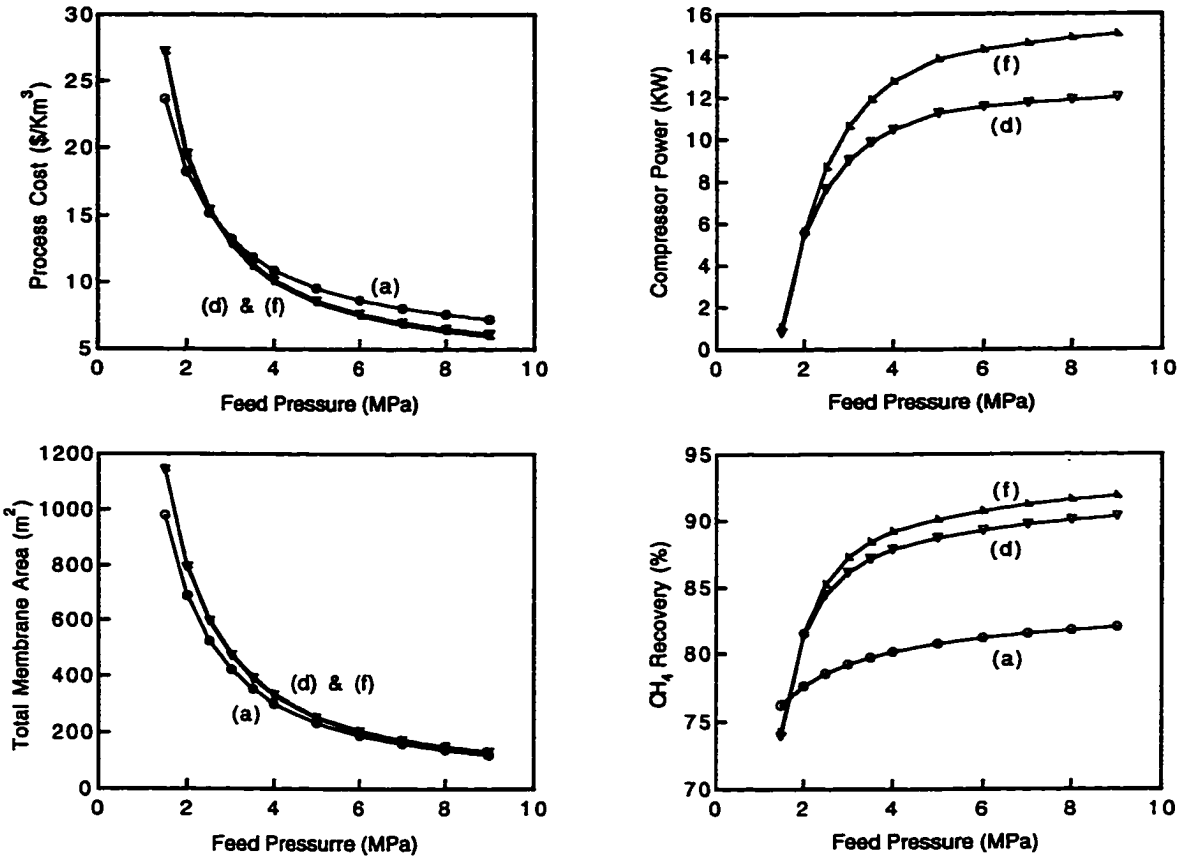

Figure 4.2: Effect of feed pressure on optimal separation system for natural gas treatment: (a) single stage; (d) two stage with permeate recycle; (f) three stage with residue recycle.

low process costs. It is important to note we have assumed there is no cost associated with increasing the feed pressure. Increasing feed pressure improves the process costs and the CH_4 recoveries, especially when the pressure is less than 40 MPa. Although not shown here, we also have investigated the effect of feed flow rate. Increasing feed flow rate increases the membrane area and compressor power linearly, while the process cost and CH_4 recovery essentially are unchanged. This behavior occurs because the permeator model does not account for concentration polarization [79].

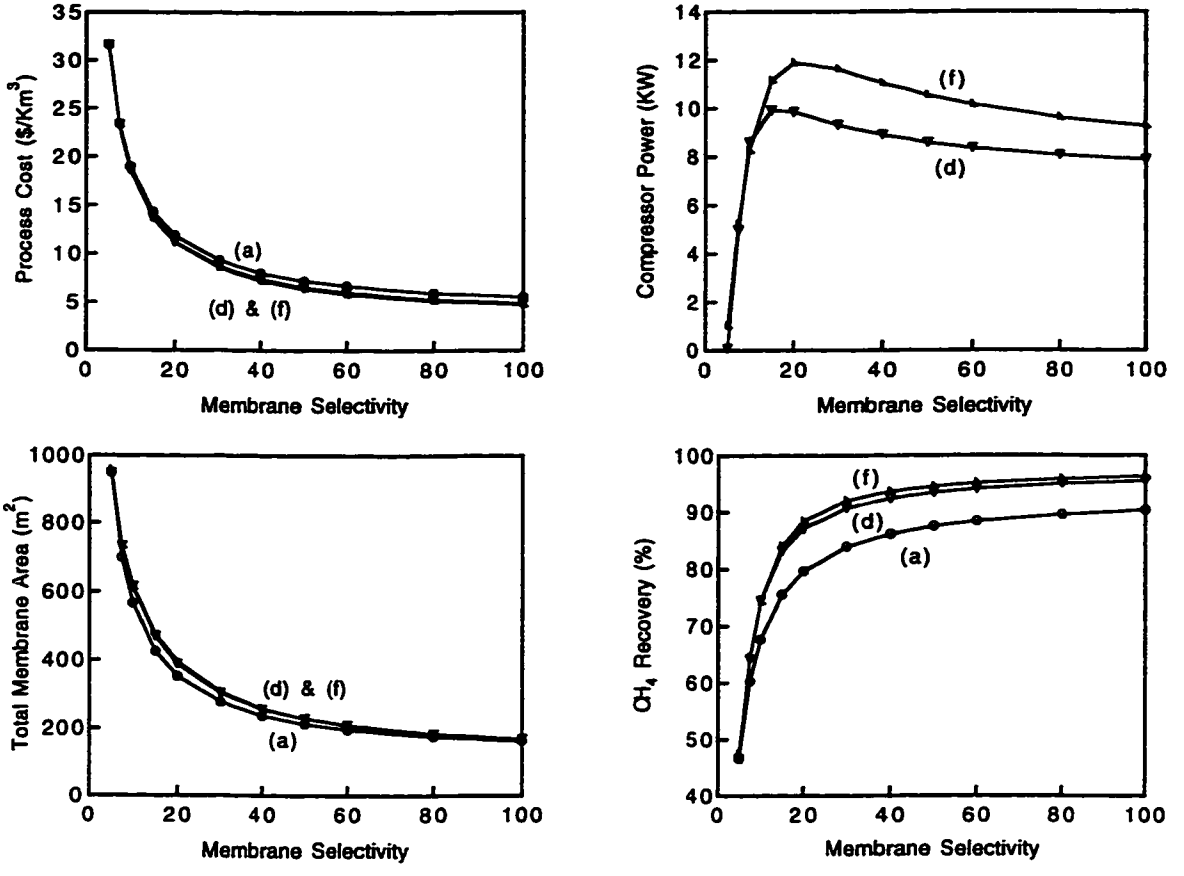

Figure 4.3: Effect of membrane selectivity on optimal separation system for natural gas treatment: (a) single stage; (d) two stage with permeate recycle; (f) three stage with residue recycle.

The feed flow rate has no effect on the optimal operating conditions, but it does change the size of the required equipment.

4.3.2 Effect of Membrane Properties

Figure 4.3 shows the effect of membrane selectivity on three configurations (a, d, and f) with the most favorable economics. As expected, increasing selectivity significantly decreases the process cost and increases CH_4 recovery, especially when

the selectivity is relatively low. Although not shown here, we have investigated the effect of parameter C'' from 0 to 30 MPa^2m^2s/mol for the same three configurations. As expected, the process cost is the lowest if there is no permeate pressure drops (*i.e.* $C'' = 0$). As the permeate pressure drop increases, the process cost increases as more membrane area and compressor power are needed, while the CH_4 recovery decreases.

4.3.3 Effect of Economic Parameters

To investigate the effect of economic parameters on the optimal separation system, we consider variations in the capital cost of membrane housing and compressors, the expense of membrane replacement, and the price of the sales gas. For systems without recycle (configurations *a* and *c*), the operating conditions are determined solely by the membrane properties and separation requirements because no extra degree of freedom are available for economic optimization. For these configurations, variations in economic parameters change the process cost linearly and the operating conditions do not change. Therefore, we consider only the multi-stage configurations *d* and *f*.

Varying membrane housing capital from 50 to 700 $\$/m^2$ membrane results in small changes in optimal operating conditions and CH_4 recoveries, while the process cost increases in linear fashion. This indicates that membrane housing capital does not have a strong effect on the optimal separation system. The effect of compressor capital cost on the two configurations is shown in Figure 4.4. The process

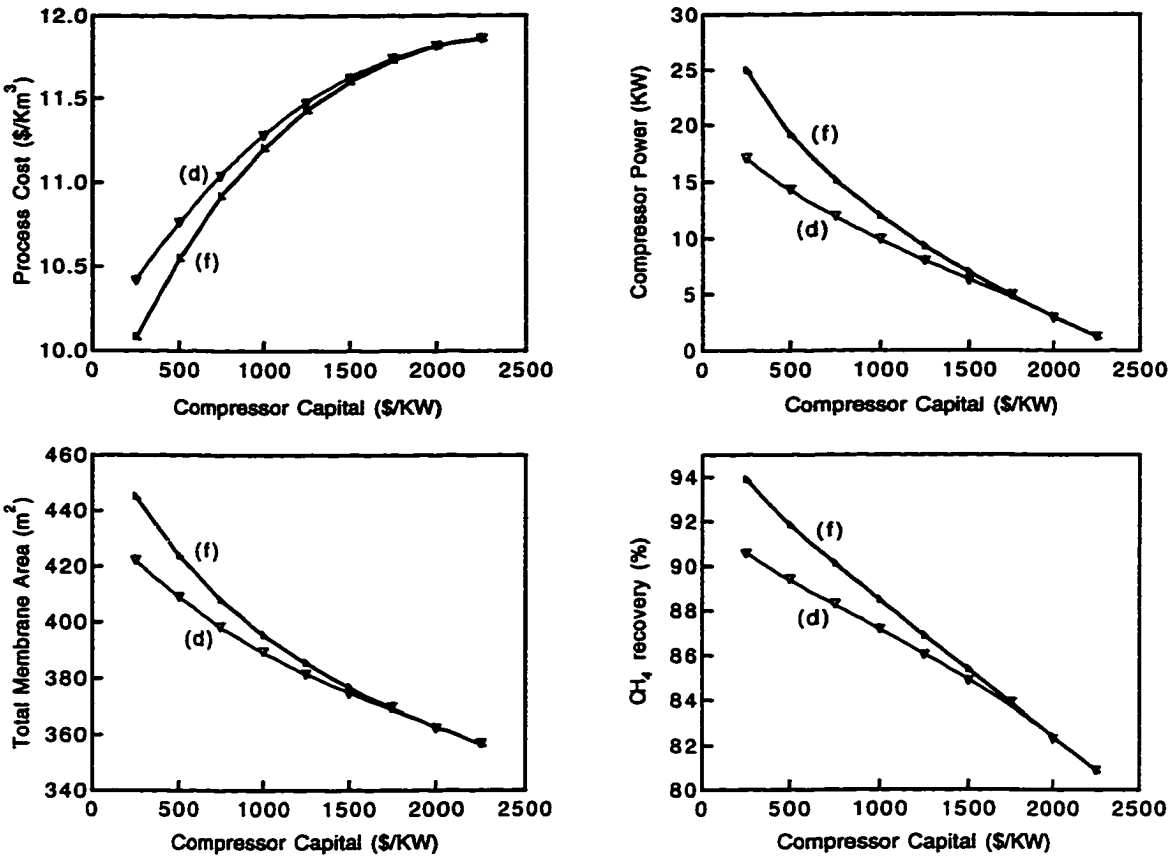

Figure 4.4: Effect of compressor capital on optimal separation system for natural gas treatment: (d) two stage with permeate recycle; (f) three stage with residue recycle.

cost increases with increasing compressor cost. However, the cost increase can be reduced substantially by optimizing the operating conditions. To balance the increased compressor cost, the compressor power and membrane area are reduced at the expense of decreased CH_4 recovery. Note that the second and third stages have very small membrane areas when compressor capital cost is very high, at which point both configurations effectively reduce to the single-stage configuration *a*.

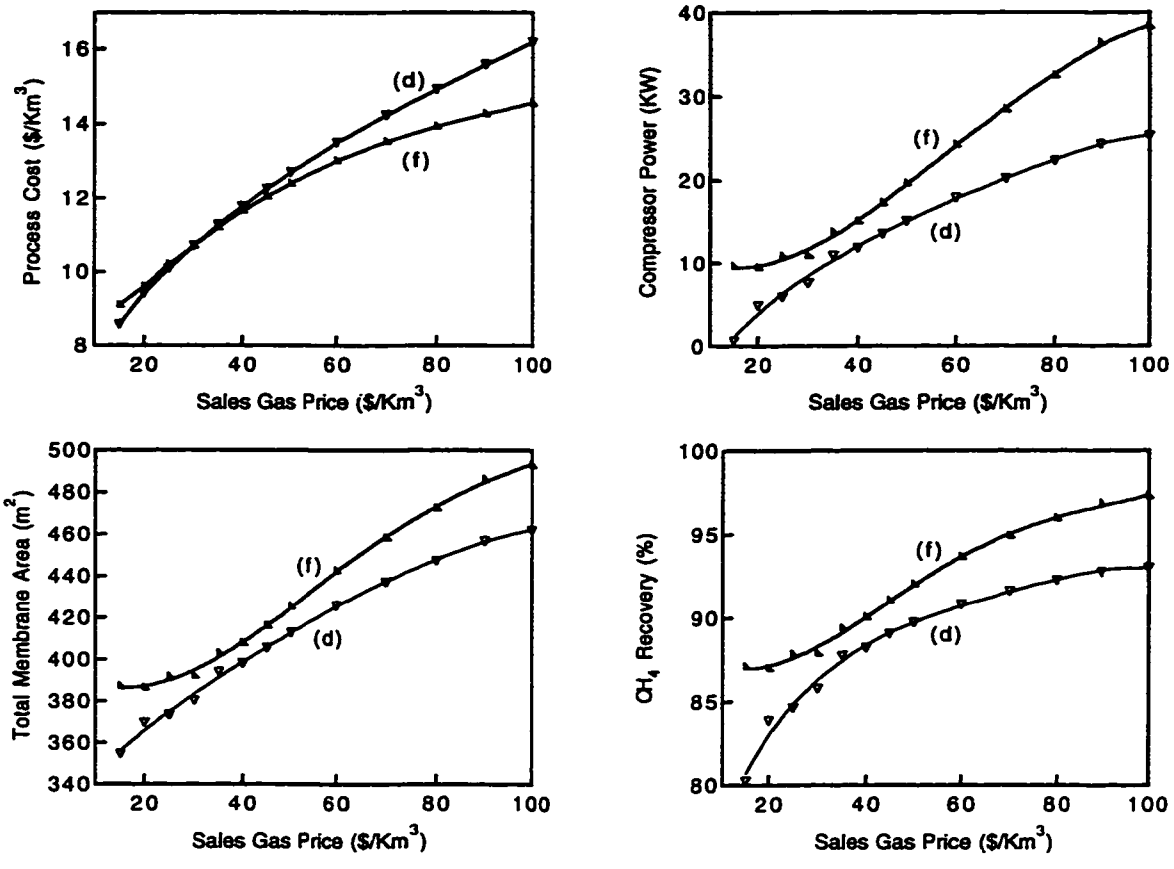

Figure 4.5: Effect of sale gas price on optimal separation system for natural gas treatment: (d) two stage with permeate recycle; (f) three stage with residue recycle.

As shown in Figure 4.5, the sales gas price has a strong effect on optimal operating conditions. Note that there is an intersection point where the process cost for the two configurations are identical. Configuration *d* is preferred when the sales gas price is low, while configuration *f* has better performance at high sales gas prices because it yields higher CH_4 recoveries. We also have investigated the effect of the membrane replacement expense from 30–150 $\$/m^2$ membrane. Although not shown here, these variations have no effect on the optimal operating conditions, while the process cost increases linearly with increasing replacement cost.

Table 4.2: Optimal separation systems at nominal conditions for enhanced oil recovery.

CF[a]	F ($\frac{\$}{Km^3}$)	n	A_n (m^2)	$W_{cp,n}$ (KW)	$p_{0,n}$ (MPa)	$U_{f,n}$ ($\frac{mol}{s}$)	$x_{f,n}$	$U_{0,n}$ ($\frac{mol}{s}$)	$x_{0,n}$	$V_{0,n}$ ($\frac{mol}{s}$)	$y_{0,n}$
e	15.355	1	530.69	56.48	0.105	14.25	0.278	8.06	0.020	6.19	0.614
		2	41.37	–	0.105	6.19	0.614	4.25	0.461	1.94	0.950
f	15.467	1	0.54	–	0.105	10.00	0.200	9.99	0.199	0.01	0.780
		2	533.84	57.13	0.105	14.33	0.281	8.06	0.020	6.26	0.617
		3	40.82	–	0.105	6.26	0.617	4.34	0.468	1.93	0.951
g	13.281	1	236.98	28.87	0.127	13.14	0.235	9.79	0.078	3.35	0.695
		2	236.30	15.74	0.105	9.79	0.078	8.06	0.020	1.73	0.347
		3	41.31	–	0.105	3.35	0.695	1.41	0.345	1.94	0.950

[a]CF–configuration; F–annual process cost; n–permeator stage number; A–membrane area; W_{cp}–compressor power; p_0–outlet permeate pressure; U_f–feed flow rate; x_f–feed concentration; U_0–residue flow rate; x_0–residue concentration; V_0–permeate flow rate; y_0–permeate concentration.

4.4 Enhanced Oil Recovery

The separation of CO_2/CH_4 in enhanced oil recovery differs from that in natural gas treatment because both the residue and permeate streams must satisfy concentration requirements. For single-stage configurations (a and b) and some two-stage configurations (c and d), the additional constraint that the permeate concentration must contain at least 95% CO_2 causes infeasibilities for a wide range of feed compositions. In fact, these configurations are feasible only when the feed CO_2 concentration is greater than 80%. Therefore, the subsequent analysis is restricted to configurations e, f, and g. Table 4.2 gives the optimal separation system for these configurations at the nominal operating conditions.

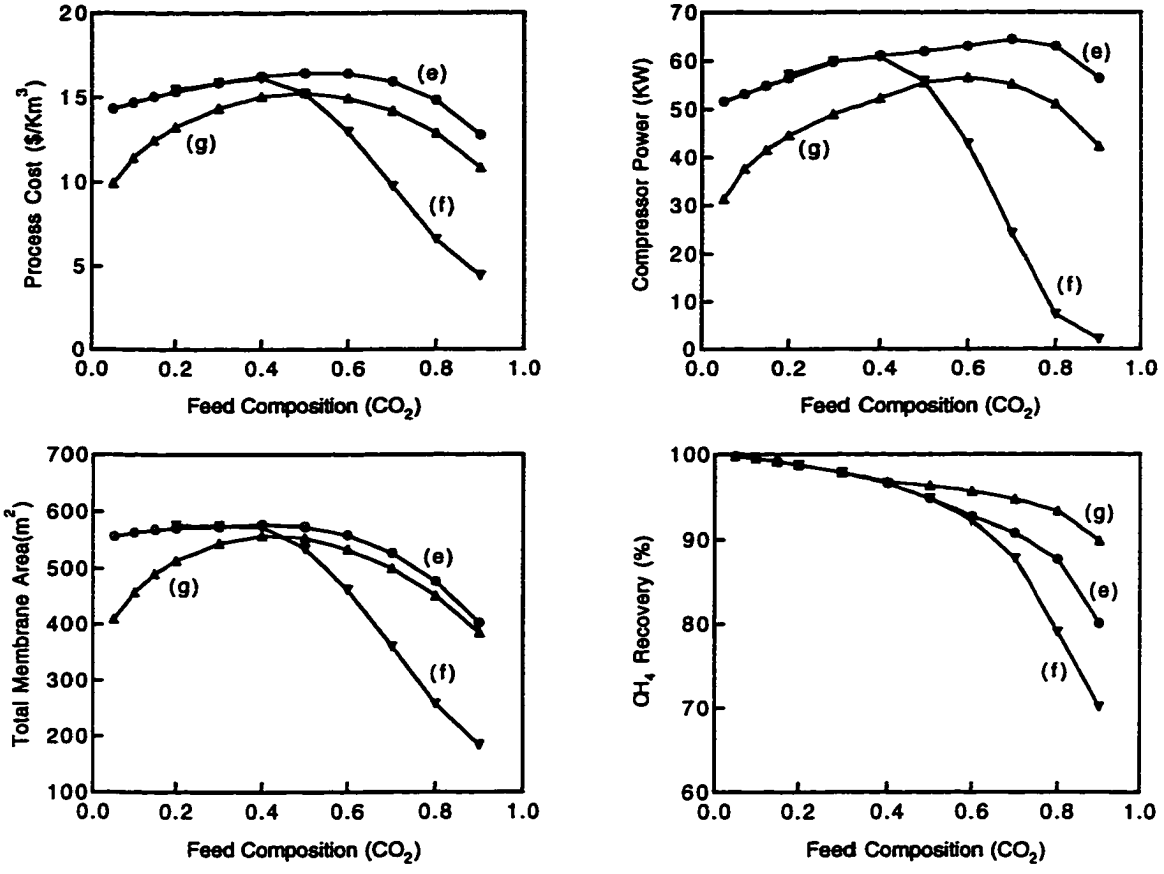

Figure 4.6: Effect of feed composition on optimal separation system for enhanced oil recovery: (e) two stage with residue recycle; (f) three stage with residue recycle; (g) three stage with permeate and residue recycle.

4.4.1 Effect of Feed Conditions

Figure 4.6 shows a comparison of the three configurations for different feed compositions. The three-stage system with permeate and residue recycle (configuration *g*) provides the lowest process cost for feed CO_2 compositions less than 50%. For higher feed concentration, the three-stage system with residue recycle (configuration *f*) becomes more cost effective. At feed compositions less than 40% CO_2, the first-stage

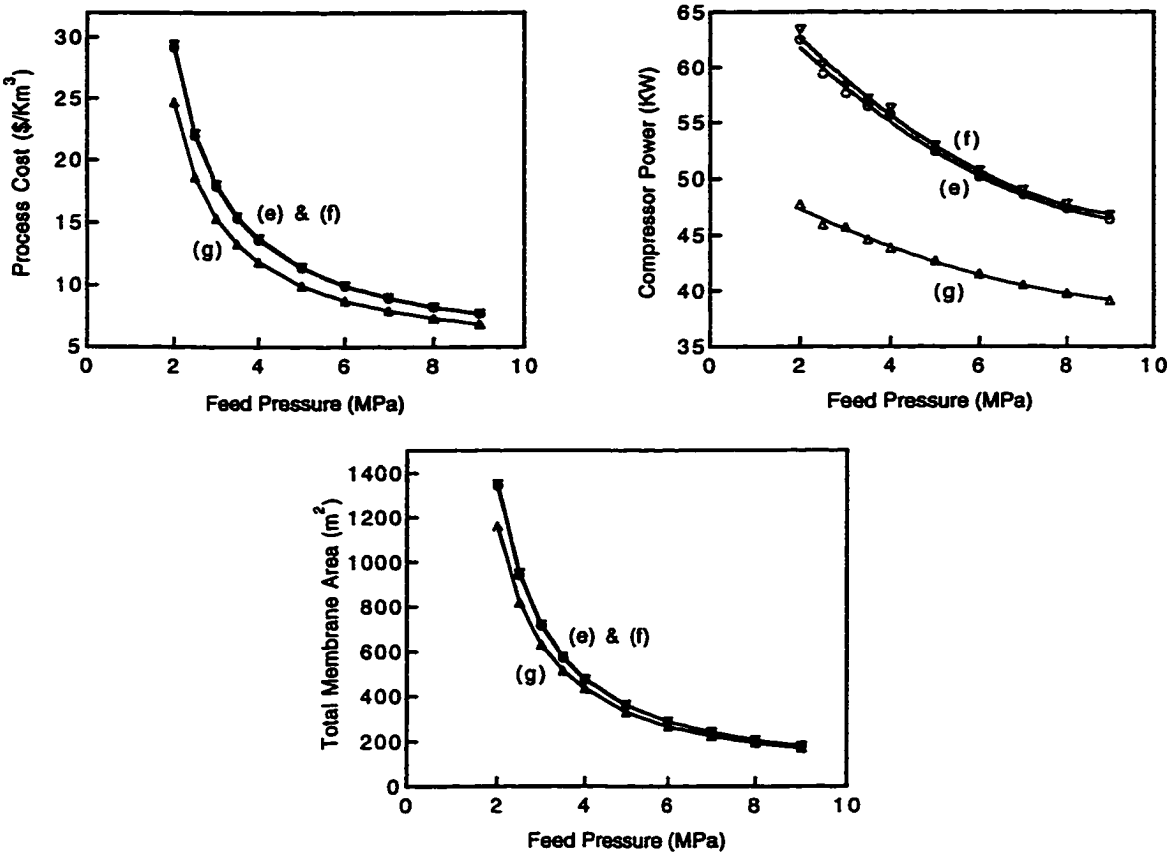

Figure 4.7: Effect of feed pressure on optimal separation system for enhanced oil recovery: (e) two stage with residue recycle; (f) three stage with residue recycle; (g) three stage with permeate and residue recycle.

membrane area of configuration f goes to zero, and the three-stage configuration becomes identical to the two-stage configuration e. The effect of feed pressure at the nominal feed composition is shown in Figure 4.7. As expected, increasing feed pressure always yields lower process cost, less membrane area, and less compressor power. It is interesting to note that configuration g has the lowest cost for all feed pressures considered.

4.4.2 Effect of Economic Parameters

The effect of membrane housing capital, compressor capital, sales gas price, and membrane replacement expense on the optimal operating conditions for the three configurations also has been investigated. It is interesting to note that variations in these parameters have much less impact on process economics than in natural gas treatment. For each configuration, optimal operating conditions are not changed significantly by variations in membrane housing from 50–700 $\$/m^2$ membrane, compressor capital from 250–2500 \$/KW, sales gas price from 15–100 $\$/Km^3$, and membrane replacement from 15–180 $\$/m^2$ membrane. The process cost increases linearly with the economic parameters, while the CH_4 recovery is always 98.79% for all configurations. This is attributable to the fact that the optimal operating conditions are dominated by the separation requirements rather than economic parameters in the objective function.

4.4.3 Effect of Separation Requirements

For the three-stage system with permeate and residue recycle (configuration g), we investigate the effect of residue and permeate composition constraints on the optimal operating conditions for a feed CO_2 concentration of 20%. Figure 4.8 shows the effect of the residue constraint (nominally 2%) on the optimal separation system. The process cost increases rapidly when the maximum CO_2 concentration in the residue is decreased as a result of increased membrane area and compressor power. It is interesting to note that the second-stage permeator and compressor are strongly

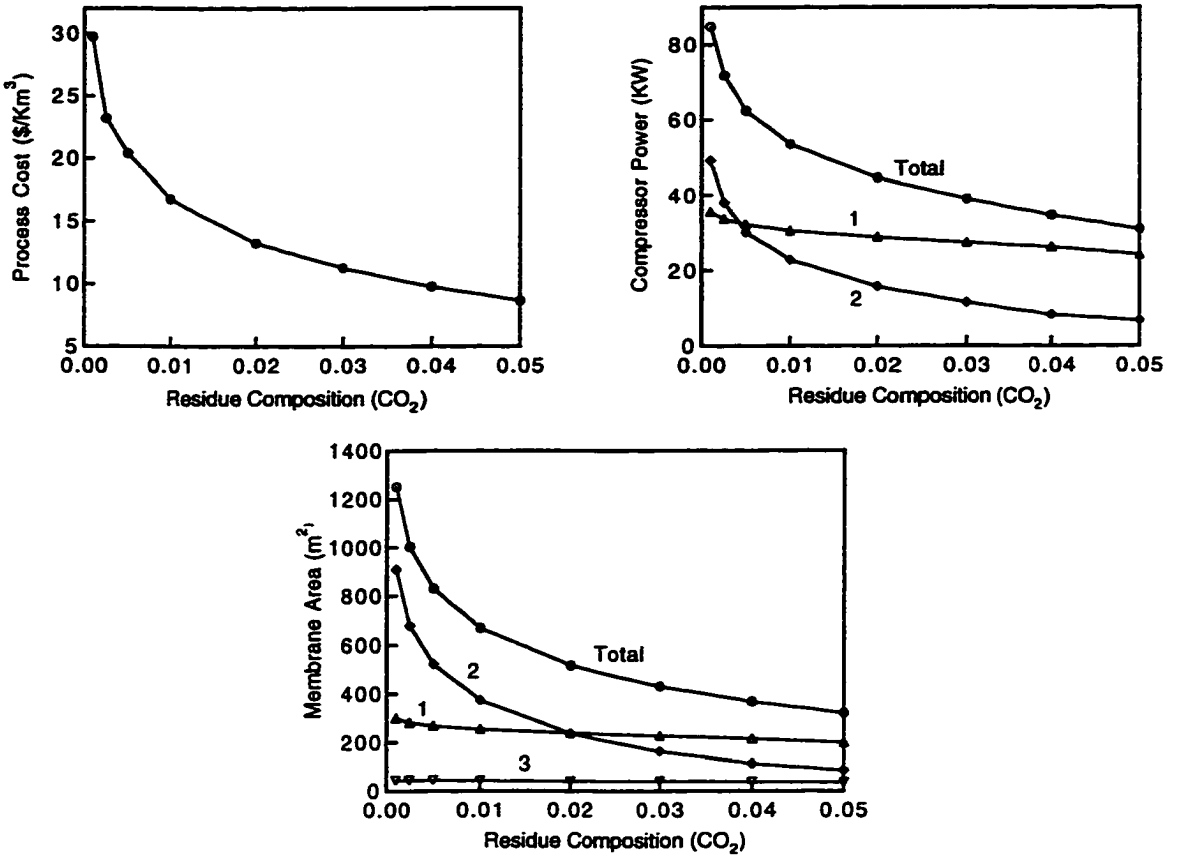

Figure 4.8: Effect of residue composition constraint on optimal separation system for enhanced oil recovery.

affected, while the other permeators and the other compressor are effectively unchanged. The effect of the permeate composition constraint (nominally 95%) is shown in Figure 4.9. The process cost increases significantly as the constraint becomes more stringent. As before, the second-stage permeator and compressor are most strongly affected by variations in this constraint. These results indicate that the proposed model and optimization procedure are sufficiently robust to optimize permeator systems with very stringent separation requirements.

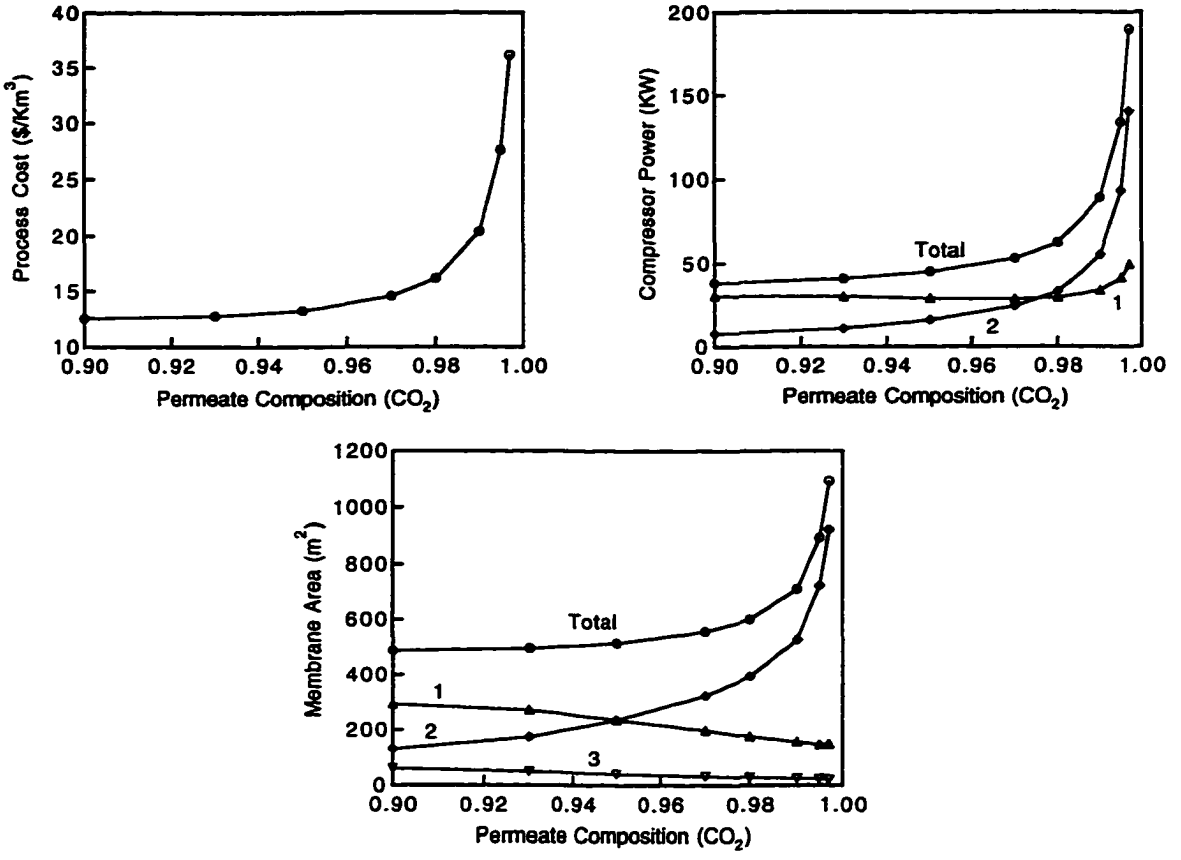

Figure 4.9: Effect of permeate composition constraint on optimal separation system for enhanced oil recovery.

4.5 Summary and Conclusions

A systematic design strategy for spiral-wound membrane systems based on an algebraic permeator model and nonlinear programming has been proposed. Case studies for the separation of CO_2/CH_4 mixtures in natural gas treatment and enhanced oil recovery have been presented. Sensitivity of the proposed designs has been investigated by changing operating conditions, membrane properties, and economic parameters. It is shown that a two-stage configuration with permeate recycle

and a three-stage configuration with residue recycle are suitable for natural gas treatment, while three-stage configurations with permeate and/or residue recycle are appropriate for enhanced oil recovery. The proposed design method provides an efficient tool for optimizing multistage membrane separation systems, including those with stringent separation requirements.

Chapter 5

Process Synthesis for Binary Gas Permeator Systems

5.1 Introduction

In Chapter 4, the approximate binary permeator model is used to develop a nonlinear programming (NLP) design strategy that allows systematic determination of the operating conditions for a specified permeator configuration. The optimization procedure is sufficiently robust to handle multi-stage configurations with very demanding separation requirements. However, the NLP strategy generally yields suboptimal designs because it is infeasible to enumerate and evaluate all possible network configurations. As mentioned in Chapter 1, the mixed-integer nonlinear programming (MINLP) methodology provides an effective approach for synthesizing multi-stage membrane separation systems.

In this chapter, we utilize the same binary model to develop a process synthesis strategy for spiral-wound membrane systems which allows simultaneous optimization of the permeator network and operating conditions. The approach is based on a permeator system superstructure which efficiently embeds a very large number of possible network configurations. The superstructure is used to develop a MINLP design strategy which automatically determines the membrane system that minimizes

the annual process cost. The methodology is applied to the separation of CO_2/CH_4 mixtures in natural gas treatment and enhanced oil recovery. Optimal separation systems are derived for different number of separation stages with both continuous and discrete membrane areas.

5.2 Problem Statement

The problem of designing spiral-wound membrane systems for gas separations can be described as:

> Given a feed mixture of known conditions, synthesize the minimum cost network of spiral-wound permeators and recycle compressors that separates the feed stream into products of specified compositions. The membrane properties and cost related parameters are assumed to be known.

The design task involves the determination of the optimal system configuration, as well as specification of the process unit sizes and operating conditions. As a first step, it is necessary to utilize a permeator model that is sufficiently accurate to predict separation performance and computationally efficient for mathematical programming. The next step is to derive a permeator system superstructure which embeds all system configurations of practical interest, formulate the superstructure as a MINLP model, and develop a suitable solution strategy. To facilitate the subsequent development, the following assumptions are invoked:

1. The feed stream contains a binary gas mixture at a relatively high pressure.

2. The feed-side pressure for each stage is equal to the pressure of the feed stream.

3. The feed-side pressure drop is negligible for each stage.

4. There is no pressure drop between permeation stages.

5. The permeate stream pressures between stages are design variables, while the product permeate stream pressure is predetermined.

6. All permeators and compressors operate at isothermal conditions.

5.3 Optimal Design Strategy

5.3.1 Permeator Superstructure

The superstructure approach to process design provides a systematic framework for simultaneous optimization of process configuration and operating conditions [28]. Superstructures have been developed for a number of membrane separation systems, including reverse osmosis [78] and pervaporation [73] networks. For gas membrane separation systems, the basic components of the superstructure are permeators, compressors, stream mixers, and stream splitters. An ideal superstructure is sufficiently "rich" to represent all process configurations of practical interest, yet sufficiently "simple" to eliminate all unreasonable configurations.

The permeator system superstructure is derived as described below [28]. Note that each separation stage may be comprised of several permeators in parallel or in series.

1. The feed stream is split into individual feed streams for each permeation stage.

2. The inlet stream to a particular stage consists of: its individual feed stream; recycle streams obtained from the permeator's effluent streams; and recycle streams obtained from the effluent streams of all other stages.

3. For each stage, the permeate and residue streams are split into: recycle streams for the particular stage; recycle streams for all other stages; and streams that are sent to the final product mixers. The permeate recycle streams must be compressed to the feed pressure before being sent to the feed stream mixers.

4. The inlet streams for the final permeate (residue) mixer are obtained from the permeate (residue) streams of all stages.

As an illustration, the system superstructure for three separation stages is shown in Figure 5.1. This superstructure is capable of representing a very large number of permeator configurations with three separation stages. Superstructures containing different number of separation stages are developed similarly.

5.3.2 Mathematical Formulation

The permeator system superstructure is mathematically modeled using the general formulation shown in (1.1). In this case, the binary variables appear linearly, so the

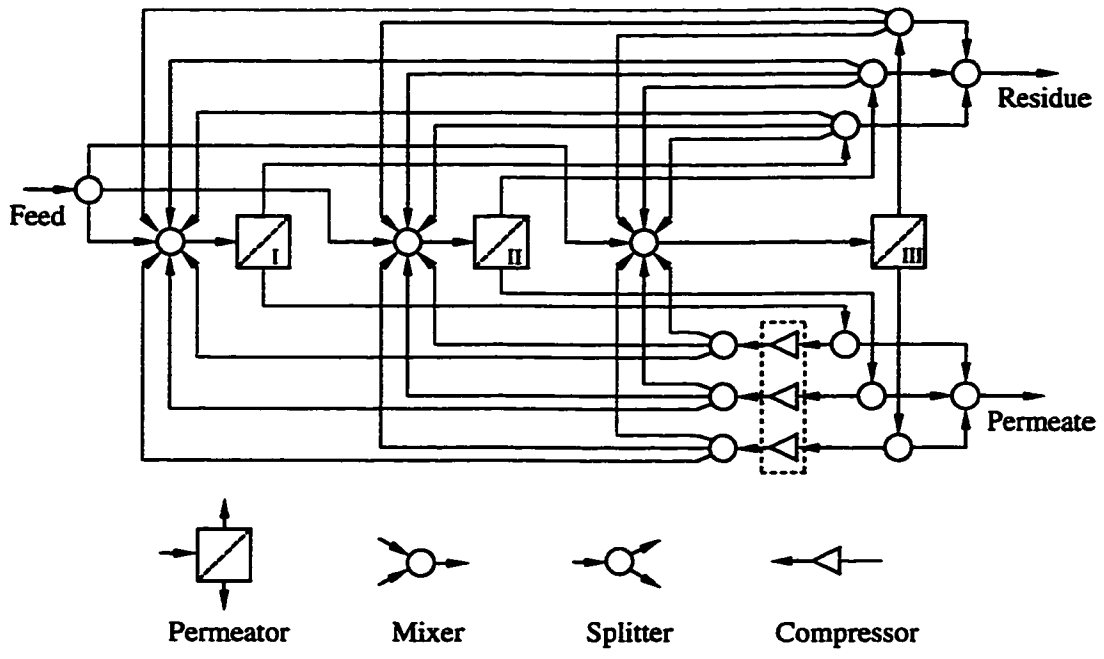

Figure 5.1: Permeator system superstructure with three permeation stages.

mathematical form can be expressed as:

$$\begin{aligned} \min: \quad & cZ + f(X) \\ \text{s.t.}: \quad & U_1 Z + h(X) = 0 \\ & U_2 Z + g(X) \leq 0 \\ & X \in R^n \\ & Z \in \{0,1\}^l \end{aligned} \tag{5.1}$$

where: X is a vector of n continuous variables that represent flow rates, pressures, and compositions of the process streams, as well as continuous properties of the process units; Z is a vector of l binary variables that denote the existence ($Z_i = 1$) or

non-existence ($Z_i = 0$) of process units and connections, as well as discrete properties of the process units; $cZ + f(X)$ is an objective function which approximates the annual cost of the membrane system; $U_1 Z + h(X)$ are m equality constraints that denote material balances, permeator model equations, and parameter definitions; $U_2 Z + g(X)$ are p inequality constraints which correspond to separation requirements, operational restrictions, and logical constraints.

Annual Process Cost

The optimal design of a membrane system entails a tradeoff between capital investments and operating expenses. The annual process cost should take into account capital investments associated with permeators and compressors, as well as operating expenses due to replacement of membrane elements, maintenance, consumption of utilities, and product losses. Depending on the application, the calculation of process costs requires different levels of accuracy. Here we focus on CO_2/CH_4 separations and utilize the approximate costing procedures presented by Spillman *et al.* [72] and Babcock *et al.* [5].

The fixed capital investment is the installed equipment cost of membrane vessels and compressors. Note that membrane housing is a capital cost, but the replacement of membrane elements is treated as an operating expense. Both membrane housing and the replacement of the elements are determined by the membrane area. Auxiliary costs associated with pipes, fittings, and assembly are included in the membrane housing cost. As a result, the fixed capital investment (F_{fc}) is only a

function of membrane area (A) and compressor power (W_{cp}) for each stage (n):

$$F_{\mathrm{fc}} = \sum_{n=1}^{N} (f_{\mathrm{mh}} A_n + f_{\mathrm{cp}} W_{\mathrm{cp},n} / \eta_{\mathrm{cp}}) \tag{5.2}$$

where N is the number of separation stages. The remaining parameters and variables are defined in Appendix D.2. The compressor power for each stage is calculated by assuming ideal gas behavior and isothermal compression [61]:

$$W_{\mathrm{cp},n} = R_{\mathrm{g}} T \left(\sum_{m=1}^{N} V_{\mathrm{b},m,n} \right) \ln \left(\frac{P}{p_{0,n}} \right), \quad n = 1, \cdots, N \tag{5.3}$$

where $V_{\mathrm{b},m,n}$ is the permeate recycle stream from the n-th stage to m-th stage. The working capital is taken as a fixed percentage (f_{wk}) of the fixed capital, and the annual capital charge (F_{cc}) is calculated by annualizing the fixed and working capitals:

$$F_{\mathrm{cc}} = f_{\mathrm{cc}} (1 + f_{\mathrm{wk}}) F_{\mathrm{fc}} \tag{5.4}$$

The annual operating costs include membrane replacement expense (F_{mr}):

$$F_{\mathrm{mr}} = \frac{f_{\mathrm{mr}}}{t_{\mathrm{m}}} \sum_{n=1}^{N} A_n \tag{5.5}$$

maintenance expense (F_{mt}):

$$F_{\mathrm{mt}} = f_{\mathrm{mt}} F_{\mathrm{fc}} \tag{5.6}$$

cost of utilities (F_{ut}):

$$F_{ut} = \frac{f_{sg} t_{wk}}{f_{hv} \eta_{cp}} \sum_{n=1}^{N} W_{cp,n} \tag{5.7}$$

and value of product losses (F_{pl}):

$$F_{pl} = f_{sg} t_{wk} \dot{V}_{pt} \frac{1 - y_{pt}}{1 - x_{pt}} \tag{5.8}$$

The annual process cost (F) is taken as the sum of the capital charge and operating expenses divided by process capacity, which is expressed as:

$$F = \left[F_{cc} + F_{mr} + F_{mt} + F_{ut} + F_{pl}\right] / (U_{f00} t_{wk}) \tag{5.9}$$

The annual process cost (F) is used as the objective function, which is minimized subject to various types of constraints described below. It is important to note that the above calculation procedure only provides an estimate of the annual process cost. As a result of the approximate permeator model and the approximate economic analysis, the MINLP strategy yields preliminary designs. These designs can be used as a basis for more detailed analysis.

Material Balance Constraints

Material balance constraints are imposed on: (*i*) splitters for the initial feed stream and the outlet streams of each stage; (*ii*) mixers for the inlet streams of each stage and the inlet streams for the final products; and (*iii*) each permeation stage. For

an N stage system, material balances on the splitters can be expressed as:

$$U_{\mathrm{f00}} = \sum_{n=1}^{N} U_{\mathrm{f0},n} \tag{5.10}$$

$$U_{0,n} = U_{\mathrm{p},n} + \sum_{m=1}^{N} U_{\mathrm{b},m,n}, \quad n = 1, \cdots, N \tag{5.11}$$

$$V_{0,n} = V_{\mathrm{p},n} + \sum_{m=1}^{N} V_{\mathrm{b},m,n}, \quad n = 1, \cdots, N \tag{5.12}$$

where: U_{f00} is the total fresh feed flow rate; $U_{\mathrm{f0},n}$ is the fresh feed flow rate for stage n; $U_{0,n}$ ($V_{0,n}$) is the total outlet residue (permeate) flow rate for stage n; $U_{\mathrm{p},n}$ ($V_{\mathrm{p},n}$) is the residue (permeate) flow rate of the final product from stage n; and $U_{\mathrm{b},m,n}$ ($V_{\mathrm{b},m,n}$) is the residue (permeate) flow rate of the recycle stream from the n-th stage to m-th stage. Note that only overall material balances are needed because splitters do not change stream compositions.

For the stream mixers, both overall material balances and component balances are necessary. Material balances for the inlet mixer of stage n are written as:

$$U_{\mathrm{f},n} = U_{\mathrm{f0},n} + \sum_{m=1}^{N} \left(U_{\mathrm{b},n,m} + V_{\mathrm{b},n,m} \right), \quad n = 1, \cdots, N \tag{5.13}$$

$$U_{\mathrm{f},n} x_{\mathrm{f},n} = U_{\mathrm{f0},n} x_{\mathrm{f0}} + \sum_{m=1}^{N} \left(U_{\mathrm{b},n,m} x_{0,m} + V_{\mathrm{b},n,m} y_{0,m} \right), \quad n = 1, \cdots, N \tag{5.14}$$

Note that the recycle streams are taken from the m-th stage and terminate at the n-th stage. Material balances for the product mixers are expressed as:

$$U_{\mathrm{pt}} = \sum_{n=1}^{N} U_{\mathrm{p},n} \tag{5.15}$$

$$U_{\mathrm{pt}}x_{\mathrm{pt}} = \sum_{n=1}^{N} U_{\mathrm{p},n}x_{0,n} \tag{5.16}$$

$$V_{\mathrm{pt}} = \sum_{n=1}^{N} V_{\mathrm{p},n} \tag{5.17}$$

$$V_{\mathrm{pt}}y_{\mathrm{pt}} = \sum_{n=1}^{N} V_{\mathrm{p},n}y_{0,n} \tag{5.18}$$

where U_{pt} and x_{pt} are the total flow rate and concentration of the final residue product, and V_{pt} and y_{pt} are the total flow rate and concentration of the final permeate product. Material balances about each permeation stage yield:

$$U_{\mathrm{f},n} = U_{0,n} + V_{0,n}, \quad n = 1, \cdots, N \tag{5.19}$$

$$U_{\mathrm{f},n}x_{\mathrm{f},n} = U_{0,n}x_{0,n} + V_{0,n}y_{0,n}, \quad n = 1, \cdots, N \tag{5.20}$$

Permeator Model Constraints

The permeator model constraints are the approximate permeator model equations written for each stage. Some of the equations are manipulated to facilitate computer implementation. The resulting model equations are presented in Appendix D.1.

Operating Requirement Constraints

Constraints are needed to ensure the product streams satisfy the separation requirements. In CO_2/CH_4 separations, minimum purity requirements are placed on the final residue and permeate streams. In addition, a constraint which expresses that the permeate pressure for each stage must be at least as high as the pressure of the

final permeate stream is required. These constraints are expressed as:

$$x_{pt} \leq x_{out} \tag{5.21}$$

$$y_{pt} \geq y_{out} \tag{5.22}$$

$$p_{0,n} \geq p_{out} \tag{5.23}$$

Depending on the application, some of the constraints may be relaxed. For example, only (5.21) and (5.23) are required for natural gas treatment since the CO_2 enriched permeate stream has very little value.

Discrete Membrane Area Constraints

A typical spiral-wound permeator is comprised of several membrane elements placed in a cylindrical steel shell. A permeator shell normally is capable of holding from one to six spiral-wound membrane elements. Membrane area is adjusted by changing the number of elements or by connecting several permeators in series or parallel. As a result, membrane area can be considered as a discrete variable:

$$A_n = A_0 N_n^A, \quad n = 1, \cdots, N \tag{5.24}$$

where A_0 is the element membrane area and N^A ($N^{AL} \leq N^A \leq N^{AU}$) is the number of elements. Because integer variables cannot be handled directly by existing MINLP algorithms, the element number N^A must be expressed in terms of binary variables. One way to convert the integer variables N^A to binary variables Z^A is to use the

following expression [28]:

$$N_n^{\mathrm{A}} = N_n^{\mathrm{AL}} + \sum_{k=1}^{K} 2^{k-1} Z_{n,k}^{\mathrm{A}}, \quad n = 1, \cdots, N \tag{5.25}$$

where K is the minimum number of binary variable needed:

$$K = 1 + \mathrm{int}\left\{ \frac{\log(N^{\mathrm{AU}} - N^{\mathrm{AL}})}{\log(2)} \right\} \tag{5.26}$$

Note that (5.26) is used only to calculate the value of K; it is not used as a constraint equation. In the following case studies, we choose $N^{\mathrm{AL}} = 1$ and $N^{\mathrm{AU}} = 15$ to 30, which yield $K = 4$ or 5. When the membrane area is regarded as a continuous variable, the constraints (5.24) and (5.25) are not utilized.

Other Constraints

Several other types of constraints are required to have a well defined optimization problem. These include logic constraints on the binary variables, as well as nonnegativity and integrality constraints on both the continuous and binary variables. A description of these constraints is included in Appendix D.1.

5.3.3 Solution Strategy

The MINLP design model is solved using the algorithm of Viswanathan and Grossmann [75], which is available in the General Algebraic Modeling System (GAMS) [16] as the solver DICOPT++. The solution technique is based on an outer approximation approach in which the MINLP problem is decomposed into a series of

nonlinear program (NLP) and mixed-integer linear program (MILP) subproblems [64]. These subproblems can be solved using any NLP and MILP solvers that run in the GAMS environment. In this case, CONOPT2 is used for the NLP problem and XA is used for the MILP problem. The following case studies involve 100–250 continuous variables, 15–70 discrete variables, and 100–270 constraint equations. It is important to note that the MINLP formulation usually yields a nonconvex optimization problem. As a result, the solution obtained represents a local optimum. We address this problem by initializing the variables at several different points, setting reasonable bounds on variables, and adjusting the DICOPT++ options to facilitate convergence to the global optimum.

5.4 Case Studies

The MINLP design strategy is used to derive optimal permeator networks for natural gas treatment and enhanced oil recovery applications. The nominal economic parameters and operating conditions are obtained from Spillman *et al.* [72], Babcock *et al.* [5], and Lee *et al.* [52, 53].

- Operating conditions
  - natural gas processing capacity: $U_{f00} = 10$ mol/s (19,353 m^3/day)
  - feed pressure: $P = 3.5$ MPa
  - feed CO_2 concentration: $x_{f0} = 0.20$
  - product permeate pressure: $p_{out} = 0.105$ MPa

- temperature: $T = 40°C$

- Operating requirements
  - product residue CO_2 concentration less than 2%
  - product permeate CO_2 concentration greater than 95% (enhanced oil recovery only)
  - outlet permeate pressure for each stage not less than 0.105 MPa

- Membrane properties
  - CH_4 permeability: $Q_2/d = 1.48 \times 10^{-3}$ mol/MPa·m^{2}s
  - CO_2/CH_4 selectivity: $\alpha = 20$
  - pressure parameter: $C'' = 9.32$ MPa^{2}m^{2}s/mol

- Capital investment
  - membrane housing: $f_{mh} = 200$ \$/m^2 membrane
  - gas-powered compressors: $f_{cp} = 1000$ \$/KW
  - compressor efficiency: $\eta_{cp} = 70\%$
  - working capital: $f_{wk} = 10\%$ of fixed capital investment
  - capital charge: $f_{cc} = 27\%$ per year

- Operating expenses
  - membrane replacement: $f_{mr} = 90$ \$/m^2 membrane

- membrane lifetime: $t_m = 3$ years
- working time: $t_{wk} = 300$ days/year
- maintenance: $f_{mt} = 5\%$ of fixed capital investment per year
- utility and sale gas price: $f_{sg} = 35$ \$/Km^3
- sales gas gross heating value: $f_{hv} = 43$ MJ/m^3
- lost CH_4 is converted to sales gas value

The gas volumes are calculated at standard conditions of 0.102 MPa and 273 K. The pressure parameter C'' is an estimated value based on experimental data [52]. In this work, we allow the membrane area to be both a continuous variable and a discrete variable.

5.4.1 Natural Gas Treatment

For natural gas treatment, the CO_2 concentration of the residue product must be less than 2%. No constraint is placed on the permeate concentration because the permeate stream is a low grade fuel or a waste gas. Flowsheets with two, three and four separation stages are synthesized to produce process configurations and operating conditions which minimize the annual cost. A configuration with continuous membrane area provides a lower bound on the achievable annual cost for a particular number of separation stages. A configuration with discrete membrane area generally will yield a higher process cost, but the resulting flowsheet is more realistic.

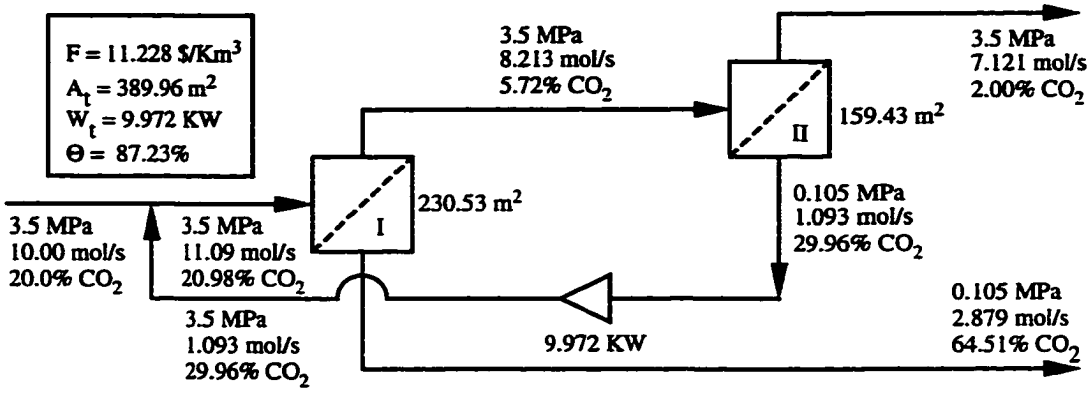

Figure 5.2: Two-stage system with continuous membrane area (natural gas treatment).

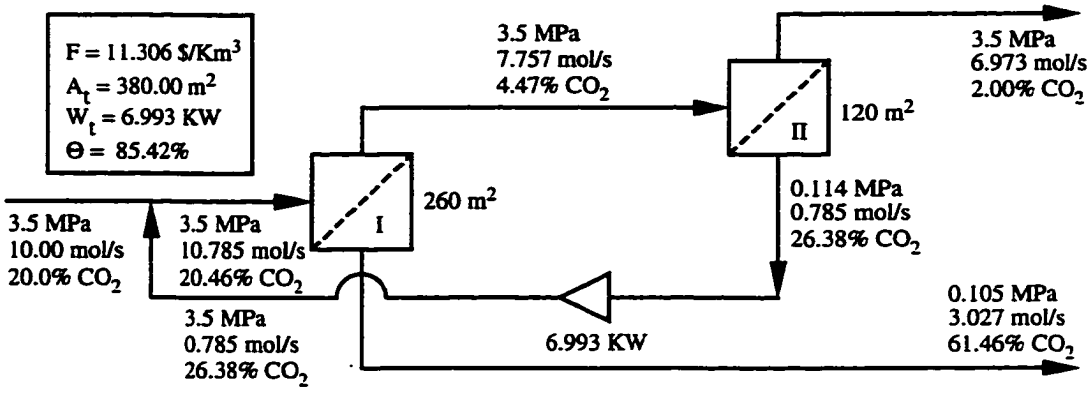

Figure 5.3: Two-stage system with membrane element area of 20 m^2 (natural gas treatment).

The optimal configuration and operating conditions for the two-stage system with continuous membrane area are shown in Figure 5.2, while the corresponding results for a discrete membrane element area of 20 m^2 are shown in Figure 5.3. Note that the system configurations for the two cases are identical, while the operating conditions are significantly different. As expected, the process cost for the discrete area case is slightly higher than that for the continuous area case. The membrane

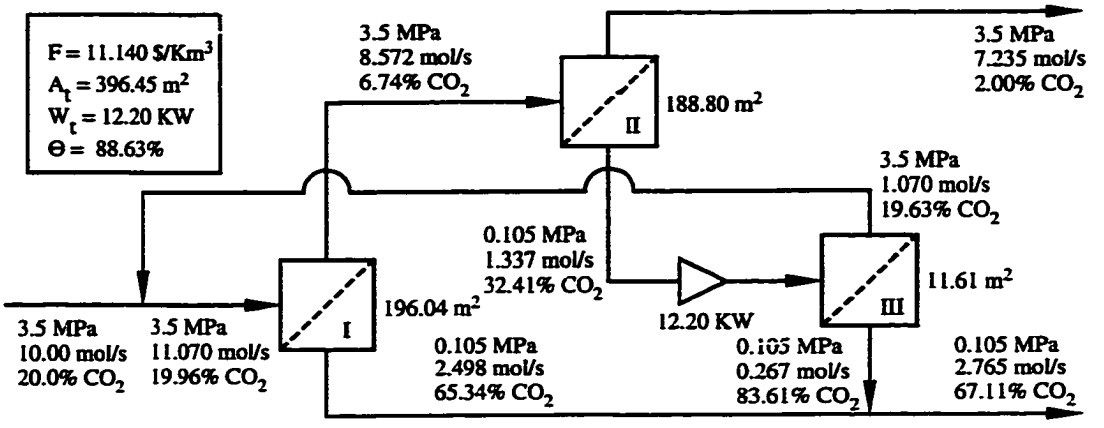

Figure 5.4: Three-stage system with continuous membrane area (natural gas treatment).

area for each individual stage is quite different, but the total membrane area is very similar. The compressor power and CH_4 recovery also differ because of the different distribution of membrane area. Note that both configurations satisfy the 98% CH_4 purity constraint placed on the product residue stream.

Figure 5.4 shows the optimal configuration and operating conditions for the three-stage system with continuous membrane area. This design represents a slight modification of the two-stage configuration (Figure 5.2) in which a small third-stage permeator is used to separate the second-stage permeate stream. The total process cost is slightly lower than that of the two-stage system because of increased CH_4 recovery. The configuration and operating conditions for the three-stage system with discrete membrane element area of 10 m^2 are shown in Figure 5.5. In this case, the system configuration is different from that obtained for the continuous area case (Figure 5.4). The discrete area configuration contains a relatively large

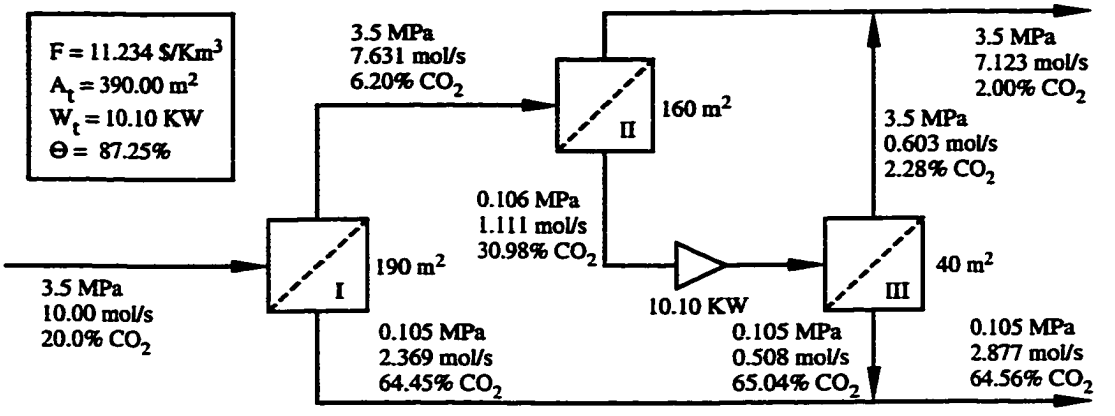

Figure 5.5: Three-stage system with membrane element area of 10 m^2 (natural gas treatment).

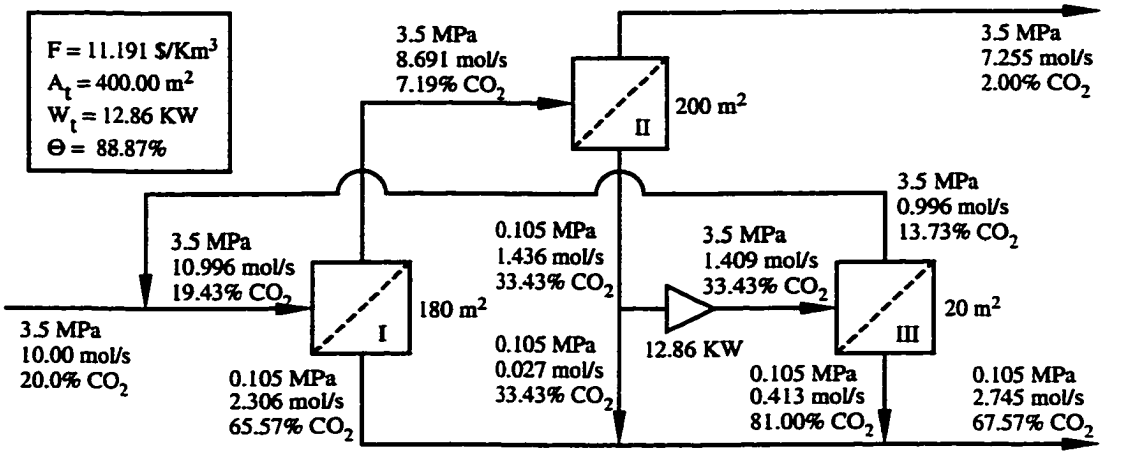

Figure 5.6: Three-stage system with membrane element area of 20 m^2 (natural gas treatment).

third stage which separates the second-stage permeate stream; this makes recycling the third-stage residue stream unnecessary. The process cost is slightly higher than that of the continuous area case. Figure 5.6 shows the design that results for a membrane element area of 20 m^2. This configuration is different from that obtained for continuous membrane area (Figure 5.4) and a discrete area of 10 m^2 (Figure

5.5). The design in Figure 5.6 is a slight modification of the continuous area design obtained by collecting a small portion of the second-stage permeate stream as the final product, while the remainder of the permeate stream is separated in the third stage. Although the process costs for the two configurations are very comparable, the configuration in Figure 5.6 may not be very practical because the flow rate of the product stream (0.027 mol/s) is very small compared to the flow rate of the second-stage permeate stream (1.436 mol/s). Additional logic constraints are required to avoid this type of situation. It is important to note that the configuration obtained for an element area of 10 m^2 (Figure 5.5) has a higher process cost than that obtained with an element area of 20 m^2 (Figure 5.6). This occurs because more binary variables are required to represent the constraint (5.25) when small element areas are used. Apparently, different local optima are found for the two cases.

The optimal configuration and operating conditions for the four-stage system with continuous membrane area are presented in Figure 5.7. This configuration is similar to that obtained for the three-stage system (Figure 5.4), except that the third stage of Figure 5.4 is divided into two smaller stages in Figure 5.7. For discrete membrane element areas of 10 m^2 and 20 m^2, optimal solutions for the four-stage system could not be obtained because membrane area and flow rate differences are too large to allow convergence of the MINLP.

Comparing the configurations and operating conditions shown in Figures 5.2–5.7, we note that the process costs and total membrane areas of the designs are very

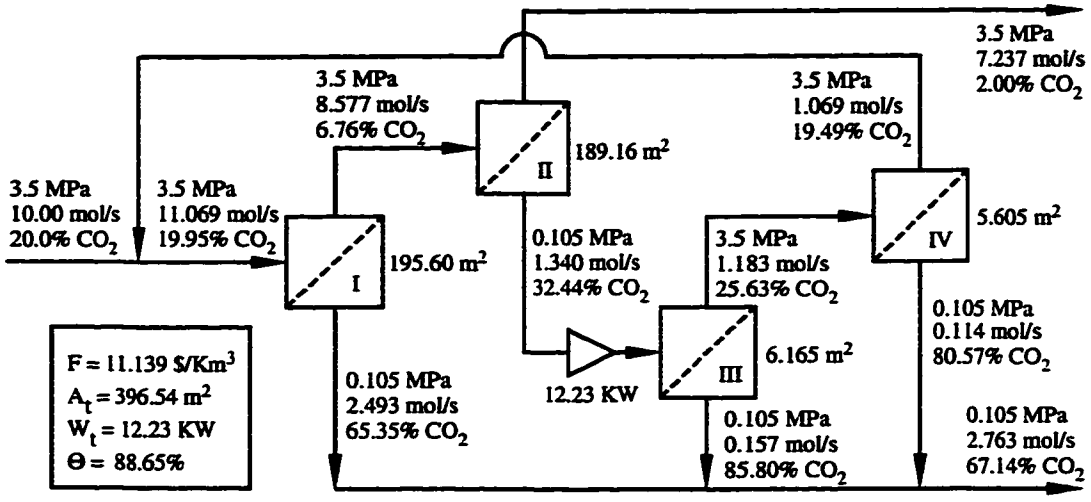

Figure 5.7: Four-stage system with continuous membrane area (natural gas treatment).

similar even though membrane areas of individual stages and operating conditions are quite different. In particular, increasing the number of membrane stages does not affect the process cost significantly. The single purity constraint on the residue concentration results in a large number of degrees of freedom, which allows the total membrane area to be allocated differently with similar overall process costs.

5.4.2 Enhanced Oil Recovery

In CO_2/CH_4 separations for enhanced oil recovery, both the residue and permeate streams must satisfy composition requirements. As in the natural gas treatment case, we design optimal separation networks for two-stage, three-stage, and four-stage membrane systems. The same nominal parameters and feed conditions are used in this application.

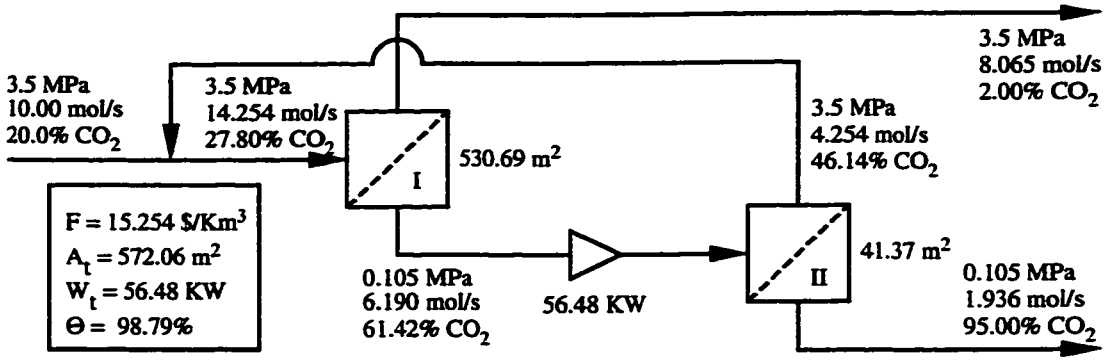

Figure 5.8: Two-stage system with continuous membrane area (enhanced oil recovery).

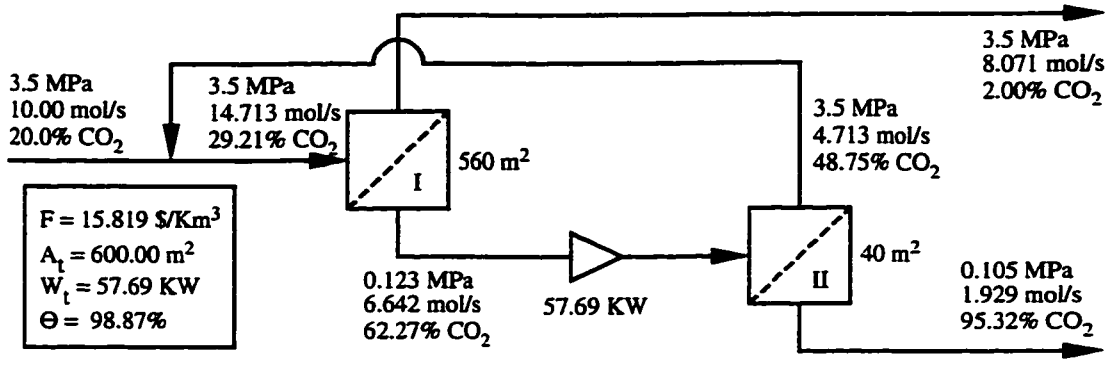

Figure 5.9: Two-stage system with membrane element area of 20 m^2 (enhanced oil recovery).

Figure 5.8 shows the optimal design for the two-stage system with continuous membrane area, while Figure 5.9 shows the optimal design for a discrete membrane element area of 20 m^2. The configurations are identical, but the total membrane area is slightly larger for the discrete area case. It is interesting to note that the larger membrane area in the discrete case results in over separation of the final permeate product. Optimal designs for the three-stage system with continuous membrane area and discrete membrane element area of 20 m^2 are shown in Figures 5.10 and 5.11,

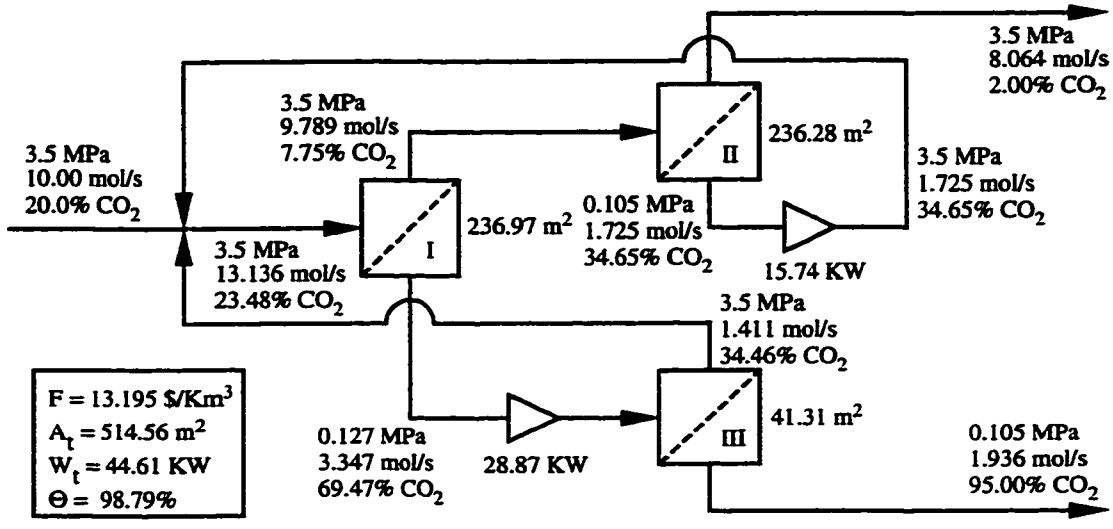

Figure 5.10: Three-stage system with continuous membrane area (enhanced oil recovery).

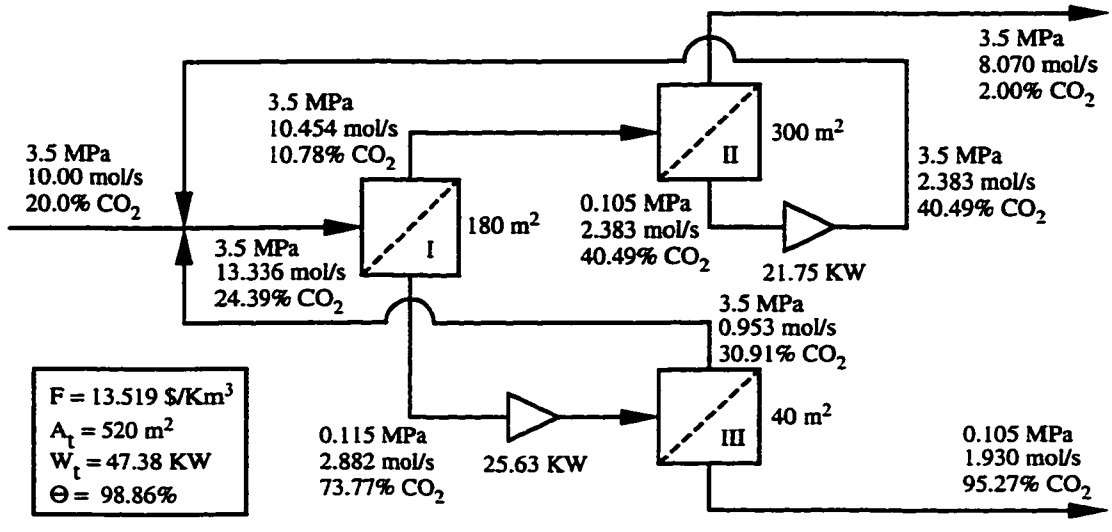

Figure 5.11: Three-stage system with membrane element area of 20 m^2 (enhanced oil recovery).

respectively. The two configurations are identical with recycle of both permeate and residue streams. A detailed investigation of this configuration with continuous membrane area is presented in Chapter 4. Using discrete membrane area significantly

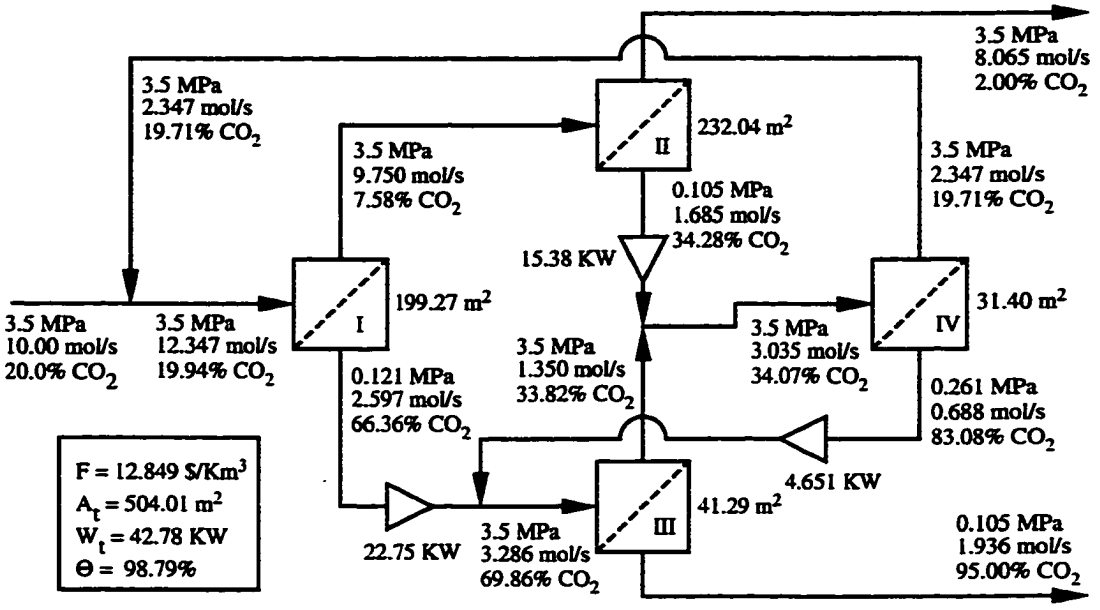

Figure 5.12: Four-stage system with continuous membrane area (enhanced oil recovery).

changes the distribution of membrane area and the operating conditions, but it has little effect on the total membrane area. Note that the permeate purity constraint is exceeded in the discrete area case. Figures 5.12 and 5.13 show optimal designs for four-stage systems with continuous membrane area and discrete membrane element area of 20 m^2, respectively. The configurations are identical and differ from the three-stage configurations (Figures 5.10 and 5.11) in that the fourth stage is used to further separate the second-stage permeate stream and the third-stage residue stream before recycling. As before, the discrete area design exceeds the permeate purity constraint.

The results in Figures 5.8–5.13 demonstrate that increasing the number of membrane stages can significantly decrease the process cost. However, the separation

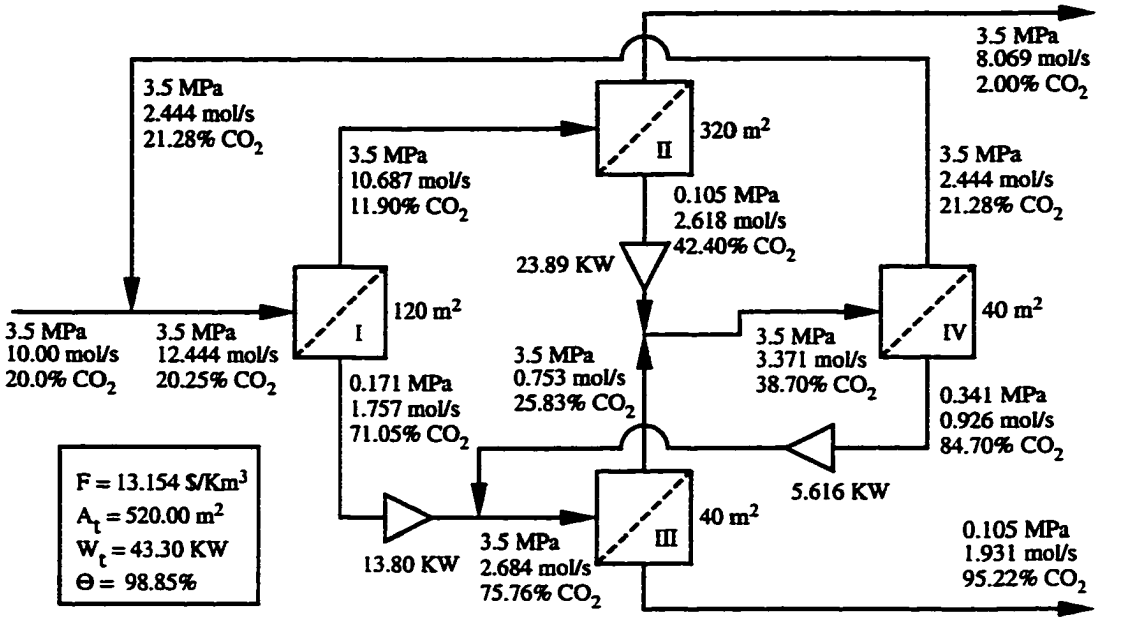

Figure 5.13: Four-stage system with membrane element area of 20 m^2 (enhanced oil recovery).

requirements on both the residue and permeate streams severely restrict the optimal process configuration and operating conditions.

5.5 Summary and Conclusions

An optimal design strategy for spiral-wound gas separation systems based on an algebraic permeator model and mixed-integer nonlinear programming (MINLP) has been developed. The proposed process synthesis approach utilizes a permeator system superstructure which embeds a very large number of possible network configurations. The superstructure is formulated as a MINLP problem and solved using standard optimization tools to yield the flowsheet which minimizes the annual process cost. Case studies for the separation of CO_2/CH_4 mixtures in natural gas treatment

and enhanced oil recovery have been presented. Optimal designs based on a reasonable estimation of process costs are derived for different number of membrane stages with both continuous and discrete membrane area. The results demonstrate that the proposed design methodology provides an effective tool for preliminary design of multi-stage membrane separation systems for binary gas mixtures.

Chapter 6

Process Synthesis for Multicomponent Gas Permeator Systems

6.1 Introduction

In Chapter 5, a MINLP synthesis strategy is developed by utilizing the binary permeator model for multi-stage membrane systems. A permeator system superstructure is used to simultaneously optimize the permeator configuration and operating conditions. In this chapter, we extend the synthesis strategy to multicomponent systems by using the approximate multicomponent model. The permeator superstructure is modified to allow the feed-side pressure to be fixed or a design variable. Optimal designs are derived by solving a MINLP formulation which contains complex and highly nonlinear constraint equations. The methodology is applied to spiral-wound membrane systems separating acid gases (CO_2 and H_2S) from crude natural gas mixtures in natural gas treatment and enhanced oil recovery.

6.2 Problem Statement

The design task involves the determination of the optimal system configuration, as well as specification of the process unit sizes and operating conditions. For MINLP design, it is necessary to derive a permeator system superstructure which embeds all network configurations of practical interest, formulate the superstructure

as a MINLP model, and develop a suitable solution methodology. To facilitate the subsequent development, the following assumptions are invoked:

1. The feed stream contains a multicomponent gas mixture at known conditions.
2. The feed-side pressure for each stage can be fixed at the feed pressure or treated as a design variable.
3. The feed-side pressure drop is negligible for each stage.
4. There is no pressure drop between permeation stages.
5. The permeate stream pressures between stages are design variables, while the product permeate stream pressure is predetermined.
6. All permeators and compressors operate at isothermal conditions.

It is possible to relax some of those assumptions at the expense of a more complex MINLP model.

6.3 Optimal Design Strategy

6.3.1 Permeator System Superstructure

The multicomponent superstructure is derived using similar rules as utilized to develop the superstructure for binary gas permeator systems in Chapter 5. The only difference in the multicomponent formulation is that the fresh feed stream is compressed if a different feed-side operating pressure is needed. As an illustration, the

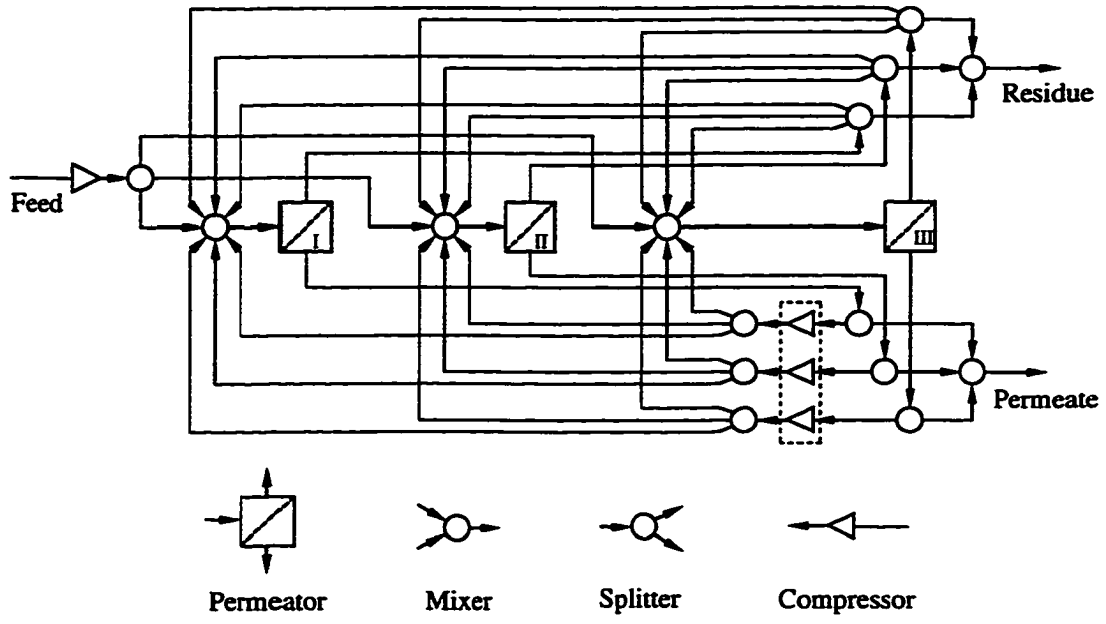

Figure 6.1: Permeator system superstructure with three permeation stages.

superstructure for three separation stages is shown in Figure 6.1. Superstructures containing different number of separation stages are developed similarly.

6.3.2 Mathematical Formulation and Solution Strategy

The multicomponent permeator system superstructure is formulated using the same general expression (5.1) as used for binary permeator systems. The major difference is that more constraint equations and variables are needed for the multicomponent case. The annual process cost is minimized subject to following types of constraints:

1. material balance constraints.

2. permeator model constraints.

3. composition sum constraints.

4. operating requirement constraints.

5. logic constraints.

6. discrete membrane area constraints.

7. nonnegativity and integrality constraints.

Detailed mathematical formulation of the objective function and constraint equations is presented in Appendix E.1. The resulting optimization problem is a mixed-integer nonlinear program (MINLP) which contains complex and highly nonlinear constraint equations. The MINLP solution provides the optimal system configuration and unit sizes, as well as optimal operating conditions for each individual stream.

As in binary case, the MINLP model is solved using the GAMS solvers DICOPT++ for the MINLP problem, CONOPT2 for the NLP problem, and XA for the MILP problem. The following case studies involve 700–2000 continuous variables, 20–70 discrete variables, and 700–2000 constraint equations. The local optimum problem is addressed by initializing the variables at several different points, setting reasonable bounds on variables, and adjusting the DICOPT++ options to facilitate convergence to the global optimum. Nevertheless, there is no guarantee that the global optimum will be found using this procedure.

6.4 Case Studies

The MINLP design strategy is used to derive optimal spiral-wound permeator networks for acid gas separations in natural gas treatment and enhanced oil recovery. The crude natural gas can be regarded as a binary mixture (CO_2 and CH_4), a four-component mixture (CO_2, H_2S, CH_4, and heavier hydrocarbons C^+H) or a five-component mixture (CO_2, H_2S, CH_4, C_2H_6, and heavier hydrocarbons C_2^+H) depending on the natural gas composition and accuracy requirements. We do not include N_2 as a separate component because the permeabilities of N_2 and CH_4 in cellulose acetate membrane are essentially identical [25, 53]. As a result, these components will have the same distribution in various streams. We investigate multistage permeator system design with different number of components while allowing the membrane area to be both a continuous variable and a discrete variable. The feed-side pressure is fixed or considered as a design variable with an upper limit.

The nominal economic parameters and operating conditions are obtained from Lee *et al.* [52, 53], Spillman *et al.* [72], and Babcock *et al.* [5].

- Operating conditions
  - natural gas processing capacity: $U_{f00} = 10$ mol/s (19,353 m^3/day)
  - product permeate pressure: $p_{out} = 0.105$ MPa
  - temperature: $T = 40°C$

- feed pressure P_f and feed concentration x_{f0} are specified in the different case studies

- Operating requirements
  - product residue CO_2 concentration less than 2%
  - product permeate CH_4 concentration less than 5% (enhanced oil recovery only)
  - outlet permeate pressure for each stage not less than 0.105 MPa

- Membrane properties
  - base component CH_4 permeability: $Q_b/d = 1.48 \times 10^{-3}$ mol/MPa·m^{2}s
  - membrane selectivities:

    $\alpha(CO_2/CH_4) = 20$ (all cases)

    $\alpha(H_2S/CH_4) = 16$ (four- and five-component cases)

    $\alpha(C^+H/CH_4) = 0.4$ (four-component case)

    $\alpha(C_2H_6/CH_4) = 0.4$ (five-component case)

    $\alpha(C_2^+H/CH_4) = 0.1$ (five-component case)
  - pressure parameter: $C'' = 9.32$ MPa^{2}m^{2}s/mol

- Capital investment
  - membrane housing: $f_{mh} = 200$ \$/m^2 membrane
  - gas-powered compressors: $f_{cp} = 1000$ \$/KW

- compressor efficiency: $\eta_{cp} = 70\%$
- working capital: $f_{wk} = 10\%$ of fixed capital investment
- capital charge: $f_{cc} = 27\%$ per year

- Operating expenses
  - membrane replacement: $f_{mr} = 90$ \$/m^2 membrane
  - membrane lifetime: $t_m = 3$ years
  - maintenance: $f_{mt} = 5\%$ of fixed capital investment per year
  - working time: $t_{wk} = 300$ days/year
  - utility and sale gas price: $f_{sg} = 35$ \$/Km^3
  - sales gas gross heating value: $f_{hv} = 43$ MJ/m^3
  - lost CH_4 is converted to sales gas value

The gas volumes are calculated at standard conditions of 0.102 MPa and 273 K. The pressure parameter C'' is an estimated value based on experimental data [52]. Note that limited permeability data have been published for the natural gas mixtures of interest. Therefore, the permeability coefficients used in this study have been derived from available information [25, 53, 58]. These values are consistent with data presented in more recent literature [11].

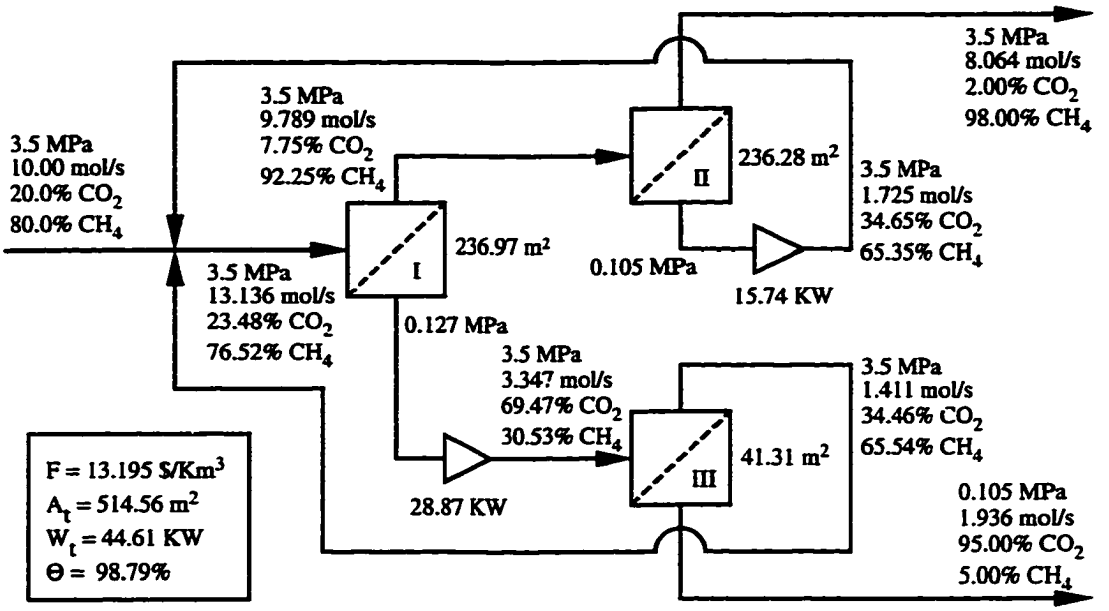

Figure 6.2: Three-stage, two-component system using binary permeator model (enhanced oil recovery).

6.4.1 Two Component Mixture

In Chapter 5, the MINLP design strategy is applied to binary separations by utilizing an approximate binary permeator model. The multicomponent model also has been used to simulate binary separations with spiral-wound permeators (Chapter 3). We have shown the models yield almost identical predictions for single-stage systems as the multicomponent model can be regarded as a generalization of the binary model. We compare these two models for the design of three-stage systems for enhanced oil recovery. In this case, the permeator feed-side pressure is chosen as the fresh feed pressure. Figures 6.2 and 6.3 show the optimal flowsheets obtained using the binary and multicomponent models, respectively. The configurations are identical, and the operating conditions are effectively identical with only small

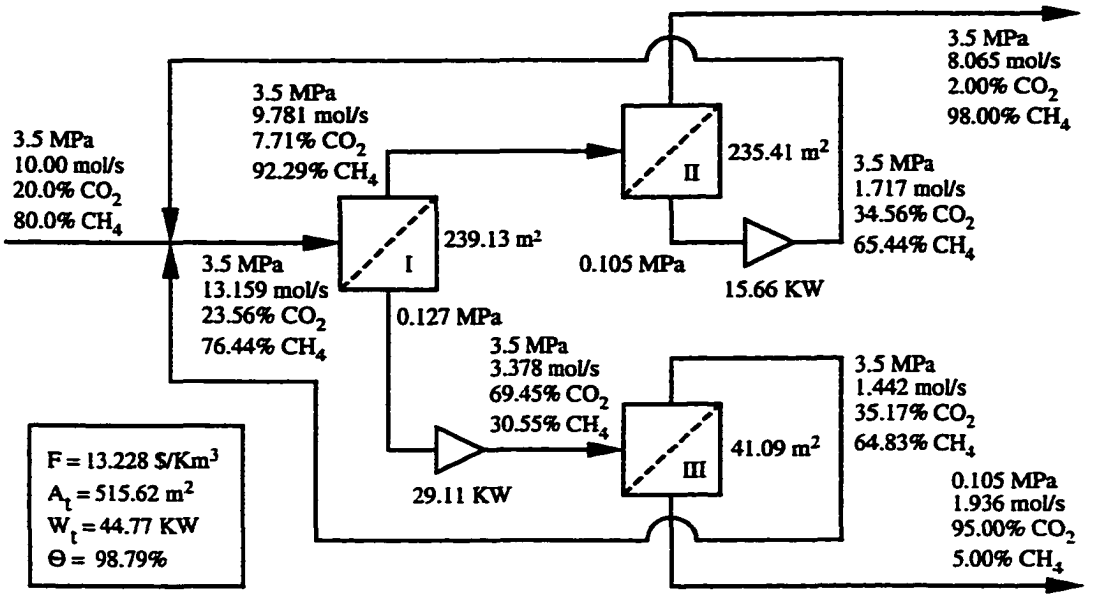

Figure 6.3: Three-stage, two-component system using multicomponent permeator model (enhanced oil recovery).

differences in the permeator and compressor unit sizes. These results demonstrate the multicomponent MINLP design strategy reduces to the binary formulation when applied to binary gas mixtures.

6.4.2 Four Component Mixture

In this case, we assume the natural gas mixture is comprised of CO_2, H_2S, CH_4, and heavier hydrocarbons C^+H. The composition of the fresh feed is chosen as 19.0% CO_2, 1.0% H_2S, 73.0% CH_4, and 7.0% C^+H, and the fresh feed pressure is 3.5 MPa. These conditions are consistent with actual applications [52, 53]. As mentioned earlier, N_2 is not explicitly included because it has the same permeability as CH_4 in cellulose acetate membrane. The permeator feed-side pressure is taken as the fresh

feed pressure. We apply the MINLP design strategy to both natural gas treatment and enhanced oil recovery applications.

For natural gas treatment, the CO_2 concentration of the residue product must be no greater than 2%. No concentration constraint is placed on the permeate stream because it is a low grade fuel or a waste gas. Flowsheets with two and three separation stages which minimize the annual cost are synthesized. A configuration with continuous membrane area provides a lower bound on the annual cost for a particular number of separation stages.

The optimal flowsheet for a two-stage system with continuous membrane area is shown in Figure 6.4, while the corresponding result for a discrete membrane element area of 20 m^2 is shown in Figure 6.5. The system configurations for the two cases are identical, while the operating conditions are significantly different. The membrane area for each individual stage is different, but the total membrane area is very similar. The total compressor power and CH_4 recovery differ because of the different distribution of membrane area. As expected, the process cost for the discrete area case is slightly higher than that obtained for continuous area. Note that both configurations satisfy the 2% CO_2 purity constraint placed on the product residue stream.

Figure 6.6 shows the optimal flowsheet for a three-stage system with continuous membrane area. This design represents a slight modification of the two-stage configuration (Figure 6.4) in which a small third-stage permeator is used to separate

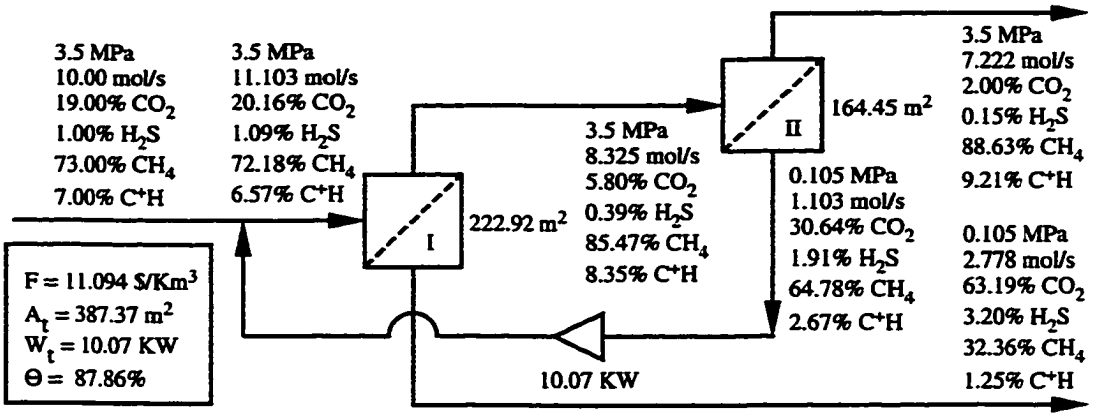

Figure 6.4: Two-stage, four-component system with continuous membrane area (natural gas treatment).

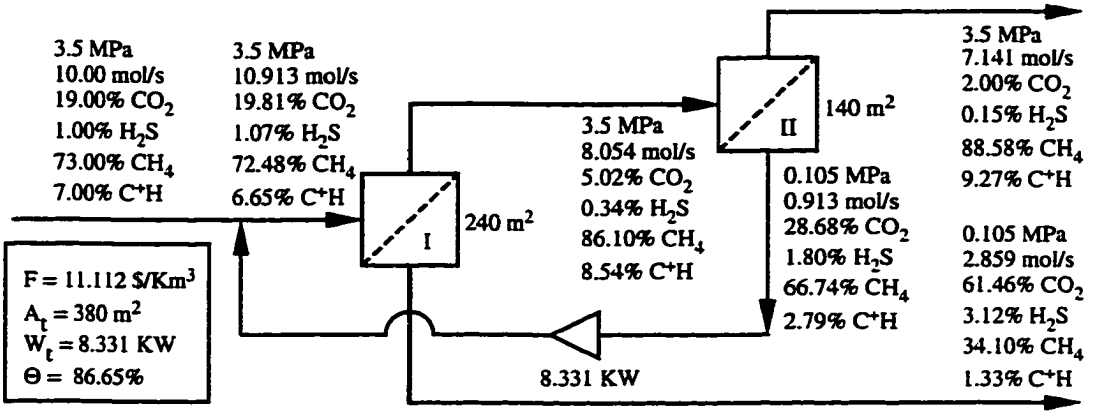

Figure 6.5: Two-stage, four-component system with membrane element area of 20 m^2 (natural gas treatment).

the second-stage permeate stream. The total process cost is slightly lower than that of the two-stage system because of increased CH_4 recovery. The optimal flowsheet for a three-stage system with discrete membrane element area of 20 m^2 is shown in Figure 6.7. In this case, the system configuration is different from that obtained for the continuous area case (Figure 6.6) in that the third-stage residue stream recycles to the second stage rather than the first stage. Even though the process costs

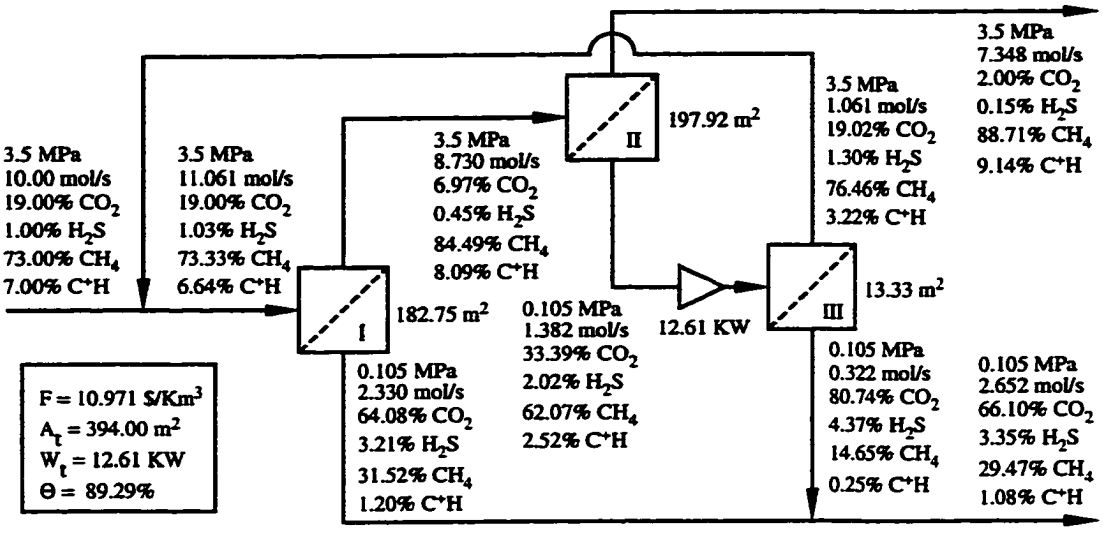

Figure 6.6: Three-stage, four-component system with continuous membrane area (natural gas treatment).

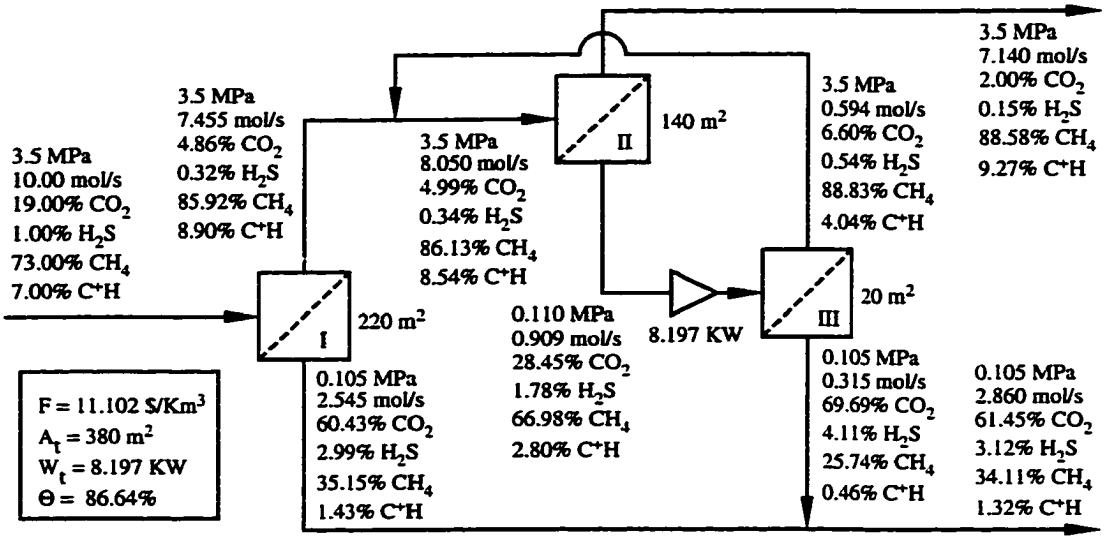

Figure 6.7: Three-stage, four-component system with membrane element area of 20 m^2 (natural gas treatment).

for the two configurations are very similar, the distributions of membrane areas and CH_4 recoveries are significantly different. As a result, different flow rates and compositions of residue and permeate products are obtained.

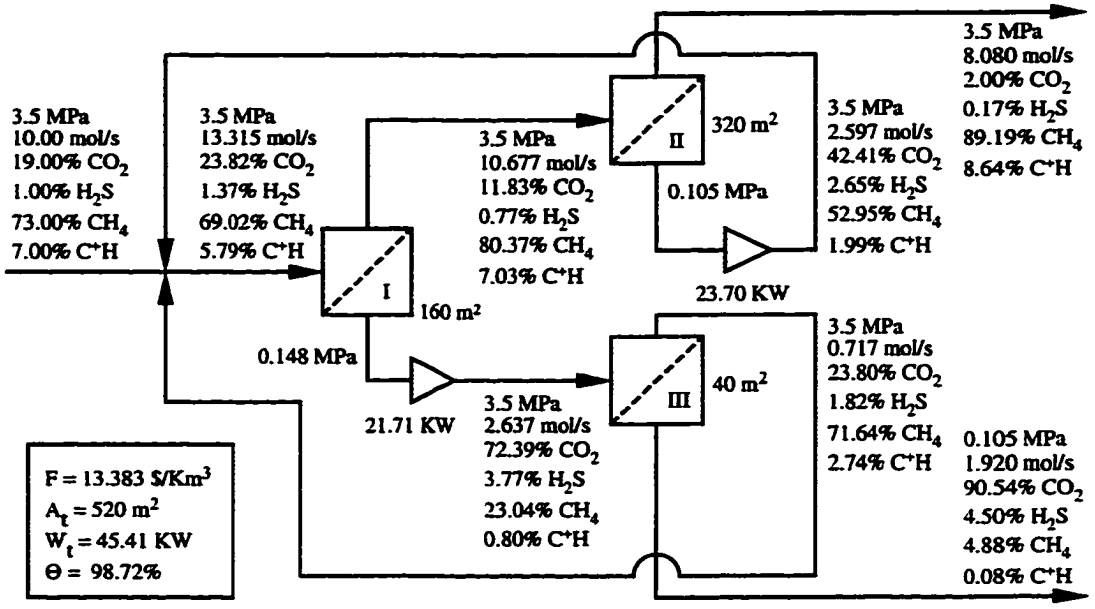

Figure 6.8: Three-stage, four-component system with membrane element area of 20 m^2 (enhanced oil recovery).

As in the binary case, the process costs and total membrane areas for different numbers of stages are very similar even though membrane areas of individual stages and operating conditions are quite different. Increasing the number of membrane stages does not affect the process cost significantly.

In acid gas separations arising in enhanced oil recovery, both the residue and permeate streams must satisfy composition constraints. We design optimal separation networks for three-stage and four-stage membrane systems. Figures 6.8 and 6.9 show the optimal designs for three-stage and four-stage systems, respectively, with a discrete membrane element area of 20 m^2. Results for continuous membrane area are not presented for the sake of brevity. Both configurations are identical to the configurations obtained for binary mixtures. The residue product concentration of

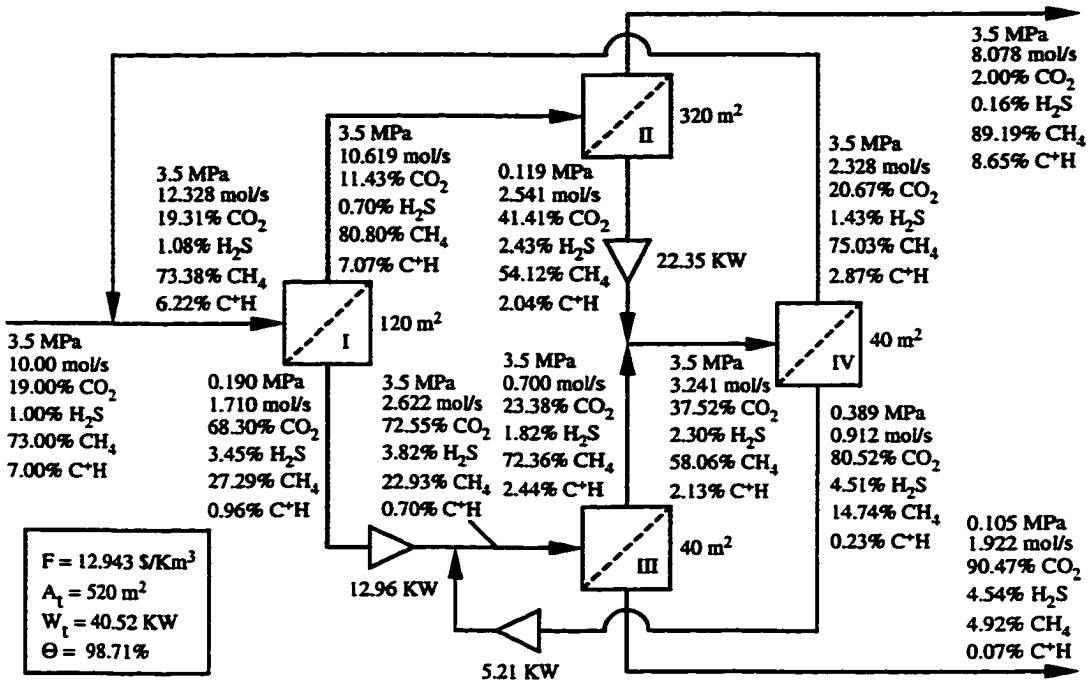

Figure 6.9: Four-stage, four-component system with membrane element area of 20 m^2 (enhanced oil recovery).

H_2S and permeate product concentration of C^+H are small compared to the major components CH_4 and CO_2. Note that increasing the number of membrane stages can significantly decrease the process cost because the separation requirements on both the residue and permeate streams severely restrict the optimal flowsheet.

6.4.3 Five Component Mixture

The MINLP design strategy is applied to a five-component natural gas mixture to investigate its robustness for wider variations in membrane selectivities and stream compositions. We choose the feed compositions for an enhanced oil recovery application [52, 53]: 19.5% CO_2, 0.5% H_2S, 73.0% CH_4, 4.0% C_2H_6, and 3.0% heavier

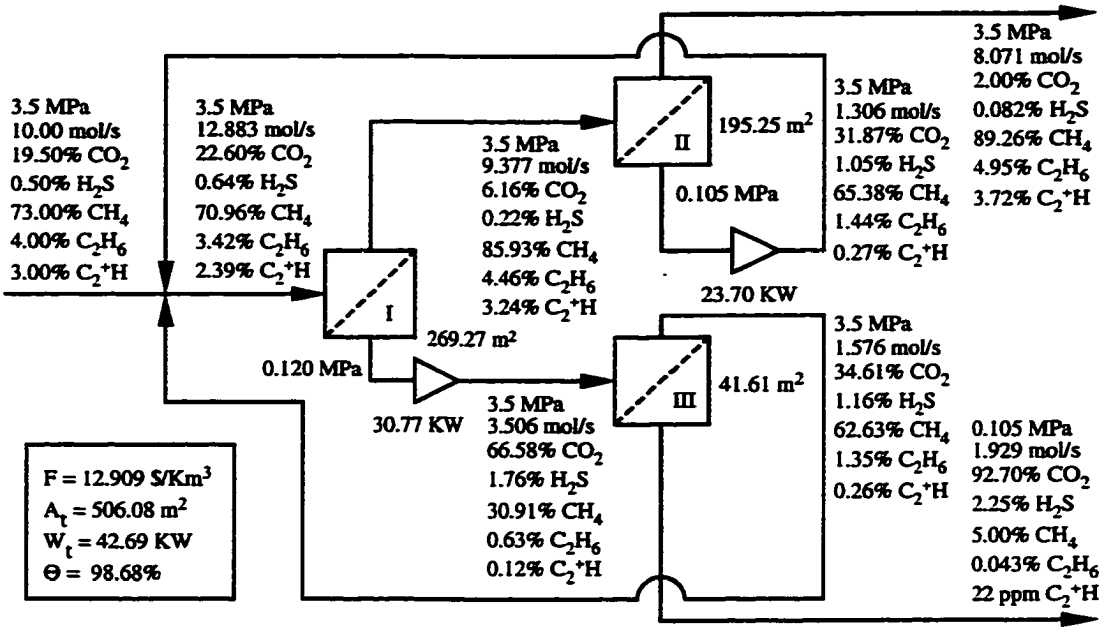

Figure 6.10: Three-stage, five-component system with continuous membrane area (enhanced oil recovery).

hydrocarbons C_2^+H. The feed-side pressure is chosen as the fresh feed pressure (3.5 MPa). Figures 6.10 and 6.11 show the optimal design obtained for three-stage and four-stage systems, respectively, with continuous membrane area. The configuration in Figure 6.10 is identical to that in Figure 6.8, while the configuration in Figure 6.11 is very similar to that in Figure 6.9. The major difference from the four-component case is that small concentrations of H_2S in the residue products (about 0.08%) and C_2^+H in the permeate product (about 20 ppm) are observed. These results indicate that the proposed MINLP design model and optimization procedure are sufficiently robust to synthesize permeator systems with very small stream concentrations.

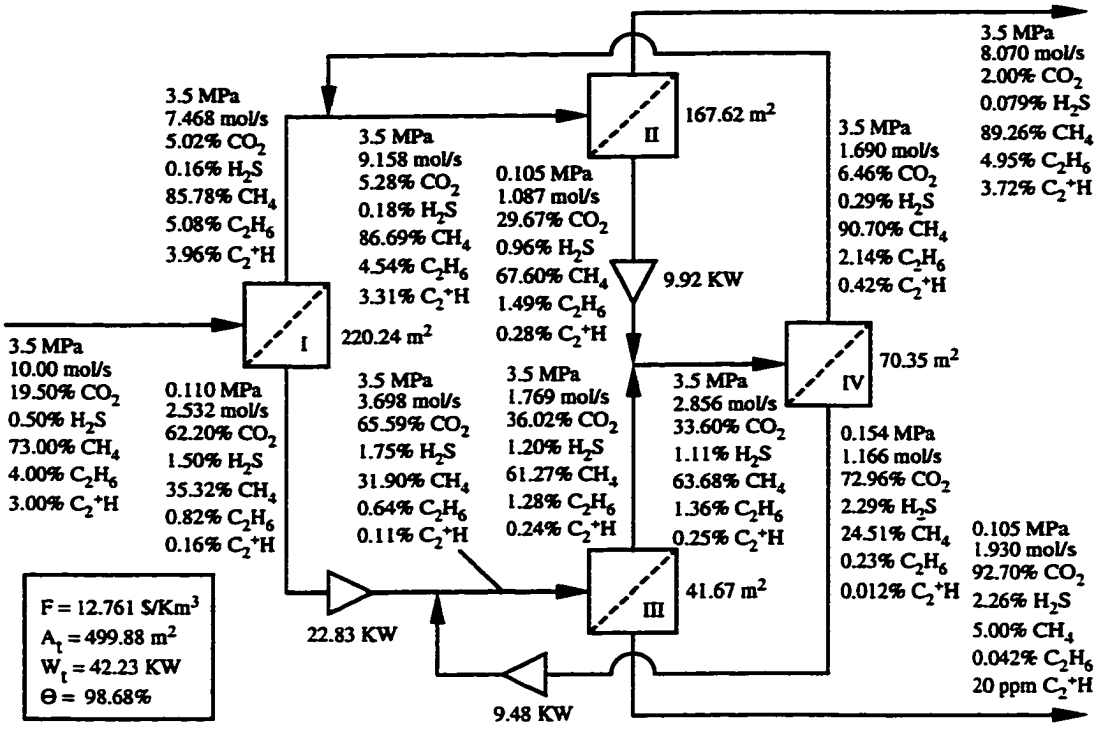

Figure 6.11: Four-stage, five-component system with continuous membrane area (enhanced oil recovery).

6.4.4 Optimization of Feed-Side Pressure

To generate the previous results, we assumed a relatively high fresh feed pressure and set the permeator feed-side pressure equal to the fresh feed pressure. In some applications, optimization of feed-side pressure may be necessary to enhance process economics. The optimal feed-side pressure represents a trade-off between compressor power and total membrane area. Furthermore, an upper limit on the pressure must be imposed due to material and mechanical limitations of the equipment. We investigate feed-side pressure optimization by utilizing the feed stream compressor in the permeator system superstructure (Figure 6.1). The four-component natural

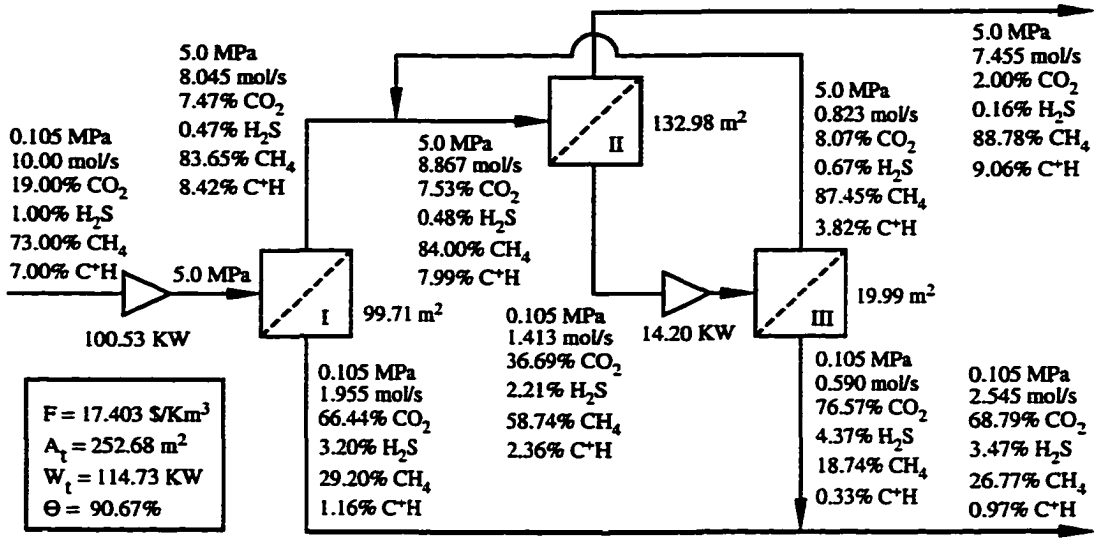

Figure 6.12: Feed-side pressure optimization for three-stage, four-component system (natural gas treatment).

gas mixture (19.0% CO_2, 1.0% H_2S, 73.0% CH_4, and 7.0% C^+H) is available at a low pressure (0.105 MPa). The upper limit for the feed-side pressure is 5.0 MPa. Figure 6.12 shows the optimal design of a three-stage configuration with continuous membrane area for natural gas treatment, while Figure 6.13 shows the optimal four-stage configuration with continuous membrane area for enhanced oil recovery. In each case, a relatively large fresh feed compressor is needed but the permeator connections are very similar to the previous cases (Figure 6.7 and 6.9). Note that the feed-side pressure goes to the upper limit for the economic parameters chosen. A lower pressure can be obtained for different economic parameters. Also note that the superstructure shown in Figure 6.1 may introduce multiple compressors which could be combined into a single compressor. A different superstructure is needed to minimize the number of compressors.

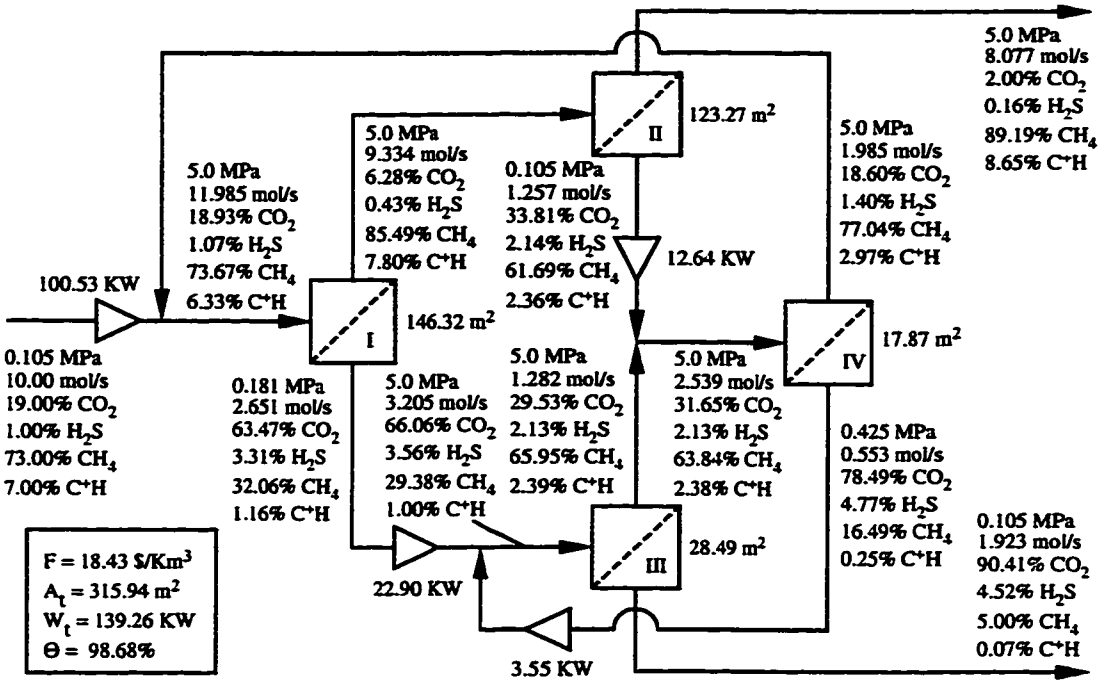

Figure 6.13: Feed-side pressure optimization for four-stage, four-component system (enhanced oil recovery).

6.5 Summary and Conclusions

An optimal design strategy utilizing an algebraic permeator model and mixed-integer nonlinear programming (MINLP) has been developed for membrane systems separating multicomponent gas mixtures. The process design approach is based on a permeator system superstructure which embeds a very large number of possible network configurations. The superstructure is formulated as a MINLP model and solved using standard optimization tools to yield the flowsheet which minimizes the annual process cost. Case studies have been presented for spiral-wound permeators separating acid gases (CO_2 and H_2S) from crude natural gas mixtures in natural gas treatment and enhanced oil recovery. Optimal designs are derived for different

number of membrane stages with both continuous and discrete membrane area. Optimization of the feed-side pressure also is investigated. The results demonstrate that the proposed design methodology provides an effective tool for preliminary design of multi-stage, multicomponent gas membrane systems, including those with very small component concentrations.

Chapter 7

Conclusions and Recommendations

The economic viability of gas membrane separation processes depends critically on process design. The competitiveness of membrane systems can be enhanced by developing improved modeling and design techniques. Available spiral-wound permeator models have several shortcomings including poor prediction accuracy and/or computational inefficiency. Existing sequential design techniques yield suboptimal flowsheets when multiple permeation stages are required.

In this research, more effective modeling and design techniques for spiral-wound membrane systems used to separate binary and multicomponent gas mixtures have been developed. The approximate permeator models are well suited for process design because the resulting nonlinear algebraic equations can be solved very efficiently and provide excellent prediction accuracy over a wide range of operating conditions. The nonlinear programming (NLP) design technique is used to optimize operating conditions and analyze parameter sensitivities for a prespecified permeator configuration. The mixed-integer nonlinear programming (MINLP) design strategy allows simultaneous optimization of permeator configuration and operating conditions to minimize the total process cost. Both modeling and design methodologies are sufficiently robust to handle gas separations with very demanding requirements. This work has yielded five journal papers (four published and one submitted) and three

conference presentations which are listed in Appendix F. To more fully conclude this work, it is necessary to provide a brief synopsis of each general area and provide recommendations for further research.

7.1 Permeator Modeling

Chapter 2 presents an approximate modeling technique for spiral-wound permeators separating binary gas mixtures. The approach is based on the assumption that the residue flow rate is constant in the direction of permeate flow. The approximate model is derived by applying this assumption to a standard fundamental model [57]. The original boundary value problem is reduced to a more tractable problem involving a small number of nonlinear algebraic equations. Additional justification for the modeling technique is obtained via comparison to one-point collocation. A nonlinear programming strategy for estimating unknown/uncertain parameters from experimental data also has been proposed. A case study of CO_2/CH_4 separations has shown that the proposed model yields accurate predictions with considerably less computing time than the fundamental model.

Chapter 3 presents two multicomponent models for spiral-wound permeators. It appears that they are the only multicomponent spiral-wound models in the open literature which account for permeate-side pressure variations. The basic transport model is derived from fundamental material balances and permeation relations, while the approximate model is derived directly from the basic model by assuming the residue flow rate is constant along the direction of permeate flow. The approximate

model is developed by using Gaussian quadrature to approximate integral expressions and the fourth-order Runge-Kutta-Gill algorithm to solve the initial value problem for the feed-side flow rate and compositions. The two models are compared for the separation of CO_2 from hydrocarbons in a four component mixture, as well as the separation of an eight component mixture. The models show close agreement for a wide range of operating conditions. In addition, a simple method for estimating uncertain/unknown model parameters from experimental data has been proposed and successfully applied to a CO_2/CH_4 mixture.

On the basis of their accuracy and efficiency, the binary and multicomponent approximate models are well suited for preliminary simulation and design of complex membrane separation systems. However, some assumptions used in the development of the basic transport models may potentially limit their applicability. Issues needing further consideration include: (*i*) flow resistance due to the porous support of the asymmetric membrane [56]; (*ii*) longitudinal mixing on the feed side [56]; (*iii*) radial mixing on the permeate side [49]; (*iv*) pressure and concentration dependent permeabilities [79]; and (*v*) nonisothermal operation [22]. The impact of each effect on permeator performance and approximate model development needs to be investigated to determine an appropriate compromise between prediction accuracy and computational efficiency.

Approximate models also should be developed for hollow-fiber membrane permeators because associated fundamental models are comprised of nonlinear ordinary

differential equations with mixed boundary conditions. Although several approximate modeling methods such as driving force approximation [17, 50, 62], finite differences [20, 50], orthogonal collocation [39] and finite elements [74] have been proposed, existing models need to be evaluated and improved for process design. The objective should be to derive models which are sufficiently accurate for prediction of permeator performance and computationally efficient for process design and optimization.

7.2 Membrane System Design

Chapter 4 presents a design strategy for spiral-wound membrane systems based on the approximate binary permeator model and nonlinear programming (NLP). The design method is applied to the separation of CO_2/CH_4 mixtures in natural gas treatment and enhanced oil recovery. Parameter sensitivities of the proposed designs have been investigated by changing operating conditions, membrane properties, and economic parameters. The NLP design strategy provides an efficient methodology for optimization of operating conditions for multistage membrane systems, including those with stringent separation requirements.

Chapter 5 presents an optimal design strategy based on the approximate binary permeator model and mixed-integer nonlinear programming (MINLP). The proposed process synthesis approach utilizes a permeator system superstructure which embeds a very large number of possible network configurations. The superstructure is formulated as a MINLP problem and solved using standard optimization tools to

yield the system configuration and operating conditions which minimize the annual process cost. The design strategy is studied for the separation of CO_2/CH_4 mixtures in natural gas treatment and enhanced oil recovery.

In Chapter 6, the MINLP design strategy is extended to multicomponent membrane systems by using the approximate multicomponent model. Case studies have been presented for spiral-wound permeators separating acid gases (CO_2 and H_2S) from crude natural gas mixtures in natural gas treatment and enhanced oil recovery. For binary and multicomponent mixtures, optimal designs are derived for different number of membrane stages with both continuous and discrete membrane area. Optimization of the feed-side pressure also is investigated. The results demonstrate that the proposed MINLP design methodologies can be effectively used for design of multi-stage gas membrane systems, including those with very small component concentrations.

The proposed NLP and MINLP design strategies provide systematic frameworks for the design and optimization of membrane gas separation systems. They are most appropriate for deriving preliminary designs due to the approximate nature of the permeator models and cost functions. A potential problem is that the NLP and MINLP formulations usually yield nonconvex optimization problems. As a result, the solutions obtained by GAMS solvers such as CONOPT and DICOPT++ only represent local optima. In this work, the problem is addressed by initializing variables at several different points, setting reasonable bounds on variables, and/or

adjusting the solver options to facilitate convergence to the global optimum. However, this approach does not ensure the global optimum will be found.

There are two possible approaches to handle the nonconvexity problem in permeator system design. The first approach utilizes convexification procedures to reduce the number of nonconvexities in the MINLP model [31, 36, 43]. This should improve the performance of MINLP solvers such as DICOPT++, although convergence to the global optimum can be ensured only if all nonconvexities are removed. The second approach involves the use of global solution algorithms for MINLP problems [1, 30, 70]. Unlike solvers such as DICOPT++, these algorithms ensure convergence to the global optimum in the presence of nonconvexities. Unfortunately, existing global optimization methods are applicable only to relatively restrictive classes of nonconvex MINLP problem [70]. Further research on global optimization procedures for membrane systems are needed.

Another software package, MINOPT (Mixed Integer Nonlinear OPTimizer), has been developed for the solution of MINLP problems [28]. MINOPT is a comprehensive and flexible optimization package which can solve MINLP formulations using a variety of algorithms including generalized benders decomposition, outer approximation with equality relaxation, and generalized cross decomposition. It also allows solution of MINLP models with differential and algebraic constraints using specified process simulators and ordinary differential equation solvers. The proposed membrane system design strategies can be further tested using MINOPT. Unfortunately,

it appears that MINOPT can only handle differential equation constraints of the initial-value type. As a result, it will be difficult to use the basic transport models for membrane system design because of the algebraic-differential-integral equations with mixed boundary conditions.

Further improvement for MINLP design is the development of improved permeator system superstructures. The superstructures proposed in this work are appropriate for applications in which there are two product streams. In some applications (especially for multicomponent mixtures), process economics may necessitate the production of multiple product streams. More general superstructures need to be developed to handle such applications. Moreover, the proposed permeator superstructures need to be modified to minimize the number of compressors and to enhance computational efficiency of the resulting MINLP problem.

To facilitate industrial application of the proposed methodology, an integrated software package could be developed to provide process engineers access to the modeling and design codes. The resulting simulator would allow engineers to evaluate the economic feasibility of membrane systems, determine the process flowsheet for preliminary design, and compare and optimize membrane system performance for different economic and operating conditions. The software package would offer the following capabilities:

1. A database of permeator properties such as membrane permeabilities and permeate pressure drop parameters.

2. Simulation of single-stage and multi-stage configurations separating binary and multicomponent mixtures.

3. Optimization of operating conditions for a specific multi-stage configuration.

4. Optimal design of multi-stage configurations for binary and multicomponent gas separations.

To make the program easy to use, a graphical user interface (GUI) can be used to input information and display results. The output could be presented in a spreadsheet and graphics format which shows the process flowsheet, operating conditions, and economic parameters. A flexible link to different optimization solvers such as those in GAMS will be an essential part of the software package.

Bibliography

[1] C. S. Adjiman, I. P. Androulakis, and C. A. Floudas. Global optimization of MINLP problems in process synthesis and design. *Computers Chem. Eng.*, 21:S445–S450, 1997.

[2] R. Agrawal. A simplified method for synthesis of gas separation membrane cascades with limited numbers of compressors. *Chem. Eng. Sci.*, 52:1029–1044, 1997.

[3] R. Agrawal and J. Xu. Gas separation membrane cascades. II. Two compressor cascades. *J. Membrane Sci.*, 112:129, 1996.

[4] R. Agrawal and J. Xu. Gas separation membrane cascades utilizing limited numbers of compressors. *AIChE J.*, 42:2141–2154, 1996.

[5] R. E. Babcock, R. W. Spillman, C. S. Goddin, and T. E. Cooley. Natural gas cleanup: A comparison of membrane and amine treatment processes. *Energy Prog.*, 8:135–142, 1988.

[6] E. M. L. Beale. The state of the art in numerical analysis. In *Integer Programming*, page 409. D. Jacobs Ed. Academic Press, 1977.

[7] B. D. Bhide and S. A. Stern. A new evaluation of membrane processes for the oxygen-enrichment of air. I. Identification of optimum operating conditions and process configuration. *J. Membrane Sci.*, 62:13–35, 1991.

[8] B. D. Bhide and S. A. Stern. A new evaluation of membrane processes for the oxygen-enrichment of air. II. Effect of economic parameters and membrane properties. *J. Membrane Sci.*, 81:37–58, 1991.

[9] B. D. Bhide and S. A. Stern. Membrane processes for the removal of acid gases from natural gas. I. Process configuration and optimization of operating conditions. *J. Membrane Sci.*, 81:209–237, 1993.

[10] B. D. Bhide and S. A. Stern. Membrane processes for the removal of acid gases from natural gas. II. Effect of operating conditions, economic parameters, and membrane properties. *J. Membrane Sci.*, 81:239–252, 1993.

[11] B. D. Bhide, A. Voskericyan, and S. A. Stern. Hybrid processes for the removal of acid gases from natural gas. *J. Membrane Sci.*, 140:27–49, 1998.

[12] R. B. Bird, W. E. Stewart, and E. D. Lightfoot. *Transport Phenomena.* Wiley International Edition, 1960.

[13] W. A. Bollinger, D. L. MacLean, and R. S. Narayan. Separation systems for oil refining and production. *Chem. Eng. Prog.*, pages 27–32, October 1982.

[14] B. Borchers and J. E. Mitchell. An improved branch and bound algorithm for mixed integer nonlinear programms. Technical Report RPI Math Report No. 200, Rensselaer Polytechnic Institute, 1991.

[15] H. I. Britt and R. H. Luecke. The estimation of parameters in nonlinear, implicit models. *Technometrics*, 15:233–247, 1973.

[16] A. Brooke, D. Kendrick, and A. Meeraus. *GAMS: A User's Guide.* Scientific Press, Palo Alto, CA, 1992.

[17] H. Chen, G. Jiang, and R. Xu. An approximate solution for countercurrent gas permeation separating multicomponent mixtures. *J. Membrane Sci.*, 95:11–19, 1994.

[18] R. T. Chern, W. J. Koros, and P. S. Fedkiw. Simulation of a hollow-fiber separation: The effects of process and design variables. *Ind. Eng. Chem. Des. Dev.*, 24:1015–1022, 1985.

[19] A. B. Coady and J. A. Davis. CO_2 recovery by gas permeation. *Chem. Eng. Prog.*, pages 44–49, October 1982.

[20] D. T. Coker, B. D. Freeman, and G. K. Fleming. Modeling multicomponent gas separation using hollow-fiber membrane contactors. *AIChE J.*, 44:1289–1302, 1998.

[21] T. E. Cooley and W. L. Dethloff. Field tests show membrane processes attractive. *Chem. Eng. Prog.*, pages 45–50, October 1985.

[22] A. E. Cornelissen. Heat effect in gas permeation, with special reference to spiral-wound membranes. *J. Membrane Sci.*, 76:185, 1993.

[23] V. G. Dovi, A. P. Reverberi, and L. Maga. Optimal design of sequential experiments for error-in-variables models. *Comput. Chem. Engng.*, 17:111–115, 1993.

[24] M. A. Duran and I. E. Grossmann. A outer approximation algorithm for a class of mixed integer nonlinear programs. *Math Prog.*, 36:307, 1986.

[25] H. M. Ettouney, G. Al-Enezi, and R. Hughes. Modelling of enrichment of natural gas wells by membranes. *Gas Sep. Purif.*, 9:3–11, 1995.

[26] B. A. Finlayson. *Nonlinear Analysis in Chemical Engineering.* McGraw-Hill, New York, 1980.

[27] R. Fletcher and S. Leyffer. Sloving mixed integer nonliner programms by outer approximation. *Math Prog.*, 66:327, 1994.

[28] C. A. Floudas. *Nonlinear and Mixed-Integer Optimization.* Scientific Press, Oxford, 1995.

[29] C. A. Floudas, A. Aggarwal, and A. R. Ciric. Global optimum search for nonconvex NLP and MINLP problems. *Computers Chem. Engng.*, 13:1117–1132, 1989.

[30] C. A. Floudas and I. E. Grossmann. Algorithmic approaches to process synthesis: Logic and global optimization. In *Proc. Foundations of Computer-Aided Design (FOCAD '94)*, pages 198–221, Snowmass, CO, 1994.

[31] C. A. Floudas and G. E. Paules. A mixed-integer nonlinear programming formulation for the synthesis of heat integrated distillation sequences. *Computers Chem. Eng.*, 12(6):531, 1988.

[32] F. J. C. Fournie and J. P. Agostini. Permeation membranes can efficiently replace conventional gas treatment processes. *J. Petroleum Tech.*, pages 707–712, June 1987.

[33] A. M. Geoffrion. Generalized benders decomposition. *J. Optim. Theory Appl.*, 10(4):237, 1972.

[34] I. E. Grossmann and M. M. Daichendt. New trends in optimization-based approaches to process synthesis. *Computers Chem. Eng.*, 20:665–683, 1996.

[35] I. E. Grossmann and Z. Kravanja. Mixed-integer nonlinear programming techniques for process systems engineering. *Computers Chem. Eng.*, 19:S189–S204, 1995.

[36] I. E. Grossmann and R. W. H. Sargent. Optimal design of multipurpose chemical plants. *I&EC Proc. Des. Dev.*, 18(2):343, 1979.

[37] T. Gundersen. Achievements and future challenges in industrial design applications of process system engineering. In *Process System Engineering*, page I.1.1, 1991.

[38] K. Holmberg. On the convergence of the cross decomposition. *Math Prog.*, 47:269, 1990.

[39] S. P. Kaldis, G. C. Kapantaidakis, T. I. Papadopoulos, and G. P. Sakellaropoulos. Simulation of binary gas separation in hollow fiber asymmetric membranes by orthogonal collocation. *J. Membrane Sci.*, 142:43–59, 1998.

[40] I.-W. Kim, M. J. Liebman, and T. F. Edgar. Robust error-in-variables estimation using nonlinear programming techniques. *AIChE J.*, 36:985–993, 1990.

[41] C. J. King. *Separation Processes.* McGraw-Hill, New York, 1980.

[42] G. R. Kocis and I. E. Grossmann. Relaxation strategy for the structural optimization of process flow sheets. *Ind. Eng. Chem. Res.*, 26:1869, 1987.

[43] G. R. Kocis and I. E. Grossmann. Global optimization of nonconvex MINLP problems in process synthesis. *Ind. Eng. Chem. Res.*, 27(8):1407, 1988.

[44] A. L. Kohl and F. C. Riesenfeld. *Gas Purification.* Gulf Publishing Co., Houston, TX, 1985.

[45] W. J. Koros. Gas separation. In R. W. Baker, E. L. Cussler, W. Eykamp, W. J. Koros, R. L. Riley, and H. Strathmann, editors, *Membrane Separation Systems: Recent Developments and Future Directions*, chapter 3, pages 189–241. Noyes Data Corporation, Park Ridge, NJ, 1991.

[46] W. J. Koros and R. T. Chern. Separation of gaseous mixtures with polymer membranes. In R. W. Rousseau, editor, *Handbook of Separation Process Technology*, chapter 20. Wiley-Interscience, New York, 1987.

[47] W. J. Koros and G. K. Fleming. Membrane-based gas separation. *J. Membrane Sci.*, 83:1–80, 1993.

[48] A. S. Kovvali, S. Vemury, and W. Admassu. Modeling of multicomponent countercurrent gas permeators. *Ind. Eng. Chem. Res.*, 33:896–903, 1994.

[49] A. S. Kovvali, S. Vemury, K. R. Krovvidi, and A. A. Khan. Models and analyses of membrane gas permeators. *J. Membrane Sci.*, 73:1–23, 1992.

[50] K. R. Krovvidi, A. S. Kovvali, S. Vemury, and A. A. Khan. Approximate solutions for gas permeators separating binary mixtures. *J. Membrane Sci.*, 66:103–118, 1992.

[51] H. Lababidi, G. A. Al-Enezi, and H. M. Ettouney. Optimization of module configuration in membrane gas separation. *J. Membrane Sci.*, 112:185–197, 1996.

[52] A. L. Lee and H. L. Feldkirchner. Development of a database for advanced processes to remove carbon dioxide from subquality natural gas. Topical Report GRI-93/0247, Gas Research Institute, 1993.

[53] A. L. Lee, H. L. Feldkirchner, S. A. Stern, A. Y. Houde, J. P. Gamez, and H. S. Meyer. Field tests of membrane modules for the separation of carbon dioxide for low-quality natural gas. *Gas Sep. Purif.*, 9:35–43, 1995.

[54] H. Mawengkang and B. A. Murtagh. Solving nonlinear integer programs with large scale optimization software. *Ann. Oper. Res.*, 5:425, 1986.

[55] W. H. Mazur and M. C. Chan. Membranes for natural gas sweetening and CO_2 enrichment. *Chem. Eng. Prog.*, pages 38–43, October 1982.

[56] A. G. Narinsky. Applicability conditions of idealized flow models for gas separation by asymmetric membrane. *J. Membrane Sci.*, 55:333–347, 1991.

[57] C. Y. Pan. Gas separation by permeators with high-flux asymmetric membranes. *AIChE J.*, 29:545–552, 1983.

[58] C. Y. Pan. Gas separation by high-flux, asymmetric hollow-fiber membrane. *AIChE J.*, 32:2020–2027, 1986.

[59] C. Y. Pan and H. W. Habgood. Gas separation by permeation: Part I. Calculation methods and parametric analysis. *Canadian J. Chem. Eng.*, 56:197–209, 1978.

[60] G. E. Paules and C. A. Floudas. APROS: Algorithmic development methodology for discrete-continuous optimization problems. *Oper. Res.*, 37(6):902, 1989.

[61] M. S. Peters and K. D. Timmerhaus. *Plant Design and Economics for Chemical Engineers.* McGraw-Hill, New York, 1980.

[62] T. Pettersen and K. M. Lien. A new robust design model for gas separating membrane modules based on analogy with counter-current heat exchangers. *Computers Chem. Engng.*, 18:427–439, 1994.

[63] T. Pettersen and K. M. Lien. Design studies of membrane permeator processes for gas separation. *Gas Sep. Purif.*, 9:151–169, 1995.

[64] I. Quesada and I. E. Grossmann. A LP/NLP based branch and bound algorithm for convex MINLP optimization problems. *Computers Chem. Engng.*, 16:937–947, 1992.

[65] R. Rautenbach and K. Welsch. Treatment of landfill gas by gas permeation: Pilot plant results and comparison with alternatives uses. *Gas Sep. Purif.*, 7:31–37, 1993.

[66] R. G. Rice and D. D. Do. *Applied Mathematics and Modeling for Chemical Engineers.* Wiley, New York, NY, 1995.

[67] F. G. Russell. Operating permeation systems: Field tests of DELSEP permeators. *Hydrocarb. Proc.*, pages 55–56, August 1983.

[68] W. J. Schell and C. D. Houston. Spiral-wound permeators for purification and recovery. *Chem. Eng. Prog.*, pages 33–37, October 1982.

[69] Y. Shindo, T. Hakuta, H. Yoshitome, and H. Inoue. Calculation methods for multicomponent gas separation by permeation. *Sep. Sci. Technol.*, 20:445–459, 1985.

[70] E. M. B. Smith and C. C. Pantelides. Global optimization of nonconvex MINLP. *Computers Chem. Eng.*, 21:S791–S796, 1997.

[71] R. W. Spillman. Economics of gas separation membranes. *Chem. Eng. Prog.*, pages 41–62, January 1989.

[72] R. W. Spillman, M. G. Barrett, and T. E. Cooley. Gas membrane process optimization. In *AIChE National Meeting*, New Orleans, LA, 1988.

[73] B. K. Srinivas and M. M. El-Halwagi. Optimal design of pervaporation systems for waste reduction. *Computers Chem. Engng.*, 17:957–970, 1993.

[74] M. J. Thundyil and W. J. Koros. Mathematical modeling of gas separation permeators – for radial crossflow, countercurrent, and cocurrent hollow fiber membrane modules. *J. Membrane Sci.*, 125:275–291, 1997.

[75] J. Viswanathan and I. E. Grossmann. A combined penalty function and outer-approximation method for MINLP optimization. *Computers Chem. Engng.*, 14:769–782, 1990.

[76] S. Weller and W. A. Steiner. Engineering aspects of separation of gases. *Chem. Eng. Progress*, 46:585, 1950.

[77] J. Xu and R. Agrawal. Gas separation membrane cascades. I. One compressor cascades with minimal energy losses due to mixing. *J. Membrane Sci.*, 112:115, 1996.

[78] M. Zhu, M. M. El-Halwagi, and M. Al-Ahmad. Optimal design and scheduling of flexible reverse osmosis networks. *J. Membrane Sci.*, 129:161–174, 1997.

[79] R. R. Zolandz and G. K. Fleming. Gas permeation. In W. H. Ho and K. K. Sirkar, editors, *Membrane Handbook*, chapter II. Van Nostrand and Reinhold, NY, 1989.

Appendix A

Supplement to Chapter 2

A.1 One-Point Collocation Method

One-point collocation method is applied to the fundamental permeator model of Pan [57]. Only a brief presentation of the technique is provided here; detailed descriptions of the collocation method are available elsewhere [26, 66]. The solution of the differential equations (2.1)–(2.3) is approximated as,

$$\gamma^2(h) \cong \gamma^2(h_1)l_1(h) + \gamma^2(h_2)l_2(h) \tag{A.1}$$

$$\theta(h) \cong \theta(h_1)l_1'(h) + \theta(h_2')l_2'(h) \tag{A.2}$$

$$\theta(h)y(h) \cong \theta(h_1)y(h_1)l_1'(h) + \theta(h_2')y(h_2')l_2'(h) \tag{A.3}$$

where the coefficients $\gamma(h_i)$, $\theta(h_i)$, and $y(h_i)$ are function values at the collocation point h_i, and $l_i(h)$ and $l_i'(h)$ are Lagrange interpolation polynomials. The first collocation point is $h_1 = 0.5$, and the second point is chosen according to the boundary condition as $h_2' = 0$ or $h_2 = 1$. The Lagrange polynomials are:

$$l_1(h) = \frac{h - h_2}{h_1 - h_2} = -2(h - 1) \tag{A.4}$$

$$l_2(h) = \frac{h - h_1}{h_2 - h_1} = 2(h - 0.5) \tag{A.5}$$

$$l_1'(h) = \frac{h - h_2'}{h_1 - h_2'} = 2h \tag{A.6}$$

$$l_2'(h) = \frac{h - h_1}{h_2' - h_1} = -2(h - 0.5) \tag{A.7}$$

The boundary conditions (2.5)–(2.6) are enforced as:

$$\gamma(h_2) = \gamma_0, \quad \theta(h_2') = 0, \quad \theta_2(h_2')y_2(h_2') = 0 \tag{A.8}$$

Therefore, the approximate solution is:

$$\gamma^2(h) \cong \gamma^2(h_1)l_1(h) + \gamma_0^2 l_2(h) \tag{A.9}$$

$$\theta(h) \cong \theta(h_1)l_1'(h) \tag{A.10}$$

$$\theta(h)y(h) \cong \theta(h_1)y(h_1)l_1'(h) \tag{A.11}$$

The derivatives of the Lagrange polynomials are:

$$\frac{dl_1(h)}{dh} = -2, \quad \frac{dl_2(h)}{dh} = 2, \quad \frac{dl_1'(h)}{dh} = 2 \tag{A.12}$$

By using the approximate solution to evaluate the derivatives, the differential equations (2.1)–(2.3) are reduced to:

$$-2\gamma^2(h_1) + 2\gamma_0^2 = -C\theta(h_1) \tag{A.13}$$

$$2\theta(h_1) = 1 - \phi_r(h_1) \tag{A.14}$$

$$2\theta(h_1)y(h_1) = x_f - x_r(h_1)\phi_r(h_1) \tag{A.15}$$

These algebraic equations can be written as:

$$\gamma^2(h_1) = \gamma_0^2 + \frac{1}{4}C[1-\phi_r(h_1)] \tag{A.16}$$

$$y(h_1) = \frac{x_f - x_r(h_1)\phi_r(h_1)}{1-\phi_r(h_1)} \tag{A.17}$$

$$\theta(h_1) = \frac{1}{2}[1-\phi_r(h_1)] \tag{A.18}$$

Similar to the proposed modeling technique, the values $y_f'(h_1)$, $\gamma(h_1)$, $\phi_r(h_1)$, and $y_r'(h_1)$ are determined via simultaneous solution of the nonlinear algebraic equations (2.7), (A.16), (2.15), and (2.19). The effluent permeate flow rate is:

$$\theta_0 = \theta(h_1)l_1'(h_2) = 2\theta(h_1) = 1-\phi_r(h_1) \tag{A.19}$$

The effluent permeate concentration is detemined as:

$$y_0 = \frac{\theta(h_1)y(h_1)l_1'(h_2)}{\theta_0} = \frac{1}{2}y(h_1)l_1'(h_2) = y(h_1) = \frac{x_f - x_r(h_1)\phi_r(h_1)}{1-\phi_r(h_1)} \tag{A.20}$$

Note that the approximate models obtained with the proposed technique when $M = 1$ and one-point collocation are identical with the exception of the pressure distribution functions in (2.30) and (A.16).

A.2 List of Symbols

a, b dimensionless constant defined by equation (2.9)

B permeability of the spacing materials inside the spiral-wound leaf (m^2)

C	dimensionless constant defined by equation (2.4)
C'	constant defined by equation (2.32) ($Pa^2 \cdot s/mol$)
d	effective thickness of membrane (m)
d_m	membrane leaf thickness (m)
h	$= l/L$, dimensionless leaf length variable
h_i	quadrature points of h
l	membrane leaf length variable (m)
l_1, l_2	Lagrange interpolation polynomials
l_1', l_2'	Lagrange interpolation polynomials
L	membrane leaf length (m)
M	number of quadrature points of θ_0 and y_0
N	number of quadrature points of the integral $I(\gamma, y_r')$
	number of independent experiments in parameter estimation
P	feed-side pressure (Pa)
p	permeate-side pressure (Pa)
p_0	permeate outlet pressure (Pa)
Q_1	permeability of the more permeable component ($mol/m \cdot s \cdot Pa$)
Q_2	permeability of the less permeable component ($mol/m \cdot s \cdot Pa$)
R	dimensionless permeation factor defined by equation (2.10)
R'	constant defined by equation (2.33) ($mol/Pa \cdot s$)
R_g	ideal gas constant ($m^3 \cdot Pa/kg\text{-}mol \cdot K$)

s	$= w/W$, dimensionless leaf width variable
T	temperature (K)
U_f	feed gas flow rate per membrane leaf (mol/s)
U_0	residue gas flow rate per membrane leaf (mol/s)
u	feed-side gas flow rate per unit length of membrane leaf $(mol/s{\cdot}m)$
u_f	feed gas flow rate per unit length of membrane leaf $(mol/s{\cdot}m)$
u_r	residue gas flow rate per unit length of membrane leaf $(mol/s{\cdot}m)$
V	permeate flow rate (mol/s)
V_0	permeate flow rate at permeate outlet (mol/s)
V_i	covariance matrices in parameter estimation
v_a	permeate flow rate per unit length averaged over the width of the membrane $(mol/s{\cdot}m)$
W	membrane leaf width (m)
w	membrane leaf width variable (m)
w_i, w_j	quadrature weights
x	local feed-side concentration (mole fraction)
x_0	bulk residue stream concentration at outlet (mole fraction)
x_f	feed concentration (mol fraction)
x_r	local residue concentration along outlet end of the leaf (mole fraction)
y	permeate concentration in the bulk permeate stream, (mole fraction)
y_0	permeate concentration in the bulk permeate stream at the permeate

outlet (mole fraction)

y' local permeate concentration on the membrane surface, (mole fraction)

y'_a local permeate concentration averaged over the width of the membrane (mole fraction)

y'_f local permeate concentration along inlet end of the leaf (mole fraction)

y'_j local permeate concentrations at quadrature points (mole fraction)

y'_r local permeate concentration along outlet end of the leaf (mole fraction)

z_i experimental data sets expressed in equation (2.42)

$\hat{z}_i$ estimated data sets expressed in equation (2.42)

α $= Q_1/Q_2$, membrane selectivity

γ $= p/P$, ratio of permeate pressure to feed pressure

γ_0 $= p_0/P$, ratio of permeate pressure to feed pressure at permeate outlet

μ viscosity of gas mixture $(Pa{\cdot}s)$

θ $= V/U_f$, ratio of permeate flow to feed flow

θ_0 $= V_0/U_f$, ratio of permeate flow to feed flow permeate outlet

ξ_j standard quadrature points expressed in equation (2.17)

ϕ $= u/u_f$, dimensionless feed-side gas flow rate

ϕ_r $= u_r/u_f$, dimensionless residue gas flow rate

η_0 $= U_0/U_f$, ratio of residue outlet stream flow to feed flow

ν estimated parameters expressed in equation (2.43)

Appendix B

Supplement to Chapter 3

List of Symbols

A_i dimensionless constant defined by equation (3.24)

B permeability of the spacing materials inside the spiral-wound leaf (m^2)

B_i dimensionless constant defined by equation (3.25)

C dimensionless constant defined by equation (3.13)

d effective thickness of membrane (m)

d_m membrane leaf thickness (m)

h $= l/L$, dimensionless leaf length variable

h_k quadrature points of h

l membrane leaf length variable (m)

L membrane leaf length (m)

M number of quadrature points of θ_0 and $y_{i,0}$

N number of quadrature points of the integral $I(\gamma, y'_{i,r})$

number of independent experiments in parameter estimation

n total number of components

P feed-side pressure (Pa)

p permeate-side pressure (Pa)

p_0 permeate outlet pressure (Pa)

Q_i permeabilities of the i-th permeable component $(mol/m{\cdot}s{\cdot}Pa)$

Q_b permeability of the base component $(mol/m{\cdot}s{\cdot}Pa)$

r dimensionless permeation variable defined by equation (3.12)

R dimensionless permeation factor defined by equation (3.28)

R_g ideal gas constant $(m^3{\cdot}Pa/kg\text{-}mol{\cdot}K)$

s $= w/W$, dimensionless leaf width variable

T temperature (K)

U_f feed gas flow rate per membrane leaf (mol/s)

U_0 residue gas flow rate per membrane leaf (mol/s)

u feed-side gas flow rate per unit length of membrane leaf $(mol/s{\cdot}m)$

u_f feed gas flow rate per unit length of membrane leaf $(mol/s{\cdot}m)$

u_r residue gas flow rate per unit length of membrane leaf $(mol/s{\cdot}m)$

V permeate flow rate (mol/s)

V_0 permeate flow rate at permeate outlet (mol/s)

v_a permeate flow rate per unit length averaged over the width of the membrane $(mol/s{\cdot}m)$

W membrane leaf width (m)

w membrane leaf width variable (m)

w_j quadrature weight

x_i local feed-side concentration (mole fraction)

$x_{i,0}$ bulk residue stream concentration at outlet (mole fraction)

$x_{i,f}$ feed concentration (mol fraction)

$x_{i,r}$ x_i along the outlet end of the membrane leaf (mole fraction)

y_i permeate concentration in the bulk permeate stream (mole fraction)

$y_{i,0}$ y_i at the permeate outlet (mole fraction)

y'_i local permeate concentration on the membrane surface (mole fraction)

$y'_{i,a}$ local permeate concentration averaged over the width of the membrane (mole fraction)

$y'_{i,f}$ y'_i along the inlet end of the membrane leaf (mole fraction)

$y'_{i,j}$ y'_i at the j-th quadrature point (mole fraction)

$y'_{i,r}$ y'_i along the outlet end of the membrane leaf (mole fraction)

$\bar{y}'$ composition variable defined by equation (3.17)

$\bar{y}'_f$ $\bar{y}'$ value at the feed inlet

$\bar{y}'_r$ $\bar{y}'$ value at the residue outlet

$\bar{y}'_j$ $\bar{y}'$ value at j-th quadrature point

α_i $= Q_i/Q_b$, membrane selectivity for i-th component

γ $= p/P$, ratio of permeate pressure to feed pressure

γ_0 $= p_0/P$, ratio of permeate pressure to feed pressure at permeate outlet

μ viscosity of gas mixture ($Pa{\cdot}s$)

θ $= V/U_f$, ratio of permeate flow rate to feed flow rate

θ_0 $= V_0/U_f$, ratio of permeate flow rate to feed flow rate at permeate outlet

ξ_j standard quadrature point

ϕ $= u/u_f$, dimensionless feed-side gas flow rate

ϕ_j dimensionless feed-side gas flow rate at j-th quadrature point

ϕ_r $= u_r/u_f$, dimensionless residue gas flow rate

Φ_i function expressed by equations (3.44) and (3.45)

Φ'_j function expressed by equation (3.46)

Ψ function expressed by equation (3.47)

η_0 $= L_0/U_f$, ratio of residue outlet stream flow rate to feed flow rate

Appendix C

Supplement to Chapter 4

C.1 Example of NLP Formulation

As an illustration, the formulation of the nonlinear optimization problem for a three-stage system with permeate and residue recycle (Figure 1.3g) for the enhanced oil recovery application is presented. The objective function represents the annual process cost of the membrane system. The operating requirements, material balances for each mixing point, and model equations for each permeator are posed as constraints. The nonlinear programming problem is solved with GAMS/CONOPT software running on an IBM RS-6000 workstation. It is important to note that the formulation usually yields a nonconvex optimization problem. As a result, the solution obtained represents a local optimum. This problem is addressed by checking several initial conditions. A single solution typically is obtained in a few seconds.

Annual Process Cost

The annual process cost is expressed as:

$$F = [f_{cc}(1 + f_{wk})F_{fc} + F_{mr} + f_{mt}F_{fc} + F_{ut} + F_{pl}]/(U_{f,0}t_{wk}) \qquad \text{(C.1)}$$

Fixed capital investment:

$$F_{fc} = f_{mh} \sum_{n=1}^{3} A_n + f_{cp} W_{cp} / \eta_{cp} \tag{C.2}$$

Expense of membrane replacement:

$$F_{mr} = \frac{f_{mr}}{t_m} \sum_{n=1}^{3} A_n \tag{C.3}$$

Cost of utilities:

$$F_{ut} = f_{sg} t_{wk} W_{cp} / (f_{hv} \eta_{cp}) \tag{C.4}$$

Value of lost gas:

$$F_{pl} = f_{sg} t_{wk} V_{0,3} (1 - y_{0,3}) / (1 - x_{0,2}) \tag{C.5}$$

Compressor power [61]:

$$W_{cp} = R_g T \sum_{n=1}^{2} V_{0,n} \ln \left(\frac{P}{p_{0,n}} \right) \tag{C.6}$$

Operating Requirements

$$x_{0,2} \leq 0.02 \tag{C.7}$$

$$y_{0,3} \geq 0.95 \tag{C.8}$$

$$p_{0,n} \geq 0.105 \tag{C.9}$$

$$p_{0,3} = 0.105 \tag{C.10}$$

Material Balances for Mixing Point

$$U_{f,1} = U_{f,0} + V_{0,2} + U_{0,3} \tag{C.11}$$

$$U_{f,1}x_{f,1} = U_{f,0}x_{f,0} + V_{0,2}y_{0,2} + U_{0,3}x_{0,3} \tag{C.12}$$

$$U_{f,2} = U_{0,1} \tag{C.13}$$

$$x_{f,2} = x_{0,1} \tag{C.14}$$

$$U_{f,3} = V_{0,1} \tag{C.15}$$

$$x_{f,3} = y_{0,1} \tag{C.16}$$

Model Equations for Permeator n

$$U_{f,n} = U_{0,n} + V_{0,n} \tag{C.17}$$

$$U_{f,n}x_{f,n} = U_{0,n}x_{0,n} + V_{0,n}y_{0,n} \tag{C.18}$$

$$C_n = C''U_{f,n}/(A_nP^2) \tag{C.19}$$

$$R_n = (Q_2/d)A_nP/U_{f,n} \tag{C.20}$$

$$V_{0,n} = U_{f,n}\theta_{0,n} \tag{C.21}$$

$$p_{0,n} = P\gamma_{0,n} \tag{C.22}$$

$$\gamma_n^2 = \gamma_{0,n}^2 + 0.375C_n\,(1 - \phi_{r,n}) \tag{C.23}$$

$$a_n = [\gamma_n(\alpha - 1) + 1]/[(\alpha - 1)(1 - \gamma_n)] \tag{C.24}$$

$$b_n = [\gamma_n(\alpha - 1) - \alpha]/[(\alpha - 1)(1 - \gamma_n)] \tag{C.25}$$

$$y'_{j,n} = y'_{f,n} + \xi_j(y'_{r,n} - y'_{f,n}) \tag{C.26}$$

$$\phi_{j,n} = \left(\frac{y'_{j,n}}{y'_{f,n}}\right)^{a_n} \left(\frac{1-y'_{j,n}}{1-y'_{f,n}}\right)^{b_n} \left(\frac{\alpha-(\alpha-1)y'_{j,n}}{\alpha-(\alpha-1)y'_{f,n}}\right) \quad \text{(C.27)}$$

$$I_n = (y'_{r,n} - y'_{f,n}) \sum_{j=1}^{3} \phi'_{j,n} w_j, \quad \text{(C.28)}$$

$$\phi_{r,n} = \left(\frac{y'_{r,n}}{y'_{f,n}}\right)^{a_n} \left(\frac{1-y'_{r,n}}{1-y'_{f,n}}\right)^{b_n} \left(\frac{\alpha-(\alpha-1)y'_{r,n}}{\alpha-(\alpha-1)y'_{f,n}}\right) \quad \text{(C.29)}$$

$$\alpha(1-\gamma_n)R_n = \alpha-(\alpha-1)y'_{f,n} - [\alpha-(\alpha-1)y'_{r,n}]\phi_{r,n} - (\alpha-1)I_n \quad \text{(C.30)}$$

$$y'_{f,n}/(1-y'_{f,n}) = \alpha(x_{f,n}-\gamma_n y'_{f,n})/[1-x_{f,n}-\gamma_n(1-y'_{f,n})] \quad \text{(C.31)}$$

$$y'_{r,n}/(1-y'_{r,n}) = \alpha(x_{r,n}-\gamma_n y'_{r,n})/[1-x_{r,n}-\gamma_n(1-y'_{r,n})] \quad \text{(C.32)}$$

$$\theta_{0,n} = 1-\phi_{r,n} \quad \text{(C.33)}$$

$$y_{0,n} = (x_{f,n}-x_{r,n}\phi_{r,n})/(1-\phi_{r,n}) \quad \text{(C.34)}$$

Nonnegativity Constraints

$$U_{f,n}, U_{0,n}, V_{0,n}, p_{0,n}, A_n, R_n, C_n \geq 0 \quad \text{(C.35)}$$

$$0 \leq x_{f,n}, x_{0,n}, y_{0,n}, y'_{f,n}, y'_{r,n}, y'_{j,n}, x_{r,n} \leq 1 \quad \text{(C.36)}$$

$$0 \leq \theta_{0,n}, \gamma_{0,n}, \gamma_n, \phi_{r,n}, \phi_{j,n} \leq 1 \quad \text{(C.37)}$$

$$n = 1,2,3; \quad j = 1,2,3$$

C.2 List of Symbols

a dimensionless constant defined by equation (2.9)

A membrane area (m^2)

B permeability of the spacing material inside the spiral-wound leaf (m^2)

b	dimensionless constant defined by equation (2.9)
C	dimensionless constant defined by equation (2.4)
C''	permeate-side pressure parameter defined by equation (4.1) (MPa^2s/mol)
d	thickness of membrane skin (m)
d_m	membrane leaf thickness (m)
f_{cc}	annual capital charge (%)
f_{cp}	capital cost of gas-powered compressors ($/KW)
f_{hv}	sales gas gross heating value (MJ/m^3)
f_{mh}	capital cost of membrane housing ($/m^2 membrane)
f_{mr}	expense of membrane replacement ($/m^2 membrane)
f_{mt}	maintenance rate (%)
f_{sg}	utility and sales gas price ($/Km^3)
f_{wk}	working capital rate (%)
F	annual process cost ($/Km^3)
h	$= l/L$, dimensionless leaf length variable
l	membrane leaf length variable (m)
L	membrane leaf length (m)
n	permeator stage number in a configuration
N	number of quadrature points of the integral $I(\gamma, y'_r)$
P	feed-side pressure (MPa)
p	permeate-side pressure (MPa)

p_0	permeate-side pressure at permeate outlet (MPa)
$p_{0,n}$	permeate outlet pressure for permeator n (MPa)
Q_1	permeability of the more permeable component (mol/m-s-Pa)
Q_2	permeability of the less permeable component (mol/m-s-Pa)
R	dimensionless permeation factor defined by equation (2.10)
R_g	ideal gas constant (m^3-Pa/kg-mol-K)
t_m	membrane life (years)
t_{wk}	annual working time (days)
T	temperature (K)
U_f	feed gas flow rate for each permeator (mol/s)
$U_{f,0}$	feed gas processing capacity (mol/s)
U_0	residue gas flow rate for each permeator (mol/s)
u	feed-side gas flow rate per unit length of membrane leaf (mol/s-m)
u_f	feed gas flow rate per unit length of membrane leaf (mol/s-m)
u_r	residue gas flow rate per unit length of membrane leaf (mol/s-m)
V_0	permeate flow rate at permeate outlet (mol/s)
W	membrane leaf width (m)
W_{cp}	compressor power (KW)
w_j	quadrature weights
x	local feed-side concentration (mole fraction)
x_0	bulk residue stream concentration (mole fraction)

x_f feed concentration (mol fraction)

x_r x along residue outlet of membrane leaf (mole fraction)

y_0 bulk permeate stream concentration at permeate outlet (mole fraction)

y' local permeate concentration on the membrane surface (mole fraction)

y'_f y' along feed end of membrane leaf (mole fraction)

y'_j y' at quadrature point j (mole fraction)

y'_r y' along outlet end of membrane leaf (mole fraction)

α $= Q_1/Q_2$, membrane selectivity

γ $= p/P$, ratio of permeate pressure to feed pressure

γ_0 $= p_0/P$, ratio of permeate pressure to feed pressure at permeate outlet

μ viscosity of gas mixture (Pa·s)

θ_0 $= V_0/U_f$, ratio of permeate flow to feed flow at permeate outlet

ξ_j quadrature points

ϕ $= u/u_f$, dimensionless feed-side flow rate

ϕ_r $= u_r/u_f$, dimensionless feed-side flow rate at residue outlet

η_{cp} compressor efficiency (%)

Subscripts

j index of quadrature point

n index of membrane stage

Appendix D

Supplement to Chapter 5

D.1 Other Constraints for MINLP Formulation

The formulations for permeator model constraints, logic constraints, as well as non-negativity and integrality constraints are presented as below.

Permeator Model Constraints

In the permeator model, the following equations are used to define parameters:

$$C_n = C'' U_{f,n}/(A_n P^2), \quad n = 1, \cdots, N \tag{D.1}$$

$$R_n = (Q_2/d) A_n P / U_{f,n}, \quad n = 1, \cdots, N \tag{D.2}$$

$$V_{0,n} = U_{f,n} \theta_{0,n}, \quad n = 1, \cdots, N \tag{D.3}$$

$$p_{0,n} = P \gamma_{0,n}, \quad n = 1, \cdots, N \tag{D.4}$$

$$a_n = \frac{\gamma_n(\alpha - 1) + 1}{(\alpha - 1)(1 - \gamma_n)}, \quad n = 1, \cdots, N \tag{D.5}$$

$$b_n = \frac{\gamma_n(\alpha - 1) - \alpha}{(\alpha - 1)(1 - \gamma_n)}, \quad n = 1, \cdots, N \tag{D.6}$$

The permeate-side pressure distribution is obtained from (2.13) by using a single quadrature point at $h_1 = 0.5$ [66],

$$\gamma_n^2 = \gamma_{0,n}^2 + 0.375 C_n (1 - \phi_{r,n}), \quad n = 1, \cdots, N \tag{D.7}$$

The dimensionless feed-side flow rate ϕ at each quadrature point j and the residue outlet, and the integral term I are expressed as follows:

$$y'_{j,n} = y'_{f,n} + \xi_j(y'_{r,n} - y'_{f,n}), \quad j = 1, \cdots, M; \; n = 1, \cdots, N \tag{D.8}$$

$$\phi_{j,n} = \left(\frac{y'_{j,n}}{y'_{f,n}}\right)^{a_n} \left(\frac{1 - y'_{j,n}}{1 - y'_{f,n}}\right)^{b_n} \left(\frac{\alpha - (\alpha - 1)y'_{j,n}}{\alpha - (\alpha - 1)y'_{f,n}}\right), \tag{D.9}$$

$$j = 1, \cdots, M; \; n = 1, \cdots, N$$

$$\phi_{r,n} = \left(\frac{y'_{r,n}}{y'_{f,n}}\right)^{a_n} \left(\frac{1 - y'_{r,n}}{1 - y'_{f,n}}\right)^{b_n} \left(\frac{\alpha - (\alpha - 1)y'_{r,n}}{\alpha - (\alpha - 1)y'_{f,n}}\right), \quad n = 1, \cdots, N \tag{D.10}$$

$$I_n = (y'_{r,n} - y'_{f,n}) \sum_{j=1}^{M} \phi_{j,n} w_j, \quad n = 1, \cdots, N \tag{D.11}$$

The relation (2.19) for the dimensionless permeation factor is written as:

$$\alpha(1-\gamma_n)R_n = \alpha-(\alpha-1)y'_{f,n}-[\alpha-(\alpha-1)y'_{r,n}]\phi_{r,n}-(\alpha-1)I_n, \quad n = 1, \cdots, N \tag{D.12}$$

The relation (2.7) is needed for both feed and residue ends of the permeator:

$$\frac{y'_{f,n}}{1 - y'_{f,n}} = \frac{\alpha(x_{f,n} - \gamma_n y'_{f,n})}{1 - x_{f,n} - \gamma_n(1 - y'_{f,n})}, \quad n = 1, \cdots, N \tag{D.13}$$

$$\frac{y'_{r,n}}{1 - y'_{r,n}} = \frac{\alpha(x_{r,n} - \gamma_n y'_{r,n})}{1 - x_{r,n} - \gamma_n(1 - y'_{r,n})}, \quad n = 1, \cdots, N \tag{D.14}$$

The flow rate and concentration of the effluent permeate stream from each stage are given by (2.28) and (2.29):

$$\theta_{0,n} = 1 - \phi_{r,n}, \quad n = 1, \cdots, N \tag{D.15}$$

$$y_{0,n} = \frac{x_{f,n} - x_{r,n}\phi_{r,n}}{1 - \phi_{r,n}}, \quad n = 1, \cdots, N \tag{D.16}$$

The flow rate and concentration of the effluent residue stream are constrained by material balance equations.

Logic Constraints

Logic constraints are placed on binary variables associated with the existence or nonexistence of various interconnections. The first type of logic constraint forces the flow rate to be zero if the associated connection is not utilized ($Z = 0$). If the connection is utilized ($Z = 1$), the corresponding constraint is relaxed to allow the flow rate to assume any value up to an upper bound (U^{U}). These logic relations for the feed, product, and recycle streams are expressed as follows:

$$U_{f0,n} - U^{U} Z_n^{Uf0} \leq 0, \quad n = 1, \cdots, N \tag{D.17}$$

$$U_{p,n} - U^{U} Z_n^{Up} \leq 0, \quad n = 1, \cdots, N \tag{D.18}$$

$$V_{p,n} - U^{U} Z_n^{Vp} \leq 0, \quad n = 1, \cdots, N \tag{D.19}$$

$$U_{b,m,n} - U^{U} Z_{m,n}^{Ub} \leq 0, \quad m = 1, \cdots, N; \; n = 1, \cdots, N \tag{D.20}$$

$$V_{b,m,n} - U^{U} Z_{m,n}^{Vb} \leq 0, \quad m = 1, \cdots, N; \; n = 1, \cdots, N \tag{D.21}$$

The second type of logic constraint forces the binary variable to be zero if the associated flow rate becomes zero. If the connection is utilized, the corresponding flow rate can assume any value greater than a lower bound (U^{L}). These logic relations

are expressed as:

$$U_{\mathrm{f0},n} - U^{\mathrm{L}} Z_n^{\mathrm{Uf0}} \geq 0, \quad n = 1, \cdots, N \tag{D.22}$$

$$U_{\mathrm{p},n} - U^{\mathrm{L}} Z_n^{\mathrm{Up}} \geq 0, \quad n = 1, \cdots, N \tag{D.23}$$

$$V_{\mathrm{p},n} - U^{\mathrm{L}} Z_n^{\mathrm{Vp}} \geq 0, \quad n = 1, \cdots, N \tag{D.24}$$

$$U_{\mathrm{b},m,n} - U^{\mathrm{L}} Z_{m,n}^{\mathrm{Ub}} \geq 0, \quad m = 1, \cdots, N; \; n = 1, \cdots, N \tag{D.25}$$

$$V_{\mathrm{b},m,n} - U^{\mathrm{L}} Z_{m,n}^{\mathrm{Vb}} \geq 0, \quad m = 1, \cdots, N; \; n = 1, \cdots, N \tag{D.26}$$

In practice, U^{L} is a small positive value which is chosen as the minimum flow rate allowed in the system.

The final type of logic constraint is associated with the outlet permeate pressure for each stage. If the outlet permeate stream goes to final product stream mixer, the permeate pressure must equal the product pressure. If the permeate stream is recycled to another stage, the permeate pressure can assume any value less than or equal to the feed-side pressure. By introducing a slack variable S, these logic relations can be expressed as:

$$p_{0,n} = S_n + p_{\mathrm{out}}, \quad n = 1, \cdots, N \tag{D.27}$$

$$0 \leq S_n \leq (P - p_{\mathrm{out}})(1 - Z_n^{\mathrm{Vp}}), \quad n = 1, \cdots, N \tag{D.28}$$

Note that if $Z_n^{\mathrm{Vp}} = 1$, then $S_n = 0$ and $p_{0,n} = p_{\mathrm{out}}$; if $Z_n^{\mathrm{Vp}} = 0$, then $0 \leq S_n \leq P - p_{\mathrm{out}}$ and $p_{\mathrm{out}} \leq p_{0,n} \leq P$.

Nonnegativity and Integrality Constraints

These constraints are used to specify lower and upper variable bounds to prevent undefined operations (*e.g.* division by zero) and to ensure the variables remain in a reasonable solution space. Proper selection of these bounds is very important for efficient solution of mixed-integer nonlinear models. These constraints are expressed as follows:

$$0 \leq U_{\mathrm{f0},n}, U_{\mathrm{f},n}, U_{0,n}, V_{0,n}, U_{\mathrm{p},n}, V_{\mathrm{p},n}, U_{\mathrm{b},m,n}, V_{\mathrm{b},m,n}, U_{\mathrm{pt}}, V_{\mathrm{pt}} \leq U^{\mathrm{U}} \quad \text{(D.29)}$$

$$A_n, N_n^{\mathrm{A}}, R_n, C_n \geq 0 \quad \text{(D.30)}$$

$$0 \leq x_{\mathrm{f},n}, x_{0,n}, y_{0,n}, y'_{\mathrm{f},n}, y'_{\mathrm{r},n}, y'_{j,n}, x_{\mathrm{r},n} \leq 1 \quad \text{(D.31)}$$

$$0 \leq \theta_{0,n}, \gamma_{0,n}, \gamma_n, \phi_{\mathrm{r},n}, \phi_{j,n} \leq 1 \quad \text{(D.32)}$$

$$Z_n^{\mathrm{Uf0}}, Z_n^{\mathrm{Up}}, Z_n^{\mathrm{Vp}}, Z_{m,n}^{\mathrm{Ub}}, Z_{m,n}^{\mathrm{Vb}}, Z_{n,k}^{\mathrm{A}} = 0, 1 \quad \text{(D.33)}$$

$$m = 1, \cdots, N;\ n = 1, \cdots, N;\ j = 1, \cdots, M;\ k = 1, \cdots, K$$

D.2 List of Symbols

a dimensionless constant defined by equation (2.9)

A membrane area for each stage (m^2)

A_t total membrane area of system (m^2)

B permeability of the spacing materials inside the spiral-wound leaf (m^2)

b dimensionless constant defined by equation (2.9)

C dimensionless constant defined by equation (2.4)

C'' permeate-side pressure parameter defined by equation (4.1) (MPa^2s/mol)

d thickness of membrane skin (m)

d_m thickness of membrane leaf (m)

f_{cc} annual capital charge (%/year)

f_{cp} capital cost of gas-powered compressors ($/KW)

f_{hv} sales gas gross heating value (MJ/m^3)

f_{mh} capital cost of membrane housing ($/m^2$ membrane)

f_{mr} expense of membrane replacement ($/m^2$ membrane)

f_{mt} maintenance rate (%/year)

f_{sg} utility and sales gas price ($/Km^3$)

f_{wk} working capital rate (%)

F annual process cost ($/Km^3$)

F_{cc} annual capital charge ($/year)

F_{fc} fixed capital investment ($)

F_{mr} expense of membrane replacement ($/year)

F_{mt} maintenance expense ($/year)

F_{pl} value of product losses ($/year)

F_{ut} cost of utilities ($/year)

h dimensionless leaf length variable

K minimum number of binary variables for integer conversion

L membrane leaf length (m)

M	number of quadrature points for the integral $I(\gamma, y_r')$
N	permeator stage number in configuration
N^A	number of membrane elements for each stage
N^{AL}	lower bound of membrane element number
N^{AU}	upper bound of membrane element number
P	feed-side pressure (MPa)
p	permeate-side pressure (MPa)
p_{out}	required output permeate pressure (MPa)
p_0	permeate outlet pressure for each permeator (MPa)
Q_1	permeability of the more permeable component (mol/m·s·Pa)
Q_2	permeability of the less permeable component (mol/m·s·Pa)
R	dimensionless permeation factor defined by equation (2.10)
R_g	ideal gas constant (m^3·Pa/kg-mol·K)
S	slack variable in logic constraints
t_m	membrane life (years)
t_{wk}	annual working time (days/year)
T	temperature (K)
U_f	feed gas flow rate for each permeator (mol/s)
U_{f0}	fresh feed flow rate for each permeator (mol/s)
U_{f00}	total fresh feed flow rate as processing capacity (mol/s)
U_0	flow rate of residue gas at permeator outlet (mol/s)

U_b flow rate of residue gas as recycle stream (mol/s)

U_p flow rate of residue gas as product stream (mol/s)

U_{pt} total flow rate on residue product (mol/s)

U^L upper bound on stream flow rate (mol/s)

U^U lower bound on stream flow rate (mol/s)

V_0 permeate flow rate at permeator outlet (mol/s)

V_b flow rate of permeate gas as recycle stream (mol/s)

V_p flow rate of permeate gas as product stream (mol/s)

V_{pt} total flow rate of permeate product (mol/s)

W membrane leaf width (m)

W_{cp} compressor power (KW)

W_t total compressor power (KW)

w_j quadrature weights

x local feed-side concentration (mole fraction)

x_0 bulk residue stream concentration at permeator outlet (mole fraction)

x_f feed concentration for each stage (mole fraction)

x_{f0} fresh feed concentration (mole fraction)

x_{out} required CO_2 concentration of residue product (mole fraction)

x_{pt} CO_2 concentration of residue product (mole fraction)

x_r x along outlet end of membrane leaf (mole fraction)

y_0 bulk permeate stream concentration at permeate outlet (mole fraction)

y_{pt} CO_2 concentration of permeate product (mole fraction)

y_{out} required CO_2 concentration of permeate product (mole fraction)

y' local permeate concentration on the membrane surface (mole fraction)

y'_f y' along inlet end of membrane leaf (mole fraction)

y'_j y' at quadrature point j (mole fraction)

y'_r y' along outlet end of membrane leaf (mole fraction)

Z^A binary variable used to express discrete membrane area

Z^{Ub} binary variable denoting the existence or nonexistence of U_b

Z^{Uf0} binary variable denoting the existence or nonexistence of U_{f0}

Z^{Up} binary variable denoting the existence or nonexistence of U_p

Z^{Vb} binary variable denoting the existence or nonexistence of V_b

Z^{Vp} binary variable denoting the existence or nonexistence of V_p

α $= Q_1/Q_2$, membrane selectivity

γ $= p/P$,ratio of permeate pressure to feed pressure

γ_0 $= p_0/P$, ratio of permeate pressure to feed pressure at permeate outlet

μ viscosity of gas mixture (Pa·s)

θ_0 $= V_0/U_f$, ratio of permeate flow to feed flow at permeate outlet

Θ CH_4 recovery (%)

ξ_j quadrature points

ϕ dimensionless feed-side flow rate

ϕ_r dimensionless feed-side flow rate at residue outlet

η_{cp} compressor efficiency (%)

Subscripts

i index of quadrature points for leaf length variable h

j index of quadrature points for integral function (2.18)

k index of binary variables in expression of discrete membrane area

m index of membrane stages

n index of membrane stages

Appendix E

Supplement to Chapter 6

E.1 Multicomponent MINLP Formulation

Annual Process Cost

The approximate costing procedure presented by Spillman *et al.* [72] and Babcock *et al.* [5] is utilized. As in the binary case, the fixed capital investment (F_{fc}) is only a function of total membrane area (A_t) and total compressor power (W_{t}):

$$F_{\text{fc}} = f_{\text{mh}} \sum_{n=1}^{N_{\text{s}}} A_n + f_{\text{cp}} \frac{W_{\text{t}}}{\eta_{\text{cp}}} \tag{E.1}$$

where $A_t = \sum_{n=1}^{N_s} A_n$ and N_{s} is the number of separation stages. The remaining parameters are defined in Appendix E.2. The total compressor power is taken as the summation of the fresh feed compressor power ($W_{\text{cp,f}}$) and the compressor power for each stage ($W_{\text{cp},n}$):

$$W_{\text{t}} = W_{\text{cp,f}} + \sum_{n=1}^{N_{\text{s}}} W_{\text{cp},n} \tag{E.2}$$

where compressor power is calculated by assuming ideal gas behavior and isothermal compression [61]:

$$W_{\text{cp,f}} = R_{\text{g}} T U_{\text{f00}} \ln\left(\frac{P}{P_{\text{f}}}\right) \tag{E.3}$$

$$W_{\mathrm{cp},n} = R_{\mathrm{g}}T\left(\sum_{m=1}^{N_{\mathrm{s}}} V_{\mathrm{b},m,n}\right)\ln\left(\frac{P}{p_{0,n}}\right), \quad n=1,\cdots,N_{\mathrm{s}} \tag{E.4}$$

Here $V_{\mathrm{b},m,n}$ is the permeate recycle stream from the n-th stage to m-th stage. Note that if the feed-side pressure for each stage is equal to the fresh feed pressure, the fresh feed compressor is eliminated and $W_{\mathrm{cp,f}}$ becomes zero.

The working capital is taken as a fixed percentage (f_{wk}) of the fixed capital, and the annual capital charge (F_{cc}) is calculated by annualizing the fixed and working capitals:

$$F_{\mathrm{cc}} = f_{\mathrm{cc}}(1+f_{\mathrm{wk}})F_{\mathrm{fc}} \tag{E.5}$$

The annual operating costs include membrane replacement expense (F_{mr}):

$$F_{\mathrm{mr}} = \frac{f_{\mathrm{mr}}}{t_{\mathrm{m}}}\sum_{n=1}^{N_{\mathrm{s}}} A_n \tag{E.6}$$

maintenance expense (F_{mt}):

$$F_{\mathrm{mt}} = f_{\mathrm{mt}}F_{\mathrm{fc}} \tag{E.7}$$

cost of utilities (F_{ut}):

$$F_{\mathrm{ut}} = \frac{f_{\mathrm{sg}}t_{\mathrm{wk}}}{f_{\mathrm{hv}}\eta_{\mathrm{cp}}}W_{\mathrm{t}} \tag{E.8}$$

and value of product losses (F_{pl}):

$$F_{\mathrm{pl}} = f_{\mathrm{sg}}t_{\mathrm{wk}}V_{\mathrm{pt}}\frac{y_{\mathrm{pt,k}}}{x_{\mathrm{pt,k}}} \tag{E.9}$$

The annual process cost (F) is taken as the sum of the capital charge and operating expenses divided by process capacity, which is expressed as:

$$F = \left[F_{cc} + F_{mr} + F_{mt} + F_{ut} + F_{pl}\right] / (U_{f00} t_{wk}) \tag{E.10}$$

Material Balance Constraints

Material balance constraints are imposed on: (*i*) splitters for the initial feed stream and the outlet streams of each stage; (*ii*) mixers for the inlet streams of each stage and the inlet streams for the final products; and (*iii*) each permeation stage. For an N stage system, material balances on the splitters can be expressed as:

$$U_{f00} = \sum_{n=1}^{N_s} U_{f0,n} \tag{E.11}$$

$$U_{0,n} = U_{p,n} + \sum_{m=1}^{N_s} U_{b,m,n}, \quad n = 1, \cdots, N_s \tag{E.12}$$

$$V_{0,n} = V_{p,n} + \sum_{m=1}^{N_s} V_{b,m,n}, \quad n = 1, \cdots, N_s \tag{E.13}$$

where: U_{f00} is the total fresh feed flow rate; $U_{f0,n}$ is the fresh feed flow rate for stage n; $U_{0,n}$ ($V_{0,n}$) is the total outlet residue (permeate) flow rate for stage n; $U_{p,n}$ ($V_{p,n}$) is the residue (permeate) flow rate of the final product from stage n; and $U_{b,m,n}$ ($V_{b,m,n}$) is the residue (permeate) flow rate of the recycle stream from the n-th stage to m-th stage.

For the stream mixers, both overall material balances and component balances are necessary. Material balances for the inlet mixer of stage n are written as:

$$U_{\mathrm{f},n} = U_{\mathrm{f0},n} + \sum_{m=1}^{N_\mathrm{s}} \left(U_{\mathrm{b},n,m} + V_{\mathrm{b},n,m}\right), \quad n = 1, \cdots, N_\mathrm{s} \tag{E.14}$$

$$U_{\mathrm{f},n} x_{\mathrm{f},n,i} = U_{\mathrm{f0},n} x_{\mathrm{f0},i} + \sum_{m=1}^{N_\mathrm{s}} \left(U_{\mathrm{b},n,m} x_{0,m,i} + V_{\mathrm{b},n,m} y_{0,m,i}\right), \quad n = 1, \cdots, N_\mathrm{s};\ i = 2, \cdots, N_\mathrm{c} \tag{E.15}$$

Note that the recycle streams are taken from the m-th stage and terminate at the n-th stage. Material balances for the product mixers are expressed as:

$$U_{\mathrm{pt}} = \sum_{n=1}^{N_\mathrm{s}} U_{\mathrm{p},n} \tag{E.16}$$

$$U_{\mathrm{pt}} x_{\mathrm{pt},i} = \sum_{n=1}^{N_\mathrm{s}} U_{\mathrm{p},n} x_{0,n,i}, \quad i = 2, \cdots, N_\mathrm{c} \tag{E.17}$$

$$V_{\mathrm{pt}} = \sum_{n=1}^{N_\mathrm{s}} V_{\mathrm{p},n} \tag{E.18}$$

$$V_{\mathrm{pt}} y_{\mathrm{pt},i} = \sum_{n=1}^{N_\mathrm{s}} V_{\mathrm{p},n} y_{0,n,i}, \quad i = 2, \cdots, N_\mathrm{c} \tag{E.19}$$

where U_{pt} and $x_{\mathrm{pt},i}$ are the total flow rate and concentrations of the final residue product, and V_{pt} and $y_{\mathrm{pt},i}$ are the total flow rate and concentrations of the final permeate product. Material balances about each permeation stage yield:

$$U_{\mathrm{f},n} = U_{0,n} + V_{0,n}, \quad n = 1, \cdots, N_\mathrm{s} \tag{E.20}$$

$$U_{\mathrm{f},n} x_{\mathrm{f},n,i} = U_{0,n} x_{0,n,i} + V_{0,n} y_{0,n,i}, \quad n = 1, \cdots, N_\mathrm{s};\ i = 2, \cdots, N_\mathrm{c} \tag{E.21}$$

Permeator Model Constraints

The permeator model constraints are comprised of the approximate permeator model equations written for each stage. The approximate model is described in Chapter 3. Some of the equations are manipulated to facilitate computer implementation, and some of the notation is modified to accommodate the general MINLP formulation. The following equations are used to define parameters:

$$C_n = C''U_{f,n}/(A_nP^2), \quad n = 1, \cdots, N_s \tag{E.22}$$

$$R_n = (Q_2/d)A_nP/U_{f,n}, \quad n = 1, \cdots, N_s \tag{E.23}$$

$$V_{0,n} = U_{f,n}\theta_{0,n}, \quad n = 1, \cdots, N_s \tag{E.24}$$

$$p_{0,n} = P\gamma_{0,n}, \quad n = 1, \cdots, N_s \tag{E.25}$$

The permeate-side pressure distribution is obtained from (3.30) by using a single quadrature point at $h_1 = 0.5$,

$$\gamma_n^2 = \gamma_{0,n}^2 + 0.375C_n\left(1 - \phi_{r,n}\right), \quad n = 1, \cdots, N_s \tag{E.26}$$

The relations (3.19) and (3.21) between the local feed-side concentration x_i and the local permeate-side concentration y_i' are needed for both feed and residue ends of the permeator:

$$\sum_{i=1}^{N_c} \frac{\alpha_i x_{f,n,i}\bar{y}_{f,n}'}{1 - \gamma_n + \gamma_n\alpha_i\bar{y}_{f,n}'} = 1, \quad n = 1, \cdots, N_s \tag{E.27}$$

$$\sum_{i=1}^{N_c} \frac{\alpha_i x_{r,n,i} \bar{y}'_{r,n}}{1-\gamma_n+\gamma_n \alpha_i \bar{y}'_{r,n}} = 1, \quad n = 1, \cdots, N_s \tag{E.28}$$

$$x_{f,n,i} = \gamma_n y'_{f,n,i} + \frac{(1-\gamma_n) y'_{f,n,i}}{\alpha_i \bar{y}'_{f,n}}, \quad i = 1, \cdots, N_c;\ n = 1, \cdots, N_s \tag{E.29}$$

$$x_{r,n,i} = \gamma_n y'_{r,n,i} + \frac{(1-\gamma_n) y'_{r,n,i}}{\alpha_i \bar{y}'_{r,n}}, \quad i = 1, \cdots, N_c;\ n = 1, \cdots, N_s \tag{E.30}$$

The relation (3.33) for the dimensionless permeation factor is written as:

$$(1-\gamma_n) R_n = \bar{y}'_{f,n} - \phi_{r,n} \bar{y}'_{r,n} + (\bar{y}'_{r,n} - \bar{y}'_{f,n}) \sum_{j=1}^{M} \phi_{j,n} w_j, \quad n = 1, \cdots, N_s \tag{E.31}$$

The dimensionless feed-side flow rates ϕ_j and ϕ_r and the local permeate concentration at the residue outlet $y'_{r,i}$ are determined by Runge-Kutta-Gill approximation of initial-value differential equations at each quadrature point $\bar{y}'_j$ and the residue outlet $\bar{y}'_r$. The quadrature and outlet points are determined by the following equation:

$$\bar{y}'_{j,n} = \bar{y}'_{f,n} + \xi_j (\bar{y}'_{r,n} - \bar{y}'_{f,n}), \quad j = 1, \cdots, M+1;\ n = 1, \cdots, N_s \tag{E.32}$$

in which the last point ($j = M+1$) represents the residue outlet. The Runge-Kutta-Gill equations (3.34)–(3.38) are written as:

$$K_{1,j,n} = \delta_{j,n} \cdot \mathcal{F}(\bar{y}'_{j-1,n},\ Y_{j-1,n},\ \gamma_n) \tag{E.33}$$

$$K_{2,j,n} = \delta_{j,n} \cdot \mathcal{F}(\bar{y}'_{j-1,n} + \frac{\delta_{j,n}}{2},\ Y_{j-1,n} + \frac{1}{2} K_{1,j,n},\ \gamma_n) \tag{E.34}$$

$$K_{3,j,n} = \delta_{j,n} \cdot \mathcal{F}(\bar{y}'_{j-1,n} + \frac{\delta_{j,n}}{2},\ Y_{j-1,n} + \lambda_1 K_{1,j,n} + \lambda_2 K_{2,j,n},\ \gamma_n) \tag{E.35}$$

$$K_{4,j,n} = \delta_{j,n} \cdot \mathcal{F}(\bar{y}'_{j-1,n} + \delta_{j,n},\ Y_{j-1,n} + \lambda_3 K_{2,j,n} + \lambda_4 K_{3,j,n},\ \gamma_n) \tag{E.36}$$

$$Y_{j,n} = Y_{j-1,n} + \frac{1}{6}(K_{1,j,n} + K_{4,j,n}) + \frac{1}{3}(\lambda_2 K_{2,j,n} + \lambda_4 K_{3,j,n}) \qquad \text{(E.37)}$$

where $j = 1, \cdots, M+1$; $n = 1, \cdots, N_s$, and Y and $\mathcal{F}$ are defined as:

$$Y = \left[\ln\phi,\ y'_2,\ \cdots,\ y'_{N_c}\right]^T$$

$$\mathcal{F} = \left[f_\phi,\ f_2,\ \cdots,\ f_{N_c}\right]^T$$

The functions $f_\phi,\ f_2,\ \cdots,\ f_{N_c}$ represent the right-hand sides of (3.23) and (3.26), and y'_i is the local permeate concentration of the i-th component. Note that Y and K_1–K_4 are vectors with N_c elements, while $\mathcal{F}$ is a N_c-element vector function. Thus, $Y_{j,n}$ and $K_{1,j,n}$–$K_{4,j,n}$ are three-dimensional arrays. The vector function $\mathcal{F}$ is derived from equations (3.23) and (3.26) by noting that $y'_i = Y_i$ for $i = 2, \cdots, N_c$ and $y'_1 = 1 - \sum_{i=2}^{N_c} Y_i$:

$$\mathcal{F}_1(\bar{y}', Y, \gamma) = -\frac{\mathcal{A}_1(\bar{y}', \gamma)(1 - \sum_{i=2}^{N_c} Y_i) + \sum_{i=2}^{N_c} \mathcal{A}_i(\bar{y}', \gamma) Y_i}{\mathcal{B}_1(\bar{y}', \gamma)(1 - \sum_{i=2}^{N_c} Y_i) + \sum_{i=2}^{N_c} \mathcal{B}_i(\bar{y}', \gamma) Y_i} \qquad \text{(E.38)}$$

$$\mathcal{F}_i(\bar{y}', Y, \gamma) = Y_i\left[\mathcal{A}_i(\bar{y}', \gamma) + \mathcal{B}_i(\bar{y}', \gamma)\mathcal{F}_1(\bar{y}', Y, \gamma)\right], \quad i = 2, \cdots, N_c \qquad \text{(E.39)}$$

where Y_i is the i-th element of the vector Y, and the parameters $\mathcal{A}_i$ and $\mathcal{B}_i$ are defined by equations (3.24) and (3.25) for each component i:

$$\mathcal{A}_i(\bar{y}', \gamma) = \frac{1-\gamma}{(1 - \gamma + \gamma\alpha_i\bar{y}')\bar{y}'}, \quad i = 1, \cdots, N_c \qquad \text{(E.40)}$$

$$\mathcal{B}_i(\bar{y}', \gamma) = \frac{(1-\gamma)(\alpha_i\bar{y}' - 1)}{1 - \gamma + \gamma\alpha_i\bar{y}'}, \quad i = 1, \cdots, N_c \qquad \text{(E.41)}$$

Note that the GAMS environment does not allow redefinition of functions inside the constraint definition. As a result, expressions (E.33)–(E.37) for the function $\mathcal{F}$ need to be written explicitly. The initial conditions for $Y_{j,n}$ are:

$$Y_{0,n} = \left[0,\ y'_{\mathrm{f},n,2},\ \cdots,\ y'_{\mathrm{f},n,N_\mathrm{c}}\right]^T,\quad n = 1, \cdots, N_\mathrm{s} \tag{E.42}$$

and the interval δ is chosen as the difference between $\bar{y}'$ at adjacent quadrature points:

$$\delta_{j,n} = \bar{y}'_{j,n} - \bar{y}'_{j-1,n},\quad j = 1, \cdots, M+1;\ n = 1, \cdots, N_\mathrm{s} \tag{E.43}$$

The local feed-side flow rates ϕ_j and ϕ_r and the local permeate concentration at the residue outlet $y'_{\mathrm{r},i}$ are calculated as:

$$\phi_{j,n} = \exp\left(Y_{j,n,1}\right),\quad j = 1, \cdots, M;\ n = 1, \cdots, N_\mathrm{s} \tag{E.44}$$

$$\phi_{r,n} = \exp\left(Y_{M+1,n,1}\right),\quad n = 1, \cdots, N_\mathrm{s} \tag{E.45}$$

$$y'_{\mathrm{r},n,i} = Y_{M+1,n,i},\quad n = 1, \cdots, N_\mathrm{s};\ i = 2, \cdots, N_\mathrm{c} \tag{E.46}$$

The flow rate and concentration of the effluent permeate stream from each stage are given by (3.53) and (3.54):

$$\theta_{0,n} = 1 - \phi_{\mathrm{r},n},\quad n = 1, \cdots, N_\mathrm{s} \tag{E.47}$$

$$y_{0,n,i} = \frac{x_{\mathrm{f},n,i} - x_{\mathrm{r},n,i}\phi_{\mathrm{r},n}}{1 - \phi_{\mathrm{r},n}},\quad n = 1, \cdots, N_\mathrm{s};\ i = 2, \cdots, N_\mathrm{c} \tag{E.48}$$

The flow rate and concentration of the effluent residue stream are determined by overall material balance equations.

Composition Sum Constraints

These constraints force the sum of component mole fractions to be unity:

$$\sum_{i=1}^{N_c} x_{f,n,i} = 1, \quad n = 1, \cdots, N_s \tag{E.49}$$

$$\sum_{i=1}^{N_c} y'_{f,n,i} = 1, \quad n = 1, \cdots, N_s \tag{E.50}$$

$$\sum_{i=1}^{N_c} x_{r,n,i} = 1, \quad n = 1, \cdots, N_s \tag{E.51}$$

$$\sum_{i=1}^{N_c} y'_{r,n,i} = 1, \quad n = 1, \cdots, N_s \tag{E.52}$$

$$\sum_{i=1}^{N_c} x_{0,n,i} = 1, \quad n = 1, \cdots, N_s \tag{E.53}$$

$$\sum_{i=1}^{N_c} y_{0,n,i} = 1, \quad n = 1, \cdots, N_s \tag{E.54}$$

$$\sum_{i=1}^{N_c} x_{pt,i} = 1, \quad n = 1, \cdots, N_s \tag{E.55}$$

$$\sum_{i=1}^{N_c} y_{pt,i} = 1, \quad n = 1, \cdots, N_s \tag{E.56}$$

Operating Requirement Constraints

Constraints are imposed to ensure the product streams satisfy the separation requirements. In acid gas separations from natural gas mixtures, minimum purity requirements are placed on the CO_2 concentration in the final residue product and the CH_4 concentration in the permeate product stream. In addition, a constraint which expresses that the permeate pressure for each stage must be at least as high

as the pressure of the final permeate stream is required. These constraints are expressed as:

$$x_{\mathrm{pt,CO_2}} \leq x_{\mathrm{out,CO_2}} \tag{E.57}$$

$$y_{\mathrm{pt,CH_4}} \leq y_{\mathrm{out,CH_4}} \tag{E.58}$$

$$p_{0,n} \geq p_{\mathrm{out}} \tag{E.59}$$

Depending on the application, some of the constraints may be relaxed. As in binary case, only (E.57) and (E.59) are required for natural gas treatment.

Logic Constraints

The first type of logic constraint forces the flow rate to be zero if the associated connection is not utilized ($Z = 0$). If the connection is utilized ($Z = 1$), the corresponding constraint is relaxed to allow the flow rate to assume any value up to an upper bound (U^{U}). These logic relations for the feed, product, and recycle streams are expressed as follows:

$$U_{\mathrm{f0},n} - U^{\mathrm{U}} Z_n^{\mathrm{Uf0}} \leq 0, \quad n = 1, \cdots, N_{\mathrm{s}} \tag{E.60}$$

$$U_{\mathrm{p},n} - U^{\mathrm{U}} Z_n^{\mathrm{Up}} \leq 0, \quad n = 1, \cdots, N_{\mathrm{s}} \tag{E.61}$$

$$V_{\mathrm{p},n} - U^{\mathrm{U}} Z_n^{\mathrm{Vp}} \leq 0, \quad n = 1, \cdots, N_{\mathrm{s}} \tag{E.62}$$

$$U_{\mathrm{b},m,n} - U^{\mathrm{U}} Z_{m,n}^{\mathrm{Ub}} \leq 0, \quad m = 1, \cdots, N_{\mathrm{s}};\ n = 1, \cdots, N_{\mathrm{s}} \tag{E.63}$$

$$V_{\mathrm{b},m,n} - U^{\mathrm{U}} Z_{m,n}^{\mathrm{Vb}} \leq 0, \quad m = 1, \cdots, N_{\mathrm{s}};\ n = 1, \cdots, N_{\mathrm{s}} \tag{E.64}$$

The second type of logic constraint forces the binary variable to be zero if the associated flow rate becomes zero. If the connection is utilized, the corresponding flow rate can assume any value greater than a lower bound (U^{L}). These logic relations are expressed as:

$$U_{\mathrm{f0},n} - U^{\mathrm{L}} Z_n^{\mathrm{Uf0}} \geq 0, \quad n = 1, \cdots, N_{\mathrm{s}} \tag{E.65}$$

$$U_{\mathrm{p},n} - U^{\mathrm{L}} Z_n^{\mathrm{Up}} \geq 0, \quad n = 1, \cdots, N_{\mathrm{s}} \tag{E.66}$$

$$V_{\mathrm{p},n} - U^{\mathrm{L}} Z_n^{\mathrm{Vp}} \geq 0, \quad n = 1, \cdots, N_{\mathrm{s}} \tag{E.67}$$

$$U_{\mathrm{b},m,n} - U^{\mathrm{L}} Z_{m,n}^{\mathrm{Ub}} \geq 0, \quad m = 1, \cdots, N_{\mathrm{s}};\ n = 1, \cdots, N_{\mathrm{s}} \tag{E.68}$$

$$V_{\mathrm{b},m,n} - U^{\mathrm{L}} Z_{m,n}^{\mathrm{Vb}} \geq 0, \quad m = 1, \cdots, N_{\mathrm{s}};\ n = 1, \cdots, N_{\mathrm{s}} \tag{E.69}$$

The final type of logic constraint is associated with the outlet permeate pressure for each stage. If the outlet permeate stream goes to final product stream mixer, the permeate pressure must equal the product pressure. If the permeate stream is recycled to another stage, the permeate pressure can assume any value less than or equal to the upper limit of the feed-side pressure P^{U}. By introducing a slack variable S, these logic relations can be expressed as:

$$p_{0,n} = S_n + p_{\mathrm{out}}, \quad n = 1, \cdots, N_{\mathrm{s}} \tag{E.70}$$

$$0 \leq S_n \leq (P^{\mathrm{U}} - p_{\mathrm{out}})(1 - Z_n^{\mathrm{Vp}}), \quad n = 1, \cdots, N_{\mathrm{s}} \tag{E.71}$$

Note that if $Z_n^{\mathrm{Vp}} = 1$, $p_{0,n} = p_{\mathrm{out}}$; if $Z_n^{\mathrm{Vp}} = 0$, $p_{\mathrm{out}} \leq p_{0,n} \leq P^{\mathrm{U}}$.

Discrete Membrane Area Constraints

Membrane area can be considered as a discrete variable:

$$A_n = A_0 N_n^{\mathrm{A}}, \quad n = 1, \cdots, N_{\mathrm{s}} \tag{E.72}$$

where A_0 is the element membrane area size and N^{A} ($N^{\mathrm{AL}} \leq N^{\mathrm{A}} \leq N^{\mathrm{AU}}$) is the number of elements. One way to convert the integer variables N^{A} to binary variables Z^{A} is to use the following expression [28]:

$$N_n^{\mathrm{A}} = N_n^{\mathrm{AL}} + \sum_{k=1}^{N_{\mathrm{b}}} 2^{k-1} Z_{n,k}^{\mathrm{A}}, \quad n = 1, \cdots, N_{\mathrm{s}} \tag{E.73}$$

where N_{b} is the minimum number of binary variable needed:

$$N_{\mathrm{b}} = 1 + \mathrm{int}\left\{\frac{\log(N^{\mathrm{AU}} - N^{\mathrm{AL}})}{\log(2)}\right\} \tag{E.74}$$

In the following case studies, we choose $N^{\mathrm{AL}} = 1$ and $N^{\mathrm{AU}} = 15$ to 30, which yield $N_{\mathrm{b}} = 4$ or 5.

Nonnegativity and Integrality Constraints

These constraints are used to specify lower and upper variable bounds to prevent undefined operations (*e.g.* division by zero) and to ensure the variables remain in a reasonable solution space. These constraints are expressed as follows:

$$0 \leq U_{\mathrm{f0},n}, U_{\mathrm{f},n}, U_{0,n}, V_{0,n}, U_{\mathrm{p},n}, V_{\mathrm{p},n}, U_{\mathrm{b},m,n}, V_{\mathrm{b},m,n}, U_{\mathrm{pt}}, V_{\mathrm{pt}} \leq U^{\mathrm{U}} \tag{E.75}$$

$$A_n, N_n^{\mathrm{A}}, R_n, C_n, P, p_n, \bar{y}_{\mathrm{f},n}, \bar{y}_{\mathrm{r},n}, \bar{y}'_{j,n} \geq 0 \qquad \text{(E.76)}$$

$$0 \leq x_{\mathrm{f},n,i}, x_{0,n,i}, y_{0,n,i}, y'_{\mathrm{f},n,i}, y'_{j,n,i}, y'_{\mathrm{r},n,i}, x_{\mathrm{r},n,i}, x_{\mathrm{pt},i}, y_{\mathrm{pt},i} \leq 1 \qquad \text{(E.77)}$$

$$0 \leq \theta_{0,n}, \gamma_{0,n}, \gamma_n, \phi_{\mathrm{r},n}, \phi_{j,n} \leq 1 \qquad \text{(E.78)}$$

$$Z_n^{\mathrm{Uf0}}, Z_n^{\mathrm{Up}}, Z_n^{\mathrm{Vp}}, Z_{m,n}^{\mathrm{Ub}}, Z_{m,n}^{\mathrm{Vb}}, Z_{n,k}^{\mathrm{A}} = 0, 1 \qquad \text{(E.79)}$$

$$m = 1, \cdots, N_{\mathrm{s}};\ n = 1, \cdots, N_{\mathrm{s}};\ j = 1, \cdots, M;$$

$$i = 1, \cdots, N_{\mathrm{c}};\ k = 1, \cdots, N_{\mathrm{b}}$$

E.2 List of Symbols

$\mathcal{A}_i$ dimensionless constant defined by equation (3.24)

A membrane area for each stage (m^2)

A_t total membrane area of system (m^2)

B permeability of the spacing material inside the spiral-wound leaf (m^2)

$\mathcal{B}_i$ dimensionless constant defined by equation (3.25)

C dimensionless constant defined by equation (3.13)

C'' permeate-side pressure parameter defined by equation (4.1) (MPa^2s/mol)

d thickness of membrane skin (m)

d_m thickness of membrane leaf (m)

f_{cc} annual capital charge (%/year)

f_{cp} capital cost of gas-powered compressors ($/KW)

f_{hv} sales gas gross heating value (MJ/m^3)

f_{mh} capital cost of membrane housing ($/m^2 membrane)

f_{mr} expense of membrane replacement ($/m^2 membrane)

f_{mt} maintenance rate (%/year)

f_{sg} utility and sales gas price ($/Km^3)

f_{wk} working capital rate (%)

F annual process cost ($/Km^3)

F_{cc} annual capital charge ($/year)

F_{fc} fixed capital investment ($)

F_{mr} expense of membrane replacement ($/year)

F_{mt} maintenance expense ($/year)

F_{pl} value of product losses ($/year)

F_{ut} cost of utilities ($/year)

$\mathcal{F}$ vector function expressed in (E.38)

h dimensionless leaf length variable

K_1–K_4 intermediate vector variables for Runge-Kutta-Gill expression

L membrane leaf length (m)

M number of quadrature points

N_b minimum number of binary variables for integer conversion

N_c number of components for gas mixtures

N_s permeator stage number in configuration

N^A number of membrane elements for each stage

N^{AL}	lower bound of membrane element number
N^{AU}	upper bound of membrane element number
P	feed-side pressure (MPa)
P_f	fresh feed pressure (MPa)
P^U	upper bound of feed-side pressure (MPa)
p	permeate-side pressure (MPa)
p_{out}	required outlet permeate pressure (MPa)
p_0	permeate outlet pressure for each permeator (MPa)
Q_i	permeability of the i-th component (mol/m·s·Pa)
Q_b	permeability of the base component (mol/m·s·Pa)
R	dimensionless permeation factor defined by equation (3.28)
R_g	ideal gas constant (m^3·Pa/kg-mol·K)
S	slack variable in logic constraints
t_m	membrane life (years)
t_{wk}	annual working time (days/year)
T	temperature (K)
U_f	feed flow rate for each permeator (mol/s)
U_{f0}	fresh feed flow rate for each permeator (mol/s)
U_{f00}	total fresh feed flow rate as processing capacity (mol/s)
U_0	flow rate of residue gas at permeator outlet (mol/s)
U_b	flow rate of residue gas as recycle stream (mol/s)

U_p flow rate of residue gas as product stream (mol/s)

U_{pt} total flow rate of residue product (mol/s)

U^L upper bound on stream flow rate (mol/s)

U^U lower bound on stream flow rate (mol/s)

V_0 permeate flow rate at permeator outlet (mol/s)

V_b flow rate of permeate gas as recycle stream (mol/s)

V_p flow rate of permeate gas as product stream (mol/s)

V_{pt} total flow rate of permeate product (mol/s)

W membrane leaf width (m)

W_{cp} stage compressor power (KW)

$W_{cp,f}$ fresh feed compressor power (KW)

W_t total compressor power (KW)

w_j quadrature weights

x local feed-side concentration (mole fraction)

x_0 bulk residue stream concentration at permeator outlet (mole fraction)

x_f feed concentration for each stage (mole fraction)

x_{f0} fresh feed concentration (mole fraction)

x_{out,CO_2} maximum CO_2 concentration of residue product (mole fraction)

x_{pt} concentration of residue product (mole fraction)

x_r local outlet residue concentration (mole fraction)

Y vector expressed in (E.38)

y_0 bulk permeate concentration at permeate outlet (mole fraction)

y_{pt} concentration of permeate product (mole fraction)

y_{out,CH_4} maximum CH_4 concentration of permeate product (mole fraction)

y' local permeate concentration on the membrane surface (mole fraction)

y'_f y' along inlet end of membrane leaf (mole fraction)

y'_j y' at quadrature point j (mole fraction)

y'_r y' along outlet end of membrane leaf (mole fraction)

$\bar{y}'$ composition variable defined by equation (3.17)

$\bar{y}'_f$ $\bar{y}'$ value at the feed inlet

$\bar{y}'_r$ $\bar{y}'$ value at the residue outlet

$\bar{y}'_j$ $\bar{y}'$ value at the j-th quadrature point

Z^A binary variable used to express discrete membrane area

Z^{Ub} binary variable denoting the existence or nonexistence of U_b

Z^{Uf0} binary variable denoting the existence or nonexistence of U_{f0}

Z^{Up} binary variable denoting the existence or nonexistence of U_p

Z^{Vb} binary variable denoting the existence or nonexistence of V_b

Z^{Vp} binary variable denoting the existence or nonexistence of V_p

α_i $= Q_i/Q_b$, membrane selectivity for the i-th component

γ $= p/P$, ratio of permeate pressure to feed pressure

γ_0 $= p_0/P$, ratio of permeate pressure to feed pressure at permeate outlet

μ viscosity of gas mixture (Pa·s)

θ_0 $= V_0/U_f$, ratio of permeate flow to feed flow at permeate outlet

Θ CH_4 recovery (%)

ξ_j quadrature points

ϕ dimensionless feed-side flow rate

ϕ_r dimensionless feed-side flow rate at residue outlet

η_{cp} compressor efficiency (%)

Subscripts

i index of components in gas mixture

j index of quadrature points for the summation term in equation (3.33)

k index of binary variables in expression of discrete membrane area

index of components in gas mixture

m, n index of membrane stages

q index of quadrature points for leaf length variable h

Appendix F

Resulting Publications and Presentations

1. R. Qi and M. A. Henson. Approximate modeling of spiral-wound gas permeators, *J. Membrane Sci.*, 121:11–24, 1996.

2. R. Qi and M. A. Henson. Modeling of spiral-wound permeators for multicomponent gas separations. *Ind. Eng. Chem. Res.*, 36:2320–2331, 1997.

3. R. Qi and M. A. Henson. Optimization-based design of spiral-wound membrane systems for CO_2/CH_4 separations. *Sep. Purif. Tech.*, 13:209–225, 1998.

4. R. Qi and M. A. Henson. Optimal design of spiral-wound membrane networks for gas separations. *J. Membrane Sci.*, in press.

5. R. Qi and M. A. Henson. Membrane system design for multicomponent gas mixtures via mixed-integer nonlinear programming. *AIChE J.*, submitted.

6. R. Qi and M. A. Henson. Modeling of spiral-wound permeators for multicomponent gas separations. *AIChE Spring Meeting*, Houston, TX, March 1997.

7. R. Qi and M. A. Henson. Design of gas membrane separation systems via nonlinear programming. *AIChE Annual Meeting*, Los Angeles, CA, November 1997.

8. R. Qi and M. A. Henson. A mixed-integer nonlinear programming strategy for systematic design of spiral-wound gas separation systems. *AIChE Spring Meeting*, New Orleans, LA, March 1998

Vita

Runhong Qi was born in Funing, Hebei Province, China, on April 23, 1964. He attended elementary and high schools in the Funing county from 1971 to 1980. After graduating from high school, he attended college in Tianjin University, China. He received a bachelor of engineering degree in Applied Chemistry in July 1984 and a master of engineering degree in Chemical Engineering in June 1987. After finishing his master's degree, he worked two years (July 1987 – June 1989) as an engineer in the Development Center of Petrochemical Technology at Tianjin University and five years (July 1989 – June 1994) as a faculty member (lecturer) in the Department of Chemical Engineering at Tianjin University. He received several awards for excellence in teaching and research. In August 1994, he began his doctoral studies in Chemical Engineering at Louisiana State University. During his tenure at L.S.U., he held teaching and research assistantships and received a Charles Coates Fellowship award. In December 1998, he received his doctoral degree in Chemical Engineering under the supervision of Dr. Michael A. Henson.

DOCTORAL EXAMINATION AND DISSERTATION REPORT

Candidate: Runhong Qi

Major Field: Chemical Engineering

Title of Dissertation: Modeling and Optimal Design of Spiral-Wound Membrane Systems for Gas Separations

Approved:

Major Professor and Chairman

Dean of the Graduate School

EXAMINING COMMITTEE:

Date of Examination:

August 24, 1998

IMAGE EVALUATION
TEST TARGET (QA-3)

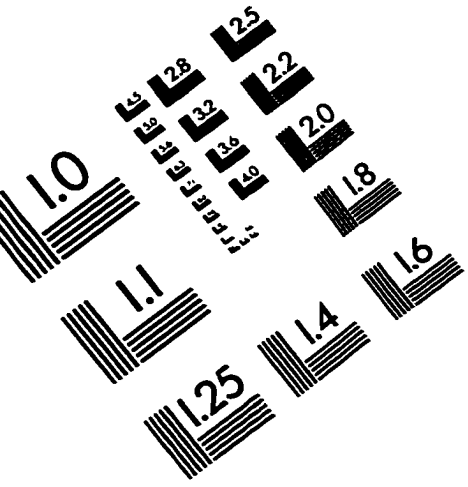

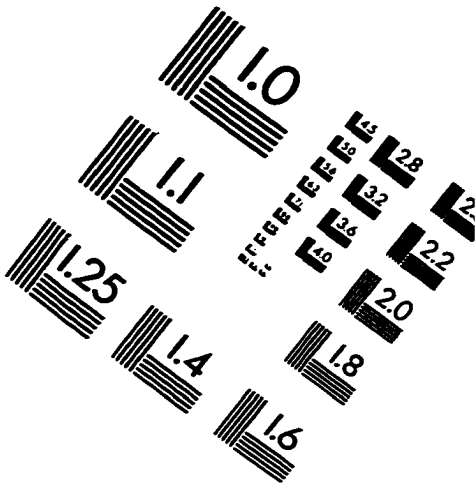

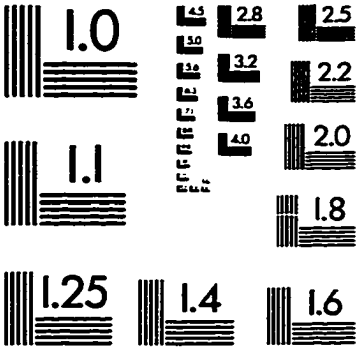

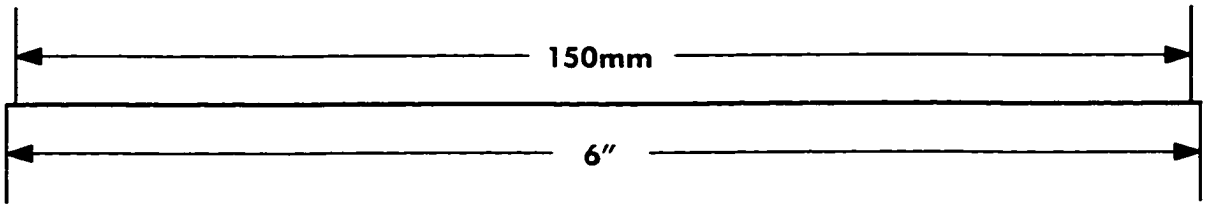

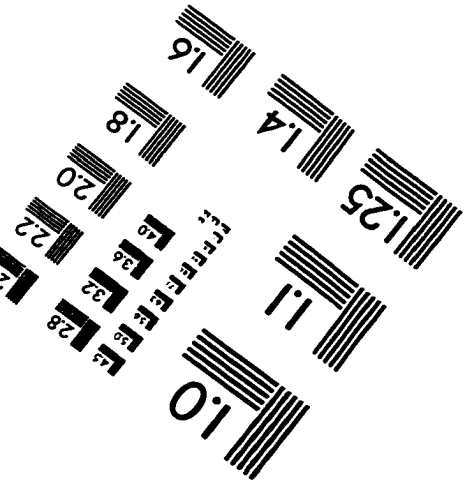

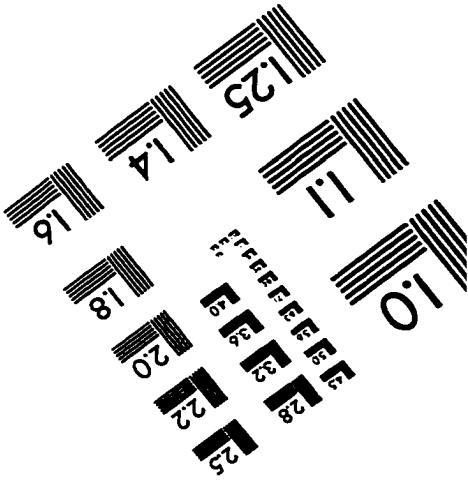

APPLIED IMAGE, Inc
1653 East Main Street
Rochester, NY 14609 USA
Phone: 716/482-0300
Fax: 716/288-5989